Energy Research and Development Division

FINAL PROJECT REPORT

High-Temperature Hybrid Compressed Air Storage:

Ultra-Low-Cost Energy Storage System Alternative to Batteries

California Energy Commission

Edmund G. Brown Jr., Governor

February 2018 | CEC-500-2018-001

PREPARED BY:

Primary Author(s):
Dr. Pirouz Kavehpour
Dr. Mohammad Janbozorgi
Walid Ismail
Sammy Houssainy

University of California, Los Angeles
420 Westwood Plaza, Room 46-147A
Los Angeles, Ca, 90095
Phone: (310)825-6494

Contract Number: EPC-14-027

PREPARED FOR:
California Energy Commission

David Chambers
Project Manager

Fernando Piña
Office Manager
ENERGY SYSTEMS RESEARCH OFFICE

Laurie ten Hope
Deputy Director
ENERGY RESEARCH AND DEVELOPMENT DIVISION

Drew Bohan
Executive Director

PREFACE

The California Energy Commission's Energy Research and Development Division supports energy research and development programs to spur innovation in energy efficiency, renewable energy and advanced clean generation, energy-related environmental protection, energy transmission and distribution and transportation.

In 2012, the Electric Program Investment Charge (EPIC) was established by the California Public Utilities Commission to fund public investments in research to create and advance new energy solution, foster regional innovation and bring ideas from the lab to the marketplace. The California Energy Commission and the state's three largest investor-owned utilities – Pacific Gas and Electric Company, San Diego Gas & Electric Company and Southern California Edison Company – were selected to administer the EPIC funds and advance novel technologies, tools and strategies that provide benefits to their electric ratepayers.

The Energy Commission is committed to ensuring public participation in its research and development programs which promote greater reliability, lower costs, and increase safety for the California electric ratepayer and include:

- Providing societal benefits.
- Reducing greenhouse gas emission in the electricity sector at the lowest possible cost.
- Supporting California's loading order to meet energy needs first with energy efficiency and demand response, next with renewable energy (distributed generation and utility scale), and finally with clean conventional electricity supply.
- Supporting low-emission vehicles and transportation.
- Providing economic development.
- Using ratepayer funds efficiently.

High Temperature Hybrid Compressed Air Storage: Ultra-Low-Cost Energy Storage System Alternative to Batteries is the final report for the High-Temperature Hybrid Compressed Air Energy Storage (Contract Number EPC-14-027, Grant Number PON-13-302, S8.2) conducted by the Regent of the University of California, Los Angeles Campus. The information from this project contributes to Energy Research and Development Division's EPIC program.

For more information about the Energy Research and Development Division, please visit the Energy Commission's website at www.energy.ca.gov/research/ or contact the Energy Commission at 916-327-1551.

ABSTRACT

Energy storage can be used to smooth fluctuations in renewable energy generation, reduce or eliminate intermittency and replace unpredictable energy with manageable, on-demand (dispatchable) power. The project team designed a fully-functional, low-cost, 74 kilowatt pilot high-temperature hybrid compressed air energy storage system that can efficiently store grid-level energy and release that energy when it is required to meet peak demand. Combining ultra-low-cost thermal energy storage with efficient compressed air energy storage, resulted in higher-than-normal efficiency system with low cost for electricity costs. The performance and operations models for the energy storage system show this type of energy storage can perform and operate at the grid level and can benefit California ratepayers with lower generation costs and reducing greenhouse gas and other emissions.

Keywords: Energy storage, CAES, thermal storage, renewables, hybrid system

Kavehpour, Pirouz, Mohammad Janbozorgi, Walid Ismail, Sammy Houssainy. University of California, Los Angeles. 2018. *High-Temperature Hybrid Compressed Air Storage: Ultra-low Cost Energy Storage System Alternatives to Batteries.* California Energy Commission. Publication Number: CEC-500-2018-001

TABLE OF CONTENTS

LIST OF FIGURES

Page

LIST OF TABLES

Page

EXECUTIVE SUMMARY

Introduction

Energy storage can be used to ease renewable energy generation by reducing or eliminating intermittency. Also, energy storage can replace unpredictable renewable energy generation with predictable, on-demand (dispatchable) power. Energy storage devices are generally categorized by performance characteristics, and the kind of applications they serve. Short-term storage, usually in minutes, can be used to provide electric grid frequency regulation and contingency power reserves. Longer-term storage, usually in hours to days can provide electric grid stability through load-leveling and peak capacity services. In addition, long-term storage can potentially providing shorter-term grid services as well. Energy storage devices used for these applications include pumped hydroelectric storage, compressed air energy storage, and certain battery technologies.

Integrating renewable energy sources to the electrical grid is more challenging because of their intermittent nature of these sources. When there is extra power generation from a combination of power plants and renewable sources, as in the middle of a sunny day, the renewable sources are often curtailed for the safety and integrity of the electrical grid. The California Public Utilities Commission has recognized more energy storage is an important step toward a greater reliance on renewable energy to meet California's electricity demands. Meeting these targets, however, requires significant improvements to energy storage systems. A large-scale energy storage system can help smooth out the fluctuations in renewable electricity generation on the grid. These systems can store excess power during periods of low demand, and provide electricity as base-load or during periods of high demand.

Numerous types of energy storage technologies with varying operating characteristics are available for commercial use including compressed air energy storage and pumped hydroelectric storage. Compressed air energy storage can offer lower capital cost, lower maintenance cost, and fewer geological restrictions, making it more appealing compared to pumped hydro storage. This project combines thermal storage and compressed air energy storage into a hybrid thermal and compressed air energy storage design.

High-temperature hybrid compressed air energy storage is a simple, yet groundbreaking energy storage system using innovative technology to store electricity with greater efficiency than conventional systems. High-temperature hybrid compressed air energy storage requires little capital expenditure and is environmentally friendly in design and operation. This inventive approach to energy storage could be instrumental in increasing California's reliance on renewable energy by improving how renewable energy is stored and used. This hybrid design incorporates two stages of heating through separate low-temperature thermal energy storage units, and achieves simplicity and practicality. The high-temperature hybrid compressed air energy system operates by storing low-cost off-peak energy as stored ambient compressed air (in an above or below ground pressure tank) and to generate on-peak electricity by (1) releasing the compressed air from the storage reservoir or pressure tank, (2) preheating the cool, high-pressure air, and (3) directing the preheated air into an expansion turbine driving an electric generator.

Project Purpose

The research team explored building and testing a low-capital-cost, durable, and efficient pilot-scale energy storage system using high-temperature compressed air that would efficiently store

grid-level electricity and release that electricity to meet peak energy demands on the grid. This energy storage system would allow power plants to store electricity generated during off-peak hours and allow the plants to use that electricity during peak-use hours, increasing reliability of the electric utility grid. The project explored the cost saving advantages of combining compressed air energy storage units with low and high-temperature thermal energy storage units to improve the overall efficiency of the high-temperature hybrid compressed air energy storage system. The high-temperature hybrid compressed air energy storage system uses grid electricity directly into the thermal storage unit through thermoelectric heaters (similar to strip or industrial space heaters) resulting in temperatures higher than traditional compressed air energy storage systems. This advanced high-temperature hybrid compressed air energy storage system could perform as well as a much larger compressed air energy storage system while costing about the same as a small conventional compressed air energy storage system.

Stakeholders included Southern California Edison, Cal-Poly Pomona and the Murry Company. The project was in Southern California Edison's service territory with Cal-Poly Pomona providing the original demonstration site on their campus. Unfortunately Cal-Poly Pomona withdrew from the project so a second demonstration site was chosen with the City of Santa Clarita. The project, however, was unable to acquire the required construction permits in time for the Murry Company to build the full size high-temperature compressed air energy storage system; and for the research team to run and test the pilot system.

For this project, a complete thermodynamic analysis of the high-temperature hybrid compressed air energy storage system was done together with the parametric studies to characterize how the operating pressure and thermal storage temperature affect the performance of the storage system. Component efficiencies and throttling losses were also investigated and modeled. Based on the modeling results, a design for a low-cost, 74 kW energy storage system was created using off-the-shelf components ready for pilot demonstration. This system can efficiently store grid-level energy and release that energy to generate electricity when required to meet peak demand, particularly for support services that help maintain grid stability and security.

The project documented and reported on the design, anticipated performance and lessons learned from the high-temperature hybrid compressed air energy storage system to increase knowledge and understanding of how these storage systems perform and the barriers to constructing and operating them.

Project Process and Results

The first of the two phases of the project was to build and test the core high temperature hybrid compressed air energy storage system. Once the low-temperature thermal energy storage unit and heat recuperator were added, the efficiency of the system was to be tested and verified 85 percent efficient. During testing, the compressed air tanks would be used to achieve the preliminary run time to "shake out" any bugs in the system before going to full pilot-scale demonstration. The second of the two project phases was to bring the system to full pilot scale and demonstrate the full capacity of 446 kilowatt-hours (kWh) with a single cycle (discharge) run time of six hours.

The high-temperature hybrid compressed air energy storage system was completely designed with all of the components (some fabricated while others purchased) and ready for construction and demonstration. However, the unexpected loss of both sites resulted in the project not having time to construct and demonstrate the system within the project term. Regardless, this project resulted in two innovative patents, six technical journal articles and a

PhD and MS student project members being hired by the National Renewable Energy Laboratory and Electricity Power Research Institute. The research has caught the attention of several microgrid companies to use the high-temperature hybrid compressed air energy storage system as an alternative to batteries on several projects in California and other states. Several utilities, including Southern California Edison, Southern California Gas and Eversource have shown interest and are considering recommending this system to their customers as an alternative to other energy storage systems.

Benefits to California

The innovation of the high-temperature hybrid compressed air energy storage system is a possible game changer for energy storage. The team's modeling showed this technology could benefit California's investor-owned electricity ratepayers by offering a more reliable, economical and safe approach to energy storage. High-temperature hybrid compressed air energy storage is a single storage system that can also be scaled for changing grid demand, reducing investment costs and providing up to 85 percent more efficiency.

According to the modeling results, using high temperature hybrid compressed air energy storage could reduce the cost of energy storage to about $100/kWh, estimating $660 million to $1.32 billion of savings annually. Calculations also showed significant reductions in greenhouse gases; 2,791 tons/MW of carbon dioxide (CO_2), 37 tons/MW of sulfur dioxide (SO_2), 5 tons/MW of oxides of nitrogen (NO_x) and 2.4 tons/MW of carbon monoxide (CO).

CHAPTER 1: Project Introduction (Energy Problem/Solution)

The California Public Utilities Commission (CPUC) has recognized that increased use of energy storage is an important step toward a greater reliance on renewable energy to meet California's electricity demands. The CPUC established energy storage procurement targets for the state's investor-owned utilities (IOUs). Meeting these procurement targets require significant improvements to conventional energy storage systems.

High-temperature hybrid compressed air energy storage (HTH-CAES) is a simple, yet groundbreaking energy storage system that will allow IOUs to meet the CPUC's stringent procurement targets at low costs. HTH-CAES uses innovative technology to store grid-level energy with greater efficiency and at lower cost than conventional systems. HTH-CAES requires little capital expenditure and is environmentally friendly in design and operation. This inventive approach to energy storage will be instrumental in increasing California's reliance on renewable energy by optimizing the way intermittent renewables energy resources are stored and used.

The project objective was to build a fully functional, low-cost, 74 kilowatt (kW) pilot HTH-CAES system that can efficiently store grid-level energy and release that energy when required to meet peak demand, particularly for ancillary services and load-following uses.

1.1 An Innovative and Low-Cost Strategy for Achieving California's Statutory Energy Storage Goals

The HTH-CAES system combines a state-of-the-art high-temperature energy storage unit with traditional compressed air energy storage technology. This combination reduces losses in air compression and shifts storage capacity to the thermal side, making possible a capital cost of $938/kW. Furthermore, the HTH-CAES system is constructed using low-cost, off-the-shelf components, resulting in significant capital cost saving. The proposed system cost for energy storage is $156/kWh installed and 7 cents/kWh/cycle levelized with a system cycle efficiency of 85% over 15,000 cycles.

1.2 HTH-CAES Offers a Significant Improvement Over Existing CAES Technologies

Energy storage can be used to level fluctuations in renewable energy generation, reduce or eliminate intermittency, and replace unpredictable energy with manageable, dispatchable power. Energy storage devices are generally categorized by performance characteristics and the kind of applications they serve. Short-term storage, usually in minutes, can be used to provide operating reserves such as frequency regulation and contingency reserves. Longer-term storage in hours to days can provide load-leveling and peak capacity services, in addition to potentially providing shorter-term grid services as well. Technologies used for these applications include pumped hydroelectric storage, compressed air energy storage, and certain battery technologies.

Among the various forms of energy storage technology, compressed air energy storage (CAES) is the most viable for long-term/large-scale storage applications. CAES has a lower capital and

maintenance cost and fewer geographic restrictions than any other competing technology. (Table 1)

Table 1: Comparing Various Energy Storage Technologies

	NaS Batteries	Fuel Cells	Thermal Storage	SMES	Pumped Hydro	Compressed Air
Power Density	Good	Very Good	Excellent	Excellent	Very Good	Very Good
Energy Density	Excellent	Very Good	Excellent	Fair	Very Good	Very Good
Life Time	15 years	20 years	20 years	20 years	30 years	30 years
Dynamic Response	ms	1s	mins	ms	5 min	5 min
Environmental Impact	Low	Low	Low	High	Moderate	Low
Cost/kW	$1800	$4000	$600	$975	$1000	$400
Efficiency %	89	59	<70	90	70-85	70-85+

In CAES technology, electricity generated during off-peak periods is stored as compressed air. Compressors are used to convert electrical energy into compressed air that is stored in large tanks or caverns. The ability of CAES to support large-scale power applications with lowest capital cost per unit of energy has captured the interest of industry in a major way. Some studies suggest that CAES systems may also be used at small-scale power levels to shift load up to three hours, curtail transmission, and hedge forecasts, among other applications.

CAES storage reservoirs for underground storage can be classified into three categories: salt, hard rock, and porous rock. These geologies are found to account for a significant fraction of United States. Previous studies indicate that more than 75% of the United States has geologic conditions that are potentially favorable for underground air storage.

While cost-effective, traditional CAES systems are disadvantaged by heat losses that occur during air compression. With advanced adiabatic (a process where heat does not enter or leave the system) CAES (AA-CAES) systems, thermal energy from air compression is stored in thermal energy storage (TES) units and returned to the compressed air during discharge. TES units consist of a thermal transport fluid, a heat exchanger, a heat reservoir, and an auxiliary circulation pump.

The higher overall efficiency of AA CAES systems has made it an attractive alternative to traditional CAES. However, AA-CAES suffers from added capital cost and increased complexity. High capital cost is one of the main hindrances to commercializing AA-CAES systems. Of the only two compressed air energy storage plants in operation (Huntorf, Germany and McIntosh, United States), neither employs AA-CAES. While the overall efficiency of AA-CAES is higher, the operating cost can be much greater with AA-CAES when compared to a traditional CAES system.

The compromise between CAES and AA-CAES is a high-temperature hybrid CAES (HTH-CAES). With HTH-CAES the TES is replaced with a low-and high-temperature energy storage unit. As with TES, the LTES unit stores the heat generated during air compression. But unlike TES, the HTES unit acts as a scalable energy reservoir without the complexity of thermal transport fluid

or recirculation pumps. The HTES unit takes advantage of the high thermal capacity of an inexpensive thermal medium to store heat that will later be used to superheat the compressed air. HTH-CAES allows for the addition of grid energy directly to the HTES through thermoelectric heaters to achieve temperatures much higher than traditional CAES and AA CAES, paving the way for a new class of energy storage systems.

With the addition of a HTES unit, the workload is shifted from pure compression to thermal storage. Separating energy storage between compressed air and thermal storage expands the energy capacity of the compressed air system without increasing the air pressure or tank capacity. HTES allows the system to be dynamically scaled up or down as the demand changes without any structural change in system configuration. More importantly, since the energy storage reservoir is now split between air compression and thermoelectric heaters, the working fluid does is not required to be compressed to the same pressures as in an AA-CAES system to achieve the same energy output. Using a smaller compression ratio, less energy is lost due to nonadiabatic conditions. That has the added benefit of allowing the LTES unit to be much less expensive than a traditional adiabatic system because the requirements are lower. This advancement in compressed air technology will allow HTH-CAES systems to perform as well as a much larger and more complex AA-CAES system, while costing about the same as a small conventional CAES system.

One major obstacle to the widespread adoption of energy storage systems is the economic justification of the systems. Converting electric energy into another form and converting it back can result in high energy losses and costs. To date, CAES technology has been associated with very inefficient or costly systems or both. This consequence has made finding investors for CAES technology especially difficult. Electric Program Investment Charge (EPIC) program funding allows the applied research to develop from the laboratory scale to pilot scale. The laboratory-scale system, which was funded by the Advanced Research Projects Agency –Energy (ARPA-E), allowed the research team to demonstrate the technology for HTH-CAES.

1.3 The Project

Having demonstrated the feasibility of this technology with a laboratory-scale prototype, the team proposed designing and constructing a pilot-scale system to further test and optimize the technology.

The thermodynamics model, which has been verified with experimental laboratory observations, shows that a pilot-scale HTH-CAES system can outperform all other compressed air systems in overall cost while providing comparable efficiency to AA-CAES.

The research team consists of professors from the mechanical and aerospace engineering department at University of California, Los Angeles (UCLA). Other than the high temperature storage unit, which was fabricated and tested in the lab, the rest of components for HTH-CAES are commercially-available, off-the-shelf types, which reduce the complexity and overall cost of the system.

This report summarizes the steps taken in this project from design and modeling of the system, including thermodynamics, heat transfer, fluid mechanics, controls, and system integration to construct the HTH-CAES system. The pitfalls that exist for such systems are identified and were overcome including unforeseen circumstances such as site change and delay in construction permit.

CHAPTER 2:
Thermodynamic Analysis

2.1 Theoretical Efficiency Limits of the Hybrid Thermal-Compressed Air Energy Storage Systems

This section provides the thermodynamic efficiency limits within which a hybrid thermal CAES system operates. The thermodynamic models assume a constant pressure cavern, typically constructed in an underground rock formation with a water-equalizing pit to maintain isobaric conditions or constant pressure. It is shown that the cavern under this assumption reduces to just a delay in operating the plant. A constant-volume cavern, on the contrary, changes the state of air through the cavern and must be considered in proper modeling of the plant. The novel premise of this work is to demonstrate and compare the fundamental differences and relationships between the efficiencies of a hybrid CAES cycle with that of an analogous Brayton power cycle (a thermodynamic cycle for a constant-pressure heat engine), for pure thermal energy storage. Specifically, the efficiency of the hybrid CAES system is compared with a regenerative and nonregenerative Brayton cycle. This unique comparison illustrates the general and fundamental differences in the roundtrip cycle efficiency definitions associated with a pure thermal energy storage system, using a Brayton cycle, versus a hybrid CAES, and the related theoretical limiting values.

2.2 Model and Assumptions

The models considered in this paper represent variations of a hybrid thermal compressed air energy storage (HT-CAES), in which part of the available input energy is spent compressing the air into a storage medium (assumed to be a cavern), and the rest is directly converted to heat and stored in a thermal energy storage (TES) medium. The nature of the TES is fundamentally different from the absorbed energy of compression, which is either discarded as in conventional CAES or stored and then used during expansion as in advanced adiabatic CAES. The inclusion of the TES intentionally takes the state of the system off the compression isentrope and fundamentally introduces an upper Carnotlike limit on the efficiency of the plant. The advanced adiabatic CAES ideally aims for the best round-trip efficiency by trying to synchronize the compression and expansion isentropes. The TES can be charged either electrically from the grid or by the surplus of photovoltaic electricity through Joule heating or by a high-temperature fluid stream. The high temperature fluid stream could also be either hot exhaust waste heat recovery or the high temperature output of a CSP plant.

In all analyses presented in this paper, all components are assumed to be internally reversible and have perfect component performance indices, that is isentropic efficiency or heat exchange effectiveness. Also, the cavern is neglected under the assumptions that 1) the cavern is fully insulated and thus no storage losses are present, and 2) the cavern is isobaric during charge and discharge. Therefore, the thermodynamic conditions of the air into and out of the cavern are the same and all the energy invested in charging the cavern is retrieved during discharge. Under these assumptions, the cavern is solely a buffer zone that introduces a delay time in the operation of the plant. An analysis of the cavern under constant volume and constant pressure is presented in this chapter. The HT-CAES can be thought of as a “broken” Brayton cycle, in which the work of compression is not supplied by the turbine, thus making it more efficient than the classical Brayton cycle commonly used in power generation units. This chapter aims to

quantify the performance of HT-CAES vs. the classical Brayton cycle, for pure thermal energy storage, and discover the efficiency limits.

2.3 HT-CAES vs. Brayton Cycle with Regeneration

To investigate the effect of temperature of the TES on the storage efficiency, a regenerative HT-CAES model is analyzed. Figure 1 shows the HT-CAES configuration in which the compressor is not powered by the turbine, as opposed to the classical Brayton cycle shown in Figure 2.

Figure 1: HT CAES With Regeneration

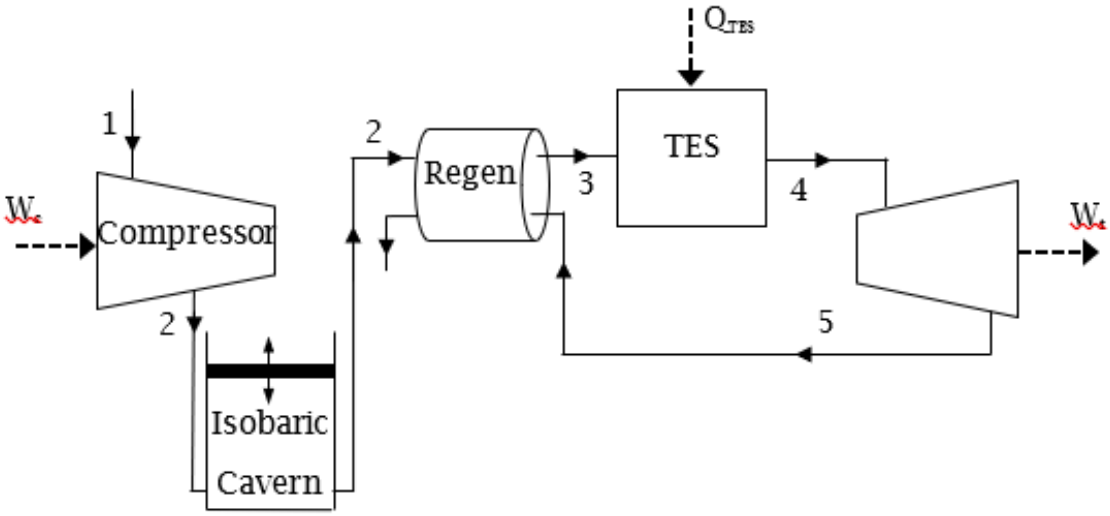

Figure 2: Brayton Cycle With Regeneration

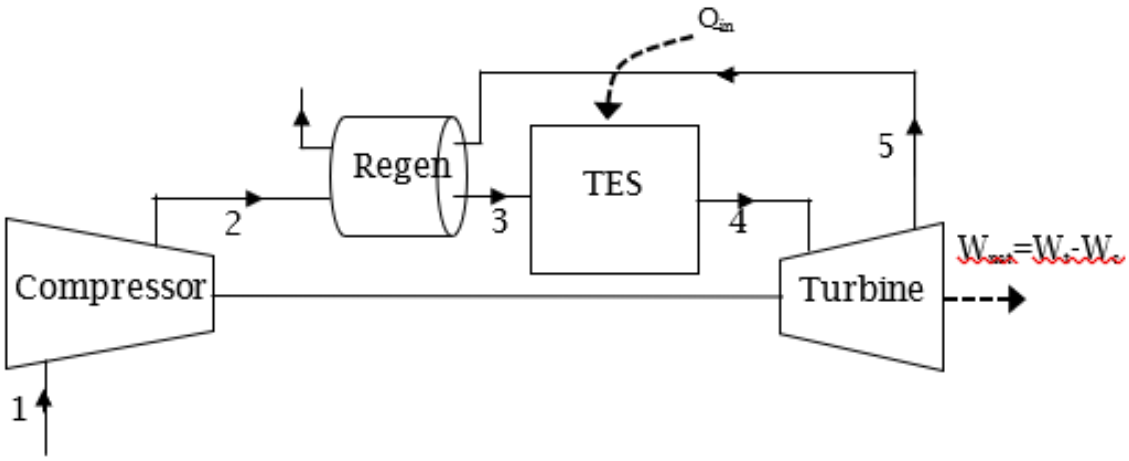

The round trip storage efficiency of the HT-CAES is given by

$$\eta_{HT-CAES,R} = \frac{\dot{W}_t}{\dot{W}_c + \dot{Q}_{TES}} \quad (1)$$

When the compressor has a compression ratio of$r$, and assuming a constant specific heat, equation (1) can be written

$$\eta_{HT-CAES,R} = \frac{T_4(1 - 1/r^{(k-1)/k})}{T_1(r^{(k-1)/k} - 1) + T_4(1 - 1/r^{(k-1)/k})} \tag{2}$$

Where k is the ratio of the specific heat. Equation (2) can be further simplified as follows

$$\eta_{HT-CAES,R} = \frac{1}{1 + \frac{T_1}{T_4} r^{(k-1)/k}} \tag{3}$$

It can be shown that the efficiency of an ideal regenerative Brayton cycle with the same compression ratio, r, and turbine inlet temperature T_4 is given by

$$\eta_{Bryaton,R} = 1 - \frac{T_1}{T_4} r^{\frac{k-1}{k}} \tag{4}$$

Eliminating $\frac{T_1}{T_4} r^{(k-1)/k}$ between equations (3) and (4) results in the following relationship between the round-trip efficiency of HT-CAES and the Brayton cycle efficiency:

$$\eta_{HT-CAES,R} = \frac{1}{2 - \eta_{Bryaton,R}} \tag{5}$$

Equation (5) can be rewritten as:

$$\eta_{HT-CAES,R} - \eta_{Brayton,R} = \frac{\left(1 - \eta_{Bryaton,R}\right)^2}{2 - \eta_{Bryaton,R}} \geq 0 \tag{6}$$

Figure 3 Efficiency equations (3) and (4), versus the turbine inlet temperature for a compression ratio of 5, and Figure 5 Equation (5).

Figure 3: Efficiency Versus Thermal Storage Temperatures

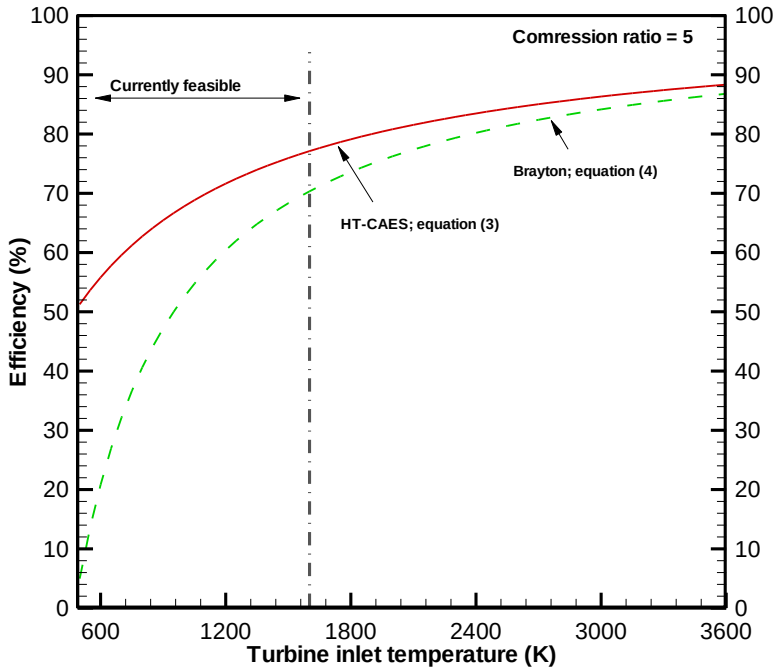

Compression ratio of five in both cycles

Figure 4: Efficiency of HT-CAES System Vs the Corresponding Brayton Cycle With Regeneration-Equation (5)

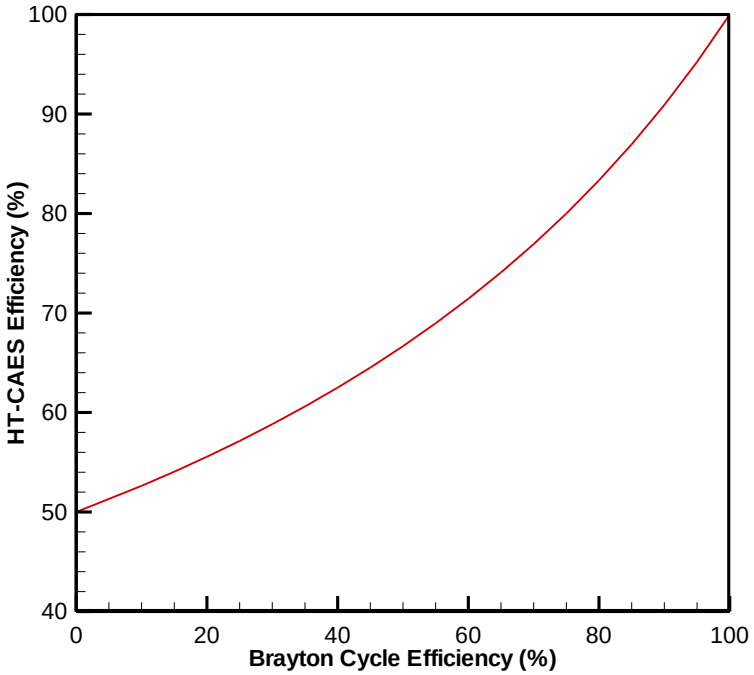

2.4 CAES vs. Brayton Cycle, Without Regeneration

2.4.1 No Heat Losses

A similar analysis is performed in the case of no regeneration. A similarly simplified and ideal configuration of the energy storage cycle with no regeneration given by Figure 5 is analyzed and compared with a Brayton cycle (Figure 5). The configuration assumes isentropic compression and expansion, for simplicity. As explained, the cavern is neglected under the assumption that no storage losses are present; therefore all energy invested in compression is retrieved during discharge. In the storage cycle, the turbine does not provide the compressor power meaning all of the turbine power is available for useful work. The compressor and thermal storage power is provided by either the electrical grid, renewable sources, or whatever power is available for storage. In contrast, the turbine is coupled with the compressor in the Brayton cycle in Figure 6.

Figure 5: Hybrid Thermal and Compressed Air Energy Storage Configuration Without Regeneration

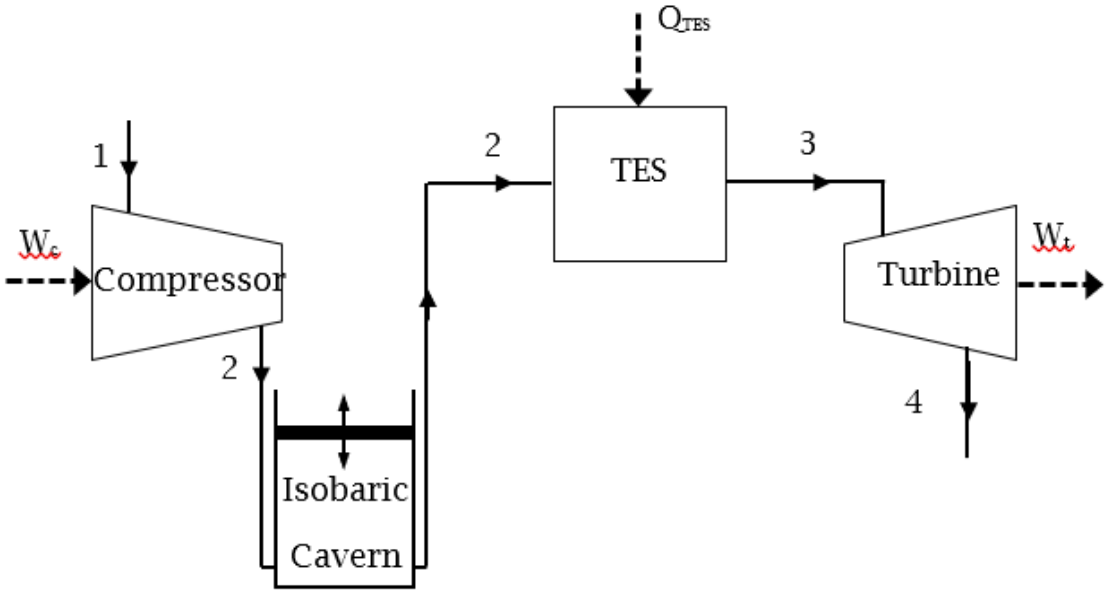

Figure 6: Brayton Cycle Without Regeneration

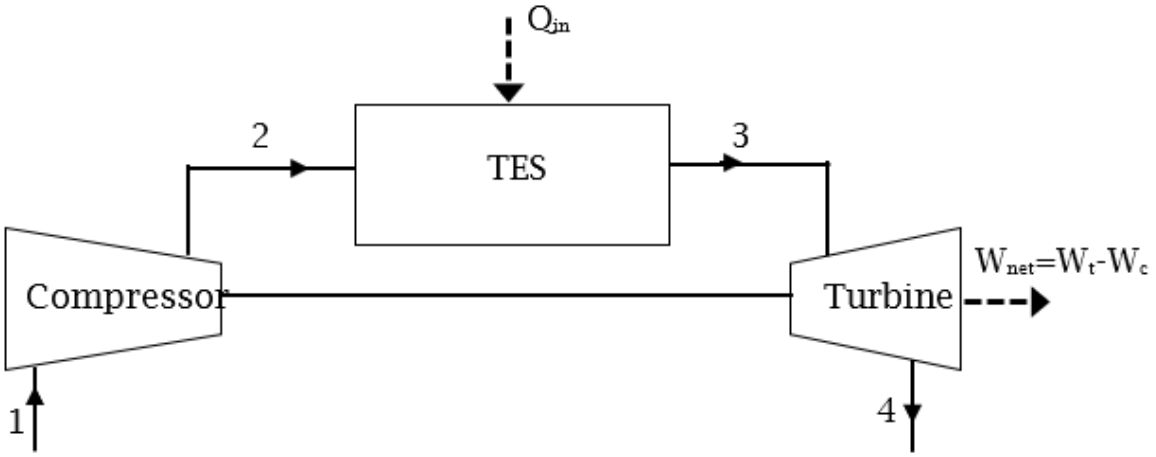

The round-trip efficiency of the simplified and ideal hybrid system given is given as

$$\eta_{HT-CAES} = \frac{\dot{W}_t}{\dot{W}_c + \dot{Q}_{HTES}} \tag{7}$$

which, assuming constant specific heat, can be simplified to get

$$\eta_{HT-CAES} = \frac{1 - T_4/T_3}{1 - T_1/T_3} \tag{8}$$

Keeping in mind that $\frac{T_4}{T_3} = \frac{T_1}{T_2}$ across the turbine and the compressor for isentropic processes, a little scrutiny reveals that the numerator of equation (8) is the Brayton cycle efficiency while the denominator is the Carnot efficiency of the associated Brayton cycle. Equation (8) can therefore be rewritten as:

$$\eta_{HT-CAES} = \frac{1 - T_1/T_2}{1 - (T_1/T_2) \times (T_2/T_3)} = \frac{\eta_{Brayton}}{\eta_{Carnot}} \tag{9}$$

A sketch of the result given by equation (9) is illustrated in Figure 7, which demonstrates that the process is 100% efficient when$T_3 = T_2$, meaning there is no heat addition provided by the thermal storage and the compression and expansion processes are along the same isentropic line. The addition of heat through the thermal storage takes the process off the compression isentrope and introduces the Carnot limit into the cycle. In the extreme of very high temperatures of thermal storage, in other words when the balance between heat and the isentropic work of compression shifts predominantly toward heat, the cycle is dominated by the Brayton cycle as the Carnot efficiency approaches unity. In another extreme where the

energy put into thermal energy storage approaches zero and $T_3 = T_2$, HT-CAES reduces to an advanced adiabatic system with a theoretical round-trip efficiency of unity, as evident from equation (9). In this limit, where advanced adiabatic CAES aims to operate, the expansion isentrope coincides with the compression isentrope. When there is economic and technological justification, this limit is theoretically the most desirable zone of operation for energy storage/retrieval. One can therefore conclude that the efficiency of a non-regenerative HT-CAES cycle is 1) always greater than the efficiency of the corresponding Brayton cycle and 2) is not bound by the Carnot efficiency.

Figure 7: Efficiency Versus Thermal Storage Temperatures of the Simplified Hybrid Compressed Air Energy Storage Cycle

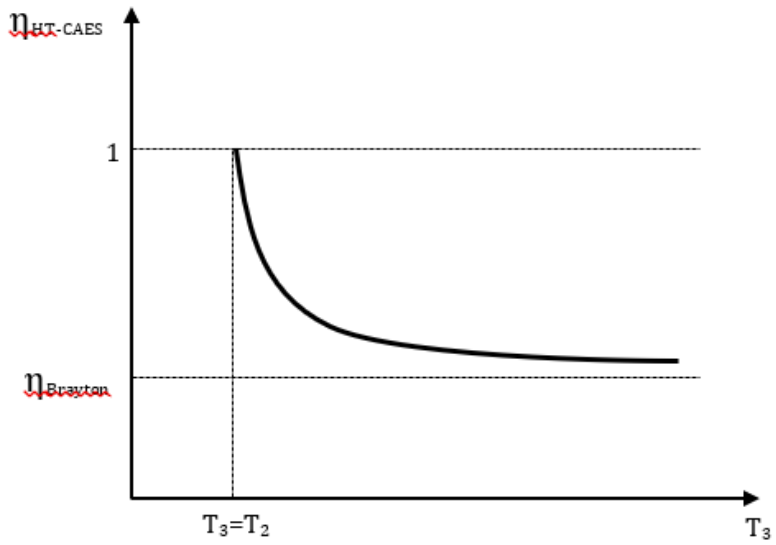

Given by Equation (9), exclusive of regeneration

2.4.2 Accounting for Heat Losses Following Compression

As noted earlier, there is an advanced adiabatic system built into the HT-CAES. In the analyses done so far, it has been assumed that the heat of compression, which is traditionally absorbed in advanced adiabatic CAES, is fully used in the system with 100% round-trip efficiency before heating the air through the TES. This section extends the analysis to take into account the heat losses following compression. The corresponding ideal and simplified model are shown in Figure 8.

Figure 8: Simplified and Ideal Hybrid Thermal and Compressed Air Energy Storage

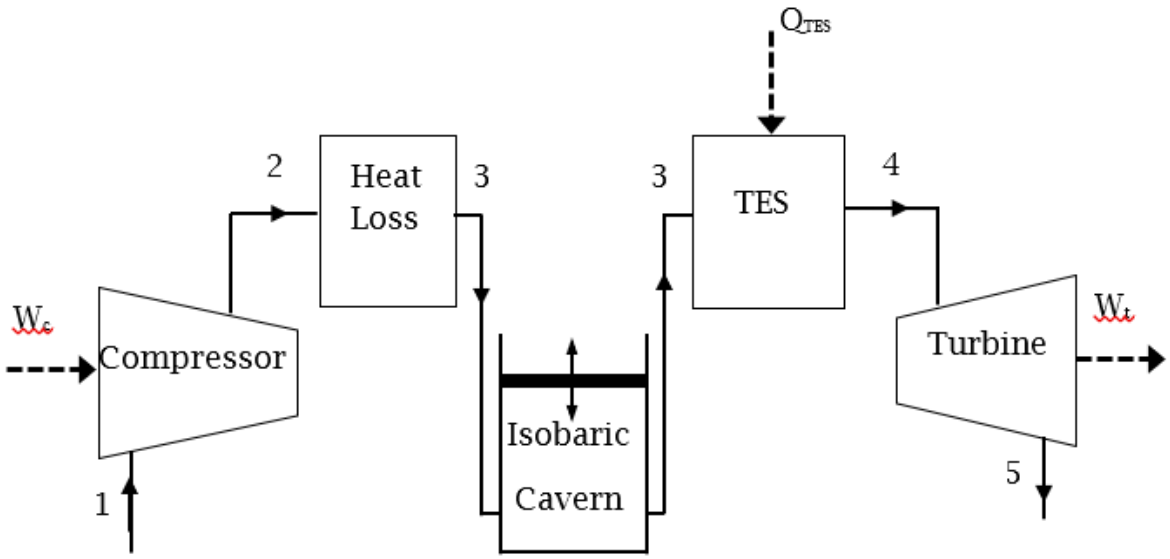

With a heat loss component following compression

The round-trip storage efficiency is calculated similar to (7), that is:

$$\eta_{HT-CAES} = \frac{\dot{W}_t}{\dot{W}_c + \dot{Q}_{HTES}} \tag{10}$$

Assuming constant specific heat, Equation (10) reduces to

$$\eta_{HT-CAES} = \frac{T_4 - T_5}{T_2 - T_1 + T_4 - T_3} \tag{11}$$

Using isentropic relations and incorporating the compression ratio, r, Equation (11) reduces to

$$\eta_{HT-CAES} = \frac{T_4\left(1 - 1/r^{(k-1)/k}\right)}{T_4(1 - T_3/T_4) - T_1(1 - r^{(k-1)/k})} \tag{12}$$

Further simplification of (12) leads to

$$\eta_{HT-CAES} = \frac{1}{\frac{(1 - T_3/T_4)}{(1 - 1/r^{(k-1)/k})} + \frac{T_1}{T_4} r^{(k-1)/k}} \tag{13}$$

Recognizing the Brayton cycle efficiency, Equation (13) can be rewritten as follows

$$\eta_{HT-CAES} = \frac{1}{\frac{(1 - T_3/T_4)}{\eta_{Brayton}} + \frac{T_1}{T_4} r^{(k-1)/k}} \tag{14}$$

An immediate observation in Equation (14) is that as T_4 increases the efficiency of the system approaches the Brayton cycle efficiency, in other words.

$$\lim_{T_4 \to \infty} \eta_{HT-CAES} = \eta_{Brayton} \tag{15}$$

A plot of the round trip efficiency, given by Equation (14), versus the expander inlet temperature (T_4) for various T_3 temperatures is provided in Figure 9. The uppermost curve in this figure represents the case where $T_3 = T_2$, which corresponds to no heat loss following compression. That is consistent with Equation (9) and the related sketch. As T_3 decreases the associated curves in Figure 9 eventually change in curvature, although all leading to the same limiting case of the Brayton cycle efficiency. The result in Figure 9 was obtained for a compression ratio of 15, a heat capacity ratio of 1.4, and an ambient temperature of 300K, which leads to a Brayton cycle efficiency of 53.87%. The decrease in the temperature, T_3, corresponds to an increase in heat loss following compression. As heat losses increase the necessary amount of heat, supplied by the TES, to reach a specified turbine inlet temperature increases. A significant increase in the necessary heat, provided by the thermal storage, overwhelmingly influences the efficiency of the system, as demonstrated by Equation (10), and eventually leads to the change in efficiency curvature.

Figure 9: A Plot of the Roundtrip Efficiency

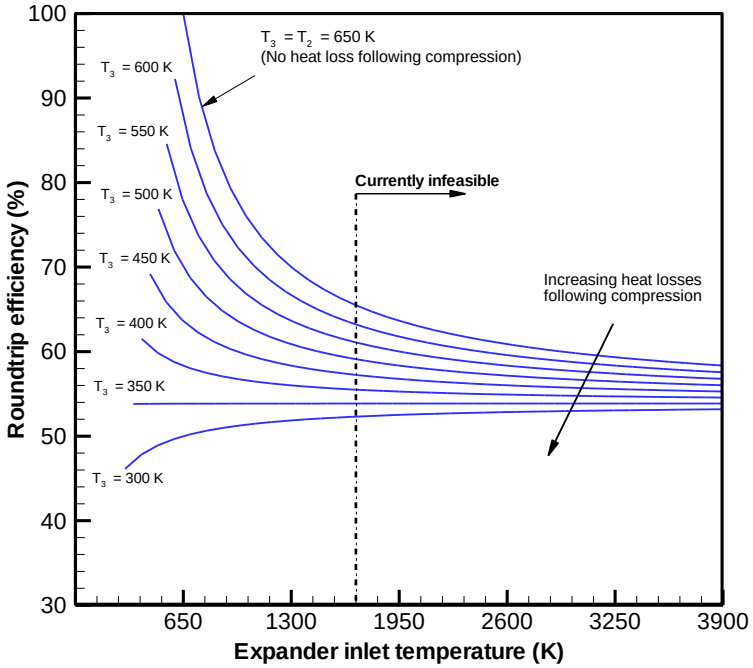

Corresponding to the Hybrid CAES cycle of Fig. 6, exclusive of regeneration) versus the turbine inlet temperature

2.5 Cyclic Cavern Analysis

This section illustrates a brief thermodynamic analysis of an isobaric and isochoric cavern. In both cases the cavern is also assumed to be adiabatic. The results below demonstrate that under the isobaric cavern assumption the thermodynamic state of the cavern, inlet, and outlet conditions remain equal and constant. The thermodynamic state of air is assumed fixed by the air pressure and temperature properties. An isochoric cavern, on the contrary, changes the state of the air through the cavern.

2.5.1 Governing Equations:

The general mass, energy and entropy balance equations together with the calorically perfect gas equations of state are given below:

$$\frac{dM}{dt} = \dot{m}_{in} - \dot{m}_{out} \qquad (A-1)$$

$$\frac{dE}{dt} = -P\frac{dV}{dt} + \dot{m}_{in}h_{in} - \dot{m}_{out}h_{out} + \dot{Q} \qquad (A-2)$$

$$\frac{dH}{dt} = V\frac{dP}{dt} + \dot{m}_{in}h_{in} - \dot{m}_{out}h_{out} + \dot{Q} \qquad (A-3)$$

$$\frac{dS}{dt} = \dot{m}_{in}s_{in} - \dot{m}_{out}s_{out} \qquad (A-4)$$

$$PV = MRT \qquad (A-5)$$

Where

$$E = Me \quad (A-6)$$

$$S = Ms \quad (A-7)$$

$$H = Mh \quad (A-8)$$

$$e = C_v T \quad (A-9)$$

$$h = C_p T \quad (A-10)$$

And e, s and h, are the specific energy, entropy, enthalpy and M is the mass of air in the cavern at any instant of time.

2.5.2 Isobaric Cavern: (P = constant)

Charge Process: *($\dot{m}_{out} = 0$)*

To analyze the conditions of the isobaric and adiabatic cavern during the charge process, Equation (A-3) is expanded while using Equation (A-1), resulting in the following equation:

$$M\frac{dT}{dt} = \dot{m}_{in}(T_o - T) \quad (A-11)$$

with the initial condition of

$$T(t=0) = T_o \quad (A-12)$$

where T_o is the temperature of the inlet air stream. Solving Equation (A-11) coupled with (A-12) results in

$$T(t) = T_o \quad (A-13)$$

meaning the isobaric cavern temperature at any instant during the charge process is equal to the constant inlet air temperature. With the cavern pressure assumed constant in this situation, the state of the cavern, which is determined by the air temperature and pressure, remains constant during the charge process.

Discharge Process: *($\dot{m}_{in} = 0$)*

Similarly, expanding Equation (A-3) and using Equation (A-1) results in the following equation

$$M\frac{dT}{dt} - \dot{m}_{out}T = -\dot{m}_{out}T \quad (A-14)$$

with the initial condition of

$$T(t=0) = T_o \quad (A-15)$$

It is immediately clear that (A-14) and (A-15) result in the following solution

$$T(t) = T_o \quad (A-16)$$

The results (A-13) and (A-16) together with the isobaric constraint, P=constant, indicate that the transients of an isobaric cavern are irrelevant. Specifically, the inlet and exit temperatures are the same. Therefore, the inlet state of the cavern air, defined by the inlet air pressure and temperature, is equal to the outlet state of the cavern air and the cavern becomes redundant in the analysis.

2.5.3 Isochoric Cavern: (V=constant)

Coupled integration of the mass and energy balance, equations (A-1) and (A-2), under calorically perfect gas equations of state and adiabatic boundary conditions enable temperature and pressure to be determined during charge and discharge and the cycle-to-cycle variations (Figure 10). Constants provided in Table 2 have been used.

Figure 10: Temperature and Pressure of an Adiabatic Cavern Cyclic Process

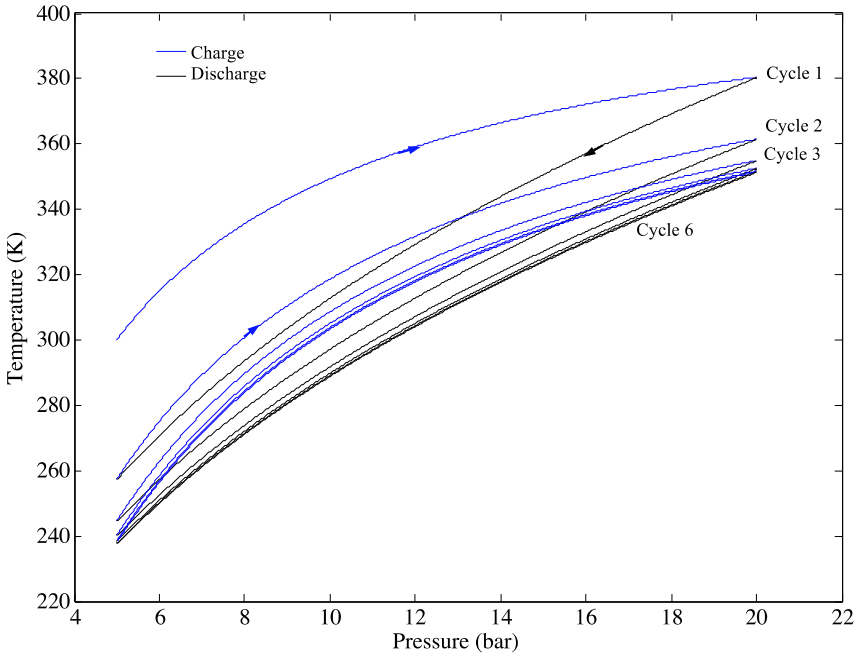

The first six cycles of the charge and discharge process are shown

Table 2: Assumed Constants for the Cyclic Isochoric and Adiabatic Cavern Example

Constant	Value
Cavern Volume, V_{cavern}	300,000 m^3
Specific Heat of Air at Constant Pressure, C_p	1 kJ/kg.K
Specific Heat of Air at Constant Volume, C_v	0.718 kJ/kg.K
Air Gas Constant, R	0.287 kJ/kg.K
Minimum Pressure, P_{min}	5 bar
Maximum Pressure, P_{max}	20 bar
Initial Cavern Temperature, T_o	300 K

Inlet Cavern Temperature, T_{in}	300 K
Mass Flow Rate, $\dot{m}$	200 kg/s

As the pressure varies between the specified maximum and minimum during the charge and discharge the temperature of the cavern reaches an equilibrium profile after about six cycles. However, the temperature and pressure remain transient and the conditions of the air through the cavern change drastically. Consequently, the state of the air into and out of the cavern is different. As a result, for a proper modeling of the plant performance the cavern internal transients must be taken into account.

2.6 Conclusion

An ideal thermodynamic model was developed for a hybrid thermal and compressed air energy storage system. The analysis considered perfect performance indices for the components (isentropic efficiency and effectiveness) and explored the integral built-in boundaries of operation of the storage cycle with respect to the corresponding Brayton and Carnot cycles. The models included cycles with and without regeneration. The following conclusions can be drawn:

1. Consistent with the advanced adiabatic compressed air energy storage concept, in the limit of no heat addition to the system the ideal cycle has 100% theoretical roundtrip efficiency. In this limit the compression and expansion occur along the same isentrope.
2. The addition of heat through thermal storage takes the expansion process off the compression isentrope and results in a nonunity round-trip efficiency even in the case of perfect components.
3. The efficiency of the storage cycle approaches that of a classical Brayton cycle as the temperature of the thermal storage increases.
4. The energy storage cycle, namely compressed air energy storage, is not bound by the Carnot efficiency, as the Carnot efficiency is limited to heat engines, not energy storage cycles.

2.7 Thermodynamic Analysis of a Simple Hybrid Thermal-Compressed Air Energy Storage System

In this section, simple high-temperature hybrid compressed air energy storage (HTH-CAES) system configuration is presented which eliminates the necessary combustion emissions in conventional CAES and addresses some of the issues in the otherwise attractive AA-CAES. The HTH-CAES allows a portion of the available energy, from the grid or renewable sources, to operate a compressor and the remainder to be converted and stored in the form of heat, through joule heating in a sensible storage medium. As a result, HTH-CAES operates on smaller volumes and lower pressures, which reduces the cost and solve some of the technical issues during expansion. This simple HTH-CAES design incorporates two stages of heating through separate low-temperature and high-temperature thermal energy storage units, which provide simplicity and practicality for future implementation. The thermodynamic analysis incorporates realistic isentropic component efficiencies and throttling losses responsible for maintaining constant pressure conditions following the cavern. While a positive-displacement machine with proper valve-timing control can adjust to the time-varying pressure in the cavern and maintain optimal performance, a variable expander assumption overestimates the power output with turbo-expanders.

The optimal performance of a turbo-expander, characterized by the isentropic efficiency, is limited to a very narrow range of inlet operating conditions of pressure, temperature and mass flow rate. Slight deviations from the design conditions result in a sharp decrease in isentropic efficiency of the machine. As a result, pressure has to be regulated to the design conditions, either via the Joule-Thomson throttling process or using an expander that is capable of taking the time-varying pressure in the cavern and delivering steady-state back pressure. This paper employs the Joule-Thomson throttling. Previous works consider only an isothermal cavern; however, the team investigated adiabatic and isothermal conditions as they represent both extremes. Most importantly, the existence of an optimum operating pressure, leading to maximum roundtrip storage efficiency, is presented and to the author's knowledge has not been formerly reported. Parametric studies, which illustrate the importance of the operating pressure and thermal storage temperature on the performance of HTH-CAES and AA-CAES systems, are presented. Moreover, the cyclic behavior and the existence of an asymptotic isentropic condition in an adiabatic cavern are reported. Lastly, the performance of an HTH-CAES system is compared with an AA-CAES system of the same power output.

2.8 Methods

While cost-effective, traditional CAES systems suffer from heat losses during compression along with carbon emissions from the combustion of fossil fuels. With AA-CAES systems, the heat of compression is stored in a thermal energy storage (TES) unit and returned to the compressed air during discharge. The higher overall efficiency of AA-CAES systems has made it an attractive alternative to traditional CAES. However, AA-CAES requires high storage and operating pressures for adequate energy densities and roundtrip efficiencies. Of the only two compressed air energy storage plants in operation (Huntorf, Germany and McIntosh, United States) neither employs AA-CAES.

The resolution between CAES and AA-CAES is the high-temperature hybrid thermal CAES (HTH-CAES). In an HTH-CAES system the TES is replaced with a low and high-temperature energy storage unit (Figure 11). As with TES in AA-CAES, the low temperature thermal energy storage (LTES) unit stores the heat of compression. But unlike TES in AA-CAES, the high temperature thermal energy storage (HTES) unit in HTH-CAES acts as a scalable energy reservoir without the complexity and limitations of a thermal transport fluid. The HTES unit takes advantage of the high thermal capacity of an inexpensive thermal medium to store heat that will later be used to heat the compressed air out of the air storage. HTH-CAES allows for direct conversion of electricity into heat through Joule heating. As a result, temperatures and volumetric energy densities well in excess of traditional CAES and AA-CAES can be achieved, while the size of the air storage can be reduced. The electricity could be supplied either from the grid or renewable source, such as wind and solar photovoltaics (PV).

Figure 11: Schematic of a High-Temperature Hybrid Compressed Air Energy Storage

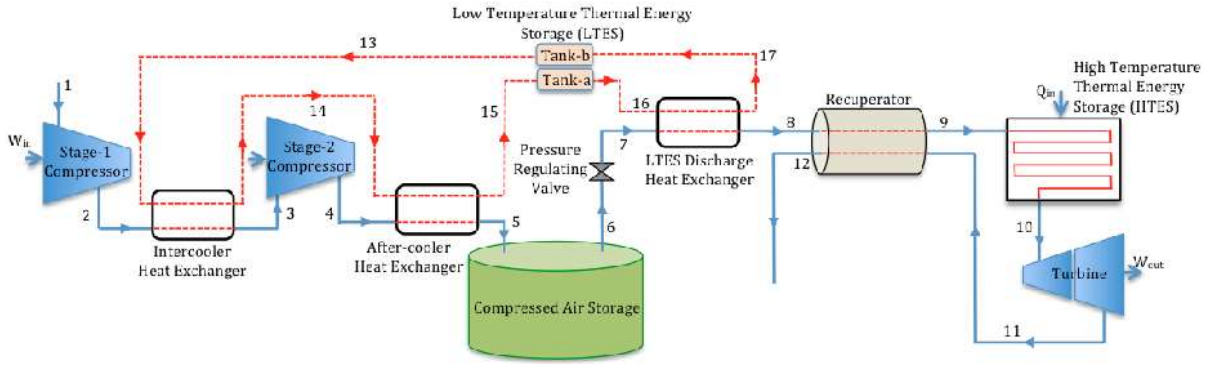

The resolution between CAES and AA-CAES is the high temperature hybrid thermal CAES (HTH-CAES). In an HTH-CAES system the TES is replaced with a low and high temperature energy storage unit. As with TES in AA-CAES, the low temperature thermal energy storage (LTES) unit stores the heat of compression. But unlike TES in AA-CAES, the high temperature thermal energy storage (HTES) unit in HTH-CAES acts as a scalable energy reservoir without the complexity and limitations of a thermal transport fluid. The HTES unit takes advantage of the high thermal capacity of an inexpensive thermal medium to store heat that will later be used to heat the compressed air out of the air storage. HTH-CAES allows for direct conversion of electricity into heat through Joule heating. As a result, temperatures and volumetric energy densities well in excess of traditional CAES and AA-CAES can be achieved, while the size of the air storage can be reduced. The electricity could be supplied either from the grid or renewable source, such as wind and PV.

With the addition of a HTES unit, the workload is shifted from pure compression to investing partially in thermal storage. This separation of energy storage between compressed air and thermal storage expands the energy capacity of the compressed air system without increasing the air pressure or cavern capacity. HTES allows the system to be dynamically scaled up or down as the load leveling demand changes without any structural change in system configuration. Figure 12 is a sketch of the T-s diagram for both AA-CAES and HTH-CAES, corresponding to the cycle in Figure 1, assuming isentropic components, an isothermal air reservoir and 100% heat exchanger and recuperator effectiveness. The process is summarized in Table 3. HTES is by nature a transient component as it depletes during the discharge process. However, it can be sized and designed to always heat up the discharging air to a constant temperature, thereby providing the expander with a steady flow. Under these conditions HTES is considered a steady component.

Table 3: Process Description Corresponding to the T-s Diagram

Process	Description
1-2	1st stage isentropic compression for both HTH-CAES and AA-CAES
2-3	Intercooling, at constant pressure, for both HTH-CAES and AA-CAES
3-4	2nd stage isentropic compression for both HTH-CAES and AA-CAES
4-5	After-cooling for both HTH-CAES and AA-CAES

6	This line represents the conditions of the isothermal cavern as it is depleted and throttled during the discharge process from pressures P_{max} to the operating pressure, P', given by points 5 and 7 respectively.
7-8	Preheating the discharging air by the LTES from the generated heat of compression. Point 8 represents the maximum temperature achievable through AA-CAES
8-8'	Isentropic expansion in AA-CAES (in Figure 1, this would correspond to 8-11)
8-9	Recuperator heat addition in HTH-CAES
9-10	Heat provided by the HTES in HTH-CAES
10-11	Isentropic expansion in HTH-CAES

As evident in Figure, 12 the addition of an HTES dramatically increases the output power and the energy density of the storage system for a given size and pressure swing in the cavern, as the AA-CAES system is limited by the amount of energy stored purely during compression.

Figure 12: T-s Diagram of AA-CAES and HTH-CAES

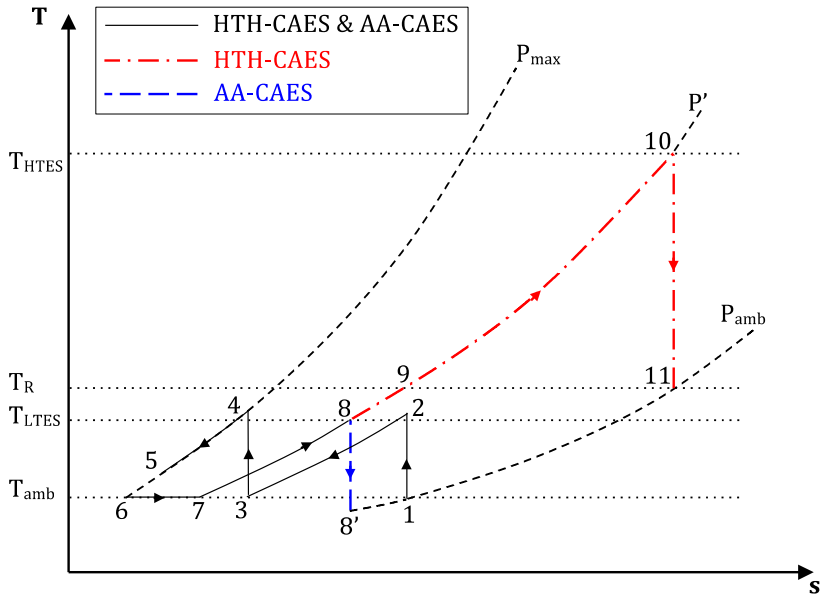

Assuming isentropic components, an isothermal cavern and 100% heat exchanger effectiveness

Table 4 represents a snapshot of one operational possibility for an isothermal cavern.

Table 4: Example of the Possible Operational Values Corresponding to the T-s Diagrams of Figure 11 and Figure 12

Variable	Value	Variable	Value
T_1	300K	T_8	357K
T_2	460.25K	T_9	820.8K
T_3	300K	T_{10}	1300K
T_4	460.25K	$T_{8'}$	225.83K

T_5	332.05K	T_{11}	820.8K
T_6, T_7	300K	P'	5bar
P_{amb}	1bar	P_{max}	20bar
P_i	4.47bar	C_r	5

Where P_i is the intercooling pressure, corresponding to minimum compression work, and $C_r=C_{LTES}/C_{air}$ is the heat capacity rate ratio, defined as the LTES heat transfer fluid (HTF) specific heat times the flow rate, over the specific heat of air, at constant pressure, times the flow rate. Data in Table 4 were also used.

Figure 13 depicts an HTH-CAES T-s diagram under an adiabatic cavern, which is essentially the same as Figure 2 except for the treatment of the cavern. As a result all values given in Table 4 are applicable with the exception of temperatures T_7 and T_6, which are now time-dependent. Lines 6' and 6 represent the instantaneous conditions in the cavern as it is charged and discharged respectively. Also, the isothermal line 7 represents the Joule-Thompson throttling, which brings the instantaneous condition of the discharging cavern air (a point along line 6) to the operating/prime pressure, P' where the prime pressure, P', is defined as the minimum cavern pressure and the discharge process pressure, which is adjusted by the pressure regulating valve. The cyclic conditions of an adiabatic cavern during the charge and discharge process, along with the respective operational values, were evaluated. The charge and discharge processes in the cavern (lines 6' and 6 respectively) tend to converge to an isentropic one after several charge and discharge cycles. All calculations presented for an adiabatic cavern in this paper represent the first charge and discharge cycle.

Figure 13: T-s Diagram of AA-CAES and HTH-CAES

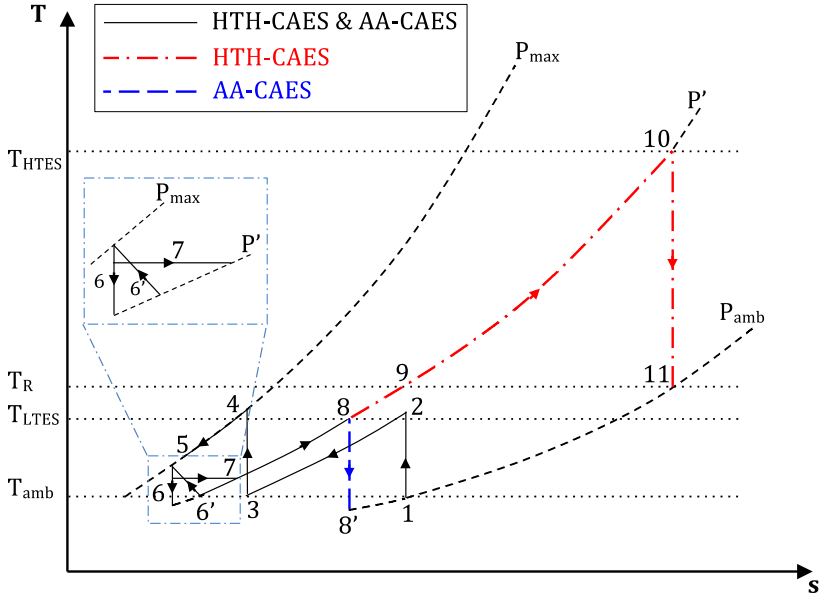

Assuming isentropic components, an adiabatic cavern, and 100% heat exchanger effectiveness

2.9 Calculations

Figure 13 represents the analyzed HTH-CAES thermodynamic cycle. During the charge process electricity from renewable sources, or the gird, is used to operate the compressor. Simultaneously or subsequently, depending on available power during the charge, electricity is converted directly into thermal energy and is stored in the HTES. Converting electricity to thermal energy can result in very high temperatures and thus high energy densities when the energy is well contained. The practical limit on how high a temperature can be reached in HTES is defined by the material properties of the storage and the electric wires. Alumina-based refractory provides service temperatures in excess of 1700C and Nichrome wires can have a continuously operating temperature of ~ 1680C. Considering that the heat of compression is absorbed during charge and is used during discharge, there is conceptually an AA-CAES built into the HTH-CAES cycle in Figure 1. The heat of compression is stored in a low-temperature thermal energy storage (LTES), which is essentially a two-tank system. Initially, tank "b" is filled with a cold heat transfer fluid (HTF) in the charge process and tank "a" is empty. As the air being compressed, tank "b" is discharged and the HTF collects the heat of compression via the LTES charge heat exchanger. The hot HTF is then stored in tank "a" for later use during the discharge process. During the discharge process, air is released from the cavern and subsequently throttled through the pressure-regulating valve to a constant pressure, herein referred to as the prime pressure, *P'*. The temperature of the discharging air is then raised through three successive stages of heating before entering the expander: LTES, recuperator, and HTES. Pressure losses within the pipes were not taken into account and all components besides the cavern are assumed to be quasi-steady. In addition, Table 5 summarizes the additional constants used in all studies presented.

Table 5: Assumed Constants

Constant	Value
Charge Time, t_{charge}	6 hours
Cavern Volume, V_{cavern}	300,000 m^3
Compressor Isentropic Efficiency, η_c	75%
Turbine Isentropic Efficiency, η_t	80%
Heat Exchanger & Recuperator Effectiveness	80%
Heat Capacity Rate Ratio of the LTES Heat Carrier Fluid to Air, $C_r=C_{LTES}/C_{air}$	5
Specific Heat of Air at Constant Pressure, C_p	1 kJ/kg.K
Specific Heat of Air at Constant Volume, C_v	0.718 kJ/kg.K
Air Gas Constant, R	0.287 kJ/kg.K
Output Power, $\dot{W}_{Output}$	100MW

A detailed outline of the calculations made for each component in the charge cycle is presented in this section. This includes all significant equations and any component specific assumptions.

2.9.1 Thermodynamic Equations

All components (compressors, heat exchangers and turbines) except for the cavern and HTES are assumed to operate quasi-steadily during charge and discharge. The team assumes the residence time within these components is much shorter than charge and discharge time scales, indicated in Table 3. Furthermore, heat capacities are assumed to be temperature independent. The charging time is fixed therefore, the cavern is charged to a peak pressure, corresponding to a specified flow rate, and is discharged until the cavern prime pressure, P', is reached.

2.9.1.1 Compressor

The required first-stage isentropic compression power is determined from the first law of thermodynamics as follows

$$\dot{W}_C = \dot{m}\,\frac{c_p T_1}{\eta_c}\left(\left(\frac{P_i}{P_1}\right)^{\frac{k-1}{k}} - 1\right) \tag{1}$$

Here T_1 and P_1 are the inlet temperature and pressure of the compressor at ambient conditions, respectively. The intercooling pressure, P_i, is given by $P_i = \sqrt{P_1 P_{max}}$, a well-known result corresponding to minimum compression power, and P_{max} is the maximum cavern pressure at the end of the charge process. The second stage compression power is calculated similarly, for a pressure swing from P_i to P_{max}. The inlet temperature of the second-stage compressor is determined by a heat exchanger energy balance that takes into account the effectiveness and the LTES heat capacity rate ratio given by Table 5.

2.9.1.2 Adiabatic Cavern

The application of the mass and energy balance under temperature-independent specific heats and adiabatic boundary conditions results in the following transient thermodynamics for the cavern:

Charge:

$$M(t) = \dot{m}t + M' \tag{2}$$

$$T(t) = \frac{M'}{M(t)}T' + \frac{\dot{m}kT_5 t}{M(t)} \tag{3}$$

$$P(t) = P' + \frac{\dot{m}kRT_5 t}{V_{cavern}} \tag{4}$$

Discharge:

$$M(t) = M_{max} - \dot{m}t \tag{5}$$

$$T(t) = T_{max}\left(1 - \frac{\dot{m}t}{M_{max}}\right)^{(k+1)} \tag{6}$$

$$P(t)V_{cavern} = M(t)RT(t) \tag{7}$$

where P' is the cavern prime pressure and T_5 is the temperature of air into the cavern, as shown in Figure 1. Also, M' is the mass of air in the cavern at the start of the charging and T' is the temperature. T_{max} and M_{max} are obtained by substituting t_{charge} in Equations (2) and (3). When the adiabatic assumption is made, $T' = T_5$ has been assumed, although it is shown that there is

a slight cycle-to-cycle variation within the first few cycles until an equilibrium is reached in the cavern. For general, though weak, temperature-dependent heat capacities, the numerical integration of mass and energy balance coupled with the equation of state will have to be resorted to determine the internal thermodynamics of the cavern.

2.9.1.3 Isothermal Cavern

Similarly, the following equations can be obtained for an isothermal cavern during charge and discharge:

Charge:

$$M(t) = \dot{m}t + M' \tag{8}$$

$$T(t) = \text{cte} \tag{9}$$

$$P(t) = P' + \frac{RT_5\dot{m}t}{V_{cavern}} \tag{10}$$

Discharge:

$$M(t) = M_{max} - \dot{m}t \tag{11}$$

$$T(t) = \text{cte} \tag{12}$$

$$P(t)V_{cavern} = M(t)RT(t) \tag{13}$$

2.9.1.4 LTES and Recuperator

The LTES working fluid storage tanks are assumed to be adiabatic. The final LTES temperature during the charge is calculated through a heat exchanger analysis using the effectiveness and the heat capacity rate ratio given by Table 3. Similarly the recuperation analysis is performed assuming the effectiveness given in Table 3.

2.9.1.5 Joule-Thomson Throttling

The air pressure is reduced to the process pressure via the Joule-Thomson throttling. It is essentially an iso-enthalpic process when the valve is fully insulated. The Joule-Thomson coefficient, $\mu_{JT} = \frac{\partial T}{\partial P}\Big]_h$, drops continuously for a given pressure as the temperature increases for air. It takes the value of $\mu_{JT} = 0.2143\ C.\text{bar}^{-1}$ at $0.0C$, 60 bar and $0.0161\ C.\text{bar}^{-1}$ at $280C$, 60 bar [21]. The former translates into a $\Delta T = 12.85C$ across the valve while the latter results in $\Delta T = 0.966C$. Considering the narrow range of variations of the Joule-Thomson coefficient, therefore, the real gas effects have been neglected and the throttling process has further assumed to be isothermal. Consequently $T_6 = T_7$ in Figure 13.

2.9.1.6 HTES and Turboexpander

As mentioned earlier, the HTES is inherently a transient component. However, it can be designed to deliver a constant temperature necessary for optimal operation of the turbo-expander. Since the plant is assumed to deliver a constant power output, $\dot{W}_{Output}$, the necessary HTES exit air temperature, T_{10}, can be determined through an energy balance of the turbo-expander as follows:

$$T_{10} = \frac{\dot{W}_{Output}}{\eta_t \dot{m}\, C_p \left[1 - \left(\frac{P_{12}}{P'}\right)^{\frac{k-1}{k}}\right]} \tag{14}$$

$P_{12} = P_1$ in Equation (14). The necessary heat addition by the HTES to air is therefore given by

$$\dot{Q}_{HTES} = \dot{m}\, c_p (T_{10} - T_9) \tag{15}$$

One way of designing the HTES for a constant exhaust temperature is through bypassing the cold air and mixing it with the hot air out of HTES, as shown in Figure 14. Part of the incoming air is bypassed around the HTES while the rest goes through it. It is assumed that the HTES length is designed for 100% effectiveness. Nonetheless, since the maximum temperature of HTES drops, so does the exhaust air temperature out of it, hence $T_{hot}(t)$. Applying the energy balance to the point where the bypass line mixes with the hot flow out of the HTES, the bypass mass flow rate,$\dot{m}_{bp}$(t), can be obtained as a function of $T_{hot}(t)$ and T_{10}:

$$\dot{m}_{bp}(t) = \dot{m} \left(\frac{T_{hot}(t) - T_{10}}{T_{hot}(t) - T_9}\right) \tag{16}$$

Therefore, fixing T_{10} in Equation (16) reduces the control problem to determining $T_{hot}(t)$.

Figure 14: Control Strategy to Keep the Temperature of the Air Out of the HTES Constant

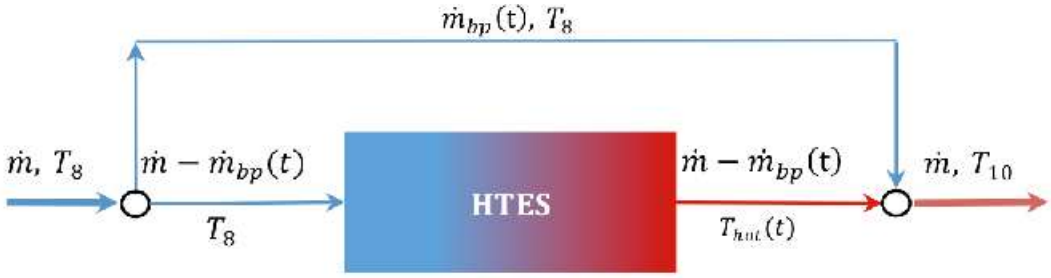

Finally, the round-trip efficiency of the system is calculated on an energy basis as follows

$$\eta_{Round\ trip} = \frac{\int_o^{t_{discharge}} \dot{W}_{Output}\, dt}{\int_0^{t_{discharge}} \dot{Q}_{HTES} dt + \int_0^{t_{charge}} \dot{W}_c dt} \tag{17}$$

2.10 Results

The effects of the prime pressure, P', defined as the minimum cavern pressure and the discharge operating pressure, are investigated in the HTH-CAES. The studies are done for an isothermal and an adiabatic cavern. The isothermal and adiabatic cavern assumptions represent the two possible extreme cavern conditions. An isothermal cavern is realized when the heat transfer between the cavern and surroundings occurs much more rapidly than the heating or cooling due to charging and discharging. Conversely, an adiabatic cavern assumption depicts

the case of small thermal equilibration time scales within the cavern, over which the heat flow across the cavern boundary is negligible. In reality, the cavern thermodynamic conditions lie somewhere between the two extremes. Finally, similar parametric studies are presented for an AA-CAES system, with the same output power of 100MW, and the results are compared with the HTH-CAES system.

2.10.1 HTH-CAES Results

For a fixed power output of 100MW, and for the constant parameters given in Table 3, the prime pressure is varied and the corresponding roundtrip efficiency of the hybrid energy storage system is calculated for various flow rates, under the assumption of an isothermal and adiabatic cavern. As shown in Figure 5, for a specified mass flow rate out of the cavern there is an optimum prime pressure for which the efficiency is a maximum.

Figure 15: Roundtrip Efficiency as a Function of the Prime Pressure for an Isothermal Cavern

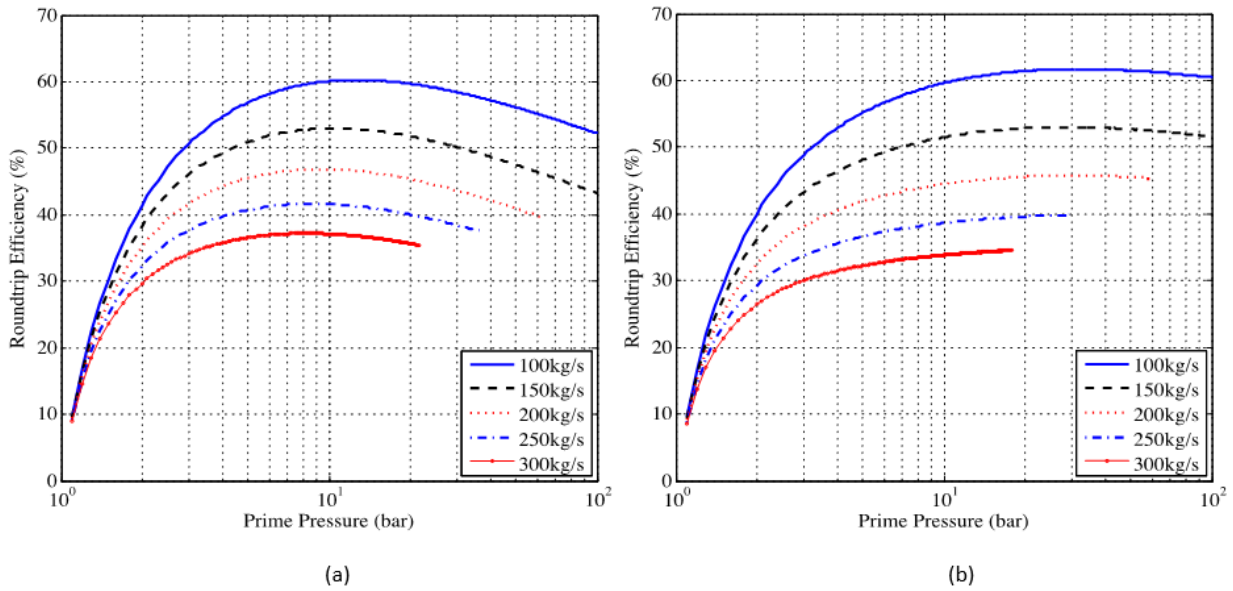

(a), adiabatic cavern (b), and a 100MW power output

Compared with the isothermal cavern, Figure 5(a), the maximum efficiency in an adiabatic cavern, Figure 5(b), occurs at a higher prime pressure for a similar mass flow rate in both cases. Nevertheless, the maximum round-trip efficiencies for adiabatic and isothermal caverns are not significantly different. For an isothermal case, the optimum prime pressure is near 10 bar, whereas for an adiabatic case it is near 20 bar. Also, the flatness of the efficiency curves around the optimum prime pressure covers a considerably wider range in an adiabatic cavern compared to an isothermal cavern.

Although distinct, nominal peak efficiencies in an isothermal cavern, given by (a), occur within a narrow prime pressure range of about 8 to 15 bar. An interesting observation is that the efficiency curves are flat around the optimum prime pressure, particularly at higher mass flow rates, which could be significant when the cost of the plant is to be optimized. The curves terminate when the temperature of air into the recuperator exceeds the turbine exhaust temperature. In this case recuperation becomes ineffective.

With a constant output power enforced throughout this paper, the efficiency of the system, given by Equation (17), is only a function of the HTES and compressor power requirements. Therefore, the point of maximum efficiency occurs when the sum of both HTES and compressor power reach a minimum. The optimum prime pressure leading to maximum efficiency, in Figure 15, is caused by the competing power requirements of the compressor and HTES. The reason behind the optimum point of operation in Figure 15 is best described by Figure 16, which is a plot of the HTES and compressor power requirement, given by equations (1) and (15), along with the sum. As the prime pressure increases, the HTES heat requirement drops, however, the compression power requirement increases, and the sum reaches a minimum at precisely the optimum efficiencies in Figure 15. Figure 16 illustrates this point for a 100MW isothermal-cavern HTH-CAES, in which the mass flow rate is 150kg/s and through the specified constants in Table 5.

Figure 16: Input Power of the HTH-CAES Compressor and HTES

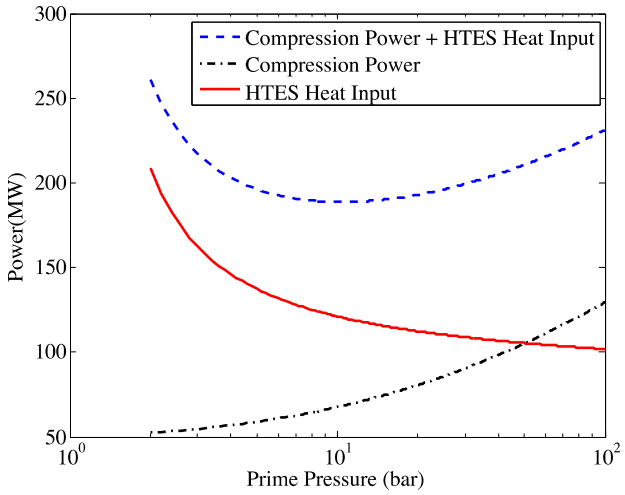

Includes the sum as a function of the prime pressure, illustrating the reason leading to an optimum efficiency in Figure 15.

Fixing the prime pressure and the mass flow rate fixes the turbine inlet temperature, that is, the HTES exit temperature, for the specified power output. Figure 17 contains such data corresponding to Figure 15 for an isothermal and an adiabatic cavern. The necessary HTES exit temperature decreases with increasing mass flow rate and increasing operating pressure. The region above the dotted horizontal line in Figure 7 entails currently infeasible turbine inlet temperatures dictated by the metallurgical limits associated with turbine blade materials [22]. The HTES exit temperatures in an adiabatic cavern, given by Figure 7(b), are identical to those corresponding to the isothermal case, Figure 7(a), with the exception that the temperatures are terminated at lower prime pressures for the adiabatic case when recuperation becomes ineffective.

Figure 17: HTES Exit Temperature vs the Prime Pressure for an Isothermal Cavern

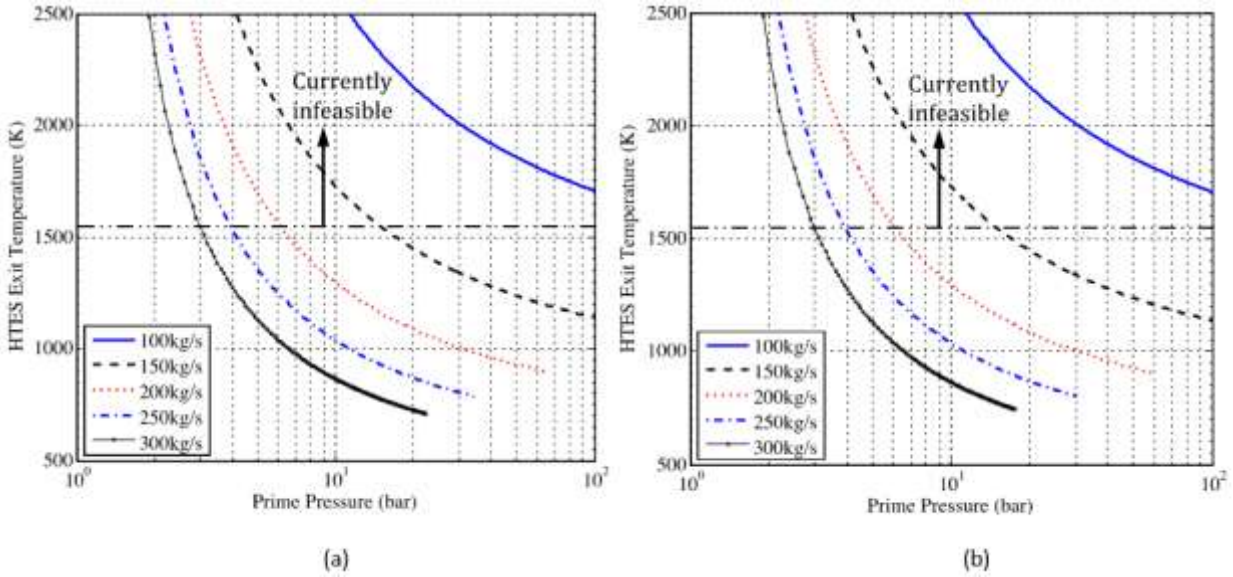

(a), an adiabatic cavern (b), and a 100MW output power.

The corresponding maximum cavern pressure as a function of the prime pressure is shown in Figure 18. The maximum pressure increases with prime pressure and flow rate.

Figure 18: Maximum Cavern Pressure as a Function of the Prime Pressure for an Isothermal Cavern

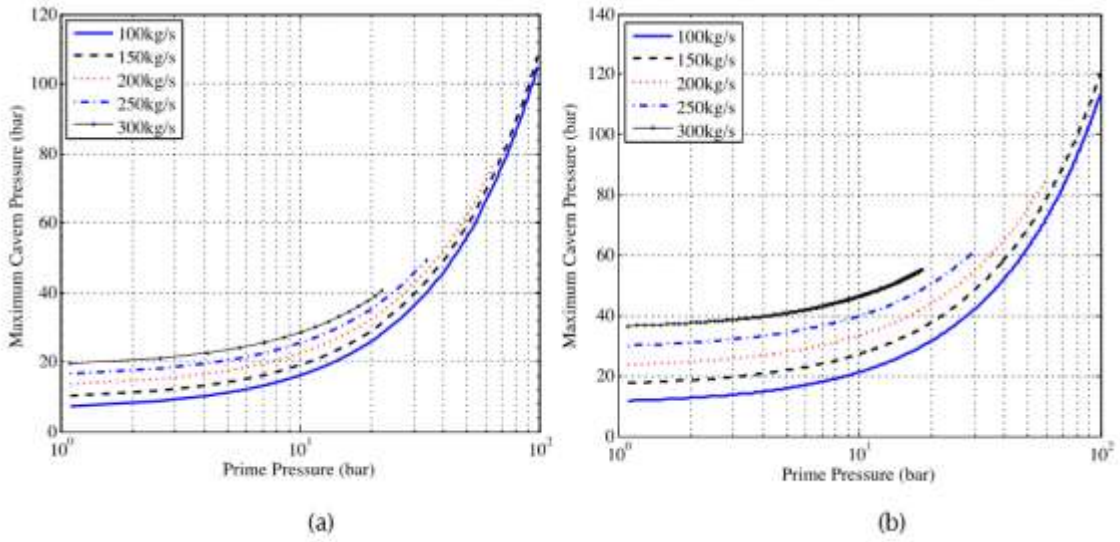

(a), and an adiabatic cavern (b)

As compared with an isothermal cavern, given by Figure 18(a), an adiabatic cavern, Figure 18(b), leads to a higher maximum pressure for the same amount of stored mass.

2.10.2 Advanced-Adiabatic CAES Results

A similar formulation was used for the calculations of an advanced-adiabatic design, however without an HTES and a recuperation component. In other words, the air out of the LTES

discharge heat exchanger goes directly into the power turbine that is where points 8 and 10 in Figure 19 coincide. In this analysis, the output power is also fixed at 100MW, and the same constants provided by Table 5 are used. The output power is a function of the LTES temperature, the prime pressure, and the mass flow rate as illustrated by Equation (14). However, without an HTES the turbine inlet temperature cannot be as easily adjusted. The LTES temperature is a function of the maximum cavern pressure, which is a function of the flow rate and the prime pressure as shown by Equations (4) and (10). Therefore, the output power is ultimately only a function of the flow rate and the prime pressure.

Figure 19: Flow Rates vs the Prime Pressure for an AA-CAES System of 100MW Power Output

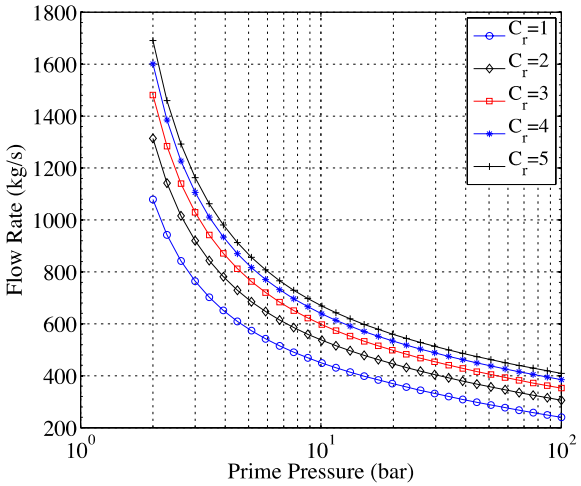

With the assumption of an isothermal cavern for various heat capacity rate ratios

The heat capacity rate ratio, C_r, is defined as $C_r = \frac{\dot{m}_{LTES}\, c_{LTES}}{\dot{m}_{air} c_{p,air}}$, where $\dot{m}_{LTES}$ is the LTES heat transfer fluid mass flow rate and c_{LTES} is the specific heat, $\dot{m}_{air}$ is the air mass flow rate and $c_{p,air}$ is the associated specific heat at constant pressure, as defined in Table 3.

As the prime pressure increases, the required flow rate to achieve a constant output power of 100MW decreases. Curves of different LTES heat capacity rate ratios are shown. For higher LTES temperatures, achieved through lower heat rate capacity ratios, lower flow rates are required to achieve the constant output power. The maximum cavern pressure, given by Equation (10), is a function of both the prime pressure and the flow rate. Figure 10 maps the maximum cavern pressure as a function of the cavern prime pressure. Evidently, a minimum value exists. The reason is that the maximum pressure is proportional to the prime pressure, as given by Equation (10), and the flow rate and the rate at which the flow rate decreases leads to the minimum cavern pressure value in Figure 20.

Figure 20: Maximum Cavern Pressure vs the Prime Pressure for an AA-CAES

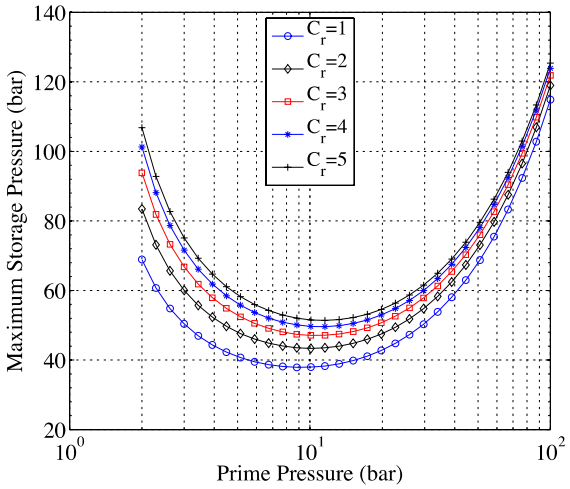

Of a constant 100MW power output and an isothermal cavern assumption

The associated LTES temperature, which is a function of the maximum cavern pressure, is shown in Figure 21. The LTES temperature increases with decreasing heat capacity rate ratio. A minimum LTES temperature value exists as the LTES is largely influenced by the trend given by the storage pressure shown in Figure 20.

Figure 21: The LTES Temperature vs the Prime Pressure of an AA-CAES

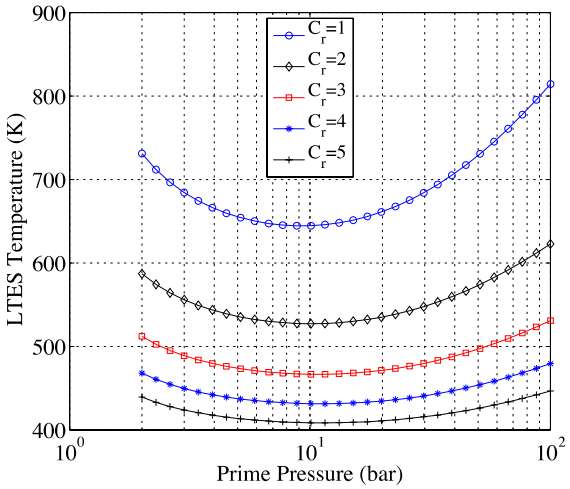

For a constant 100MW output power and an isothermal cavern

Finally, the associated round trip efficiency of the AA-CAES storage system as a function of prime pressure is shown in Figure 22. Curves for various LTES heat capacity rate ratios are plotted to illustrate the dependence of the round-trip efficiency on the LTES temperature. Lower LTES heat capacity rate ratios correspond to higher LTES temperatures and higher round trip efficiencies.

Figure 22: The Round-Trip Efficiency vs the Prime Pressure of an AA-CAES System

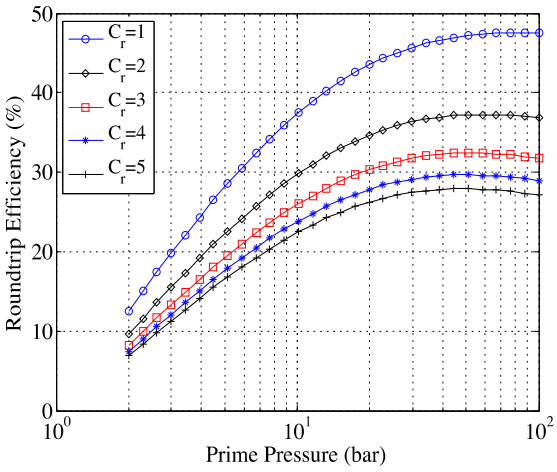

For a constant 100MW output power and an isothermal cavern assumption

In the limiting case when C_r=1, in other words when the LTES can reach the highest possible temperatures, the round-trip efficiency for the prime pressure of 50 bar is roughly 47%. Comparing results in Figure 22 with those in Figures 15, it is evident that the AA-CAES has lower efficiencies compared to HTH-CAES. There are two reasons for this: 1) throttling the cavern pressure to the constant turbine operating pressure kills the available energy between the two pressures even though the enthalpic content of the air remains constant. This energy could have otherwise been extracted via an expander, and 2) the maximum temperature of the throttled process is higher in HTH-CAES compared to AA-CAES. Throttling is often a restriction imposed by the narrow range of optimal operation of a turbo-expander. While a positive displacement machine with proper valve-timing control can adjust to a time-varying inlet pressure and maintain an optimal performance, a turbo-expander performs optimally over a narrow range of inlet operating conditions of pressure, temperature and mass flow rate. Slight deviations from the design conditions result in a sharp decrease in isentropic efficiency of the machine. This pressure must be regulated to the design conditions, either via a Joule-Thomson throttling process or using an expander that is capable of taking the time-varying pressure in the cavern and delivering a steady-state back pressure. The studies presented above quantify the performance envelope under throttling for both CAES's.

2.11 Discussion

The analyses presented are based on the assumption that pressure in the cavern monotonically increases to the peak pressure during the charge phase and monotonically drops to the prime pressure during the discharge phase. However, coupling the HTH-CAES with renewables, wind and/or solar PV for example, may invalidate this assumption, as the available power is intermittent. This fact may cause the plant to discharge before reaching the peak pressure in the cavern or charge before reaching the prime pressure in the cavern. This consideration raises the following question: If an HTH-CAES system is designed for an optimum operating pressure condition given by Figure 15, what would be the repercussions on the roundtrip efficiency if only a portion of the total storage capacity is used? More specifically, what is roundtrip efficiency if the storage pressure swings around $P\pm x$ where $P_{min}<P\pm x<P_{max}$? The answer to this question depends on the assumption/condition of the storage cavern (isothermal or adiabatic). In the case of an isothermal cavern all components and operating conditions of the cycle are

time-independent, with the exception of mass and pressure in the cavern. However, the discharge operating pressure is adjusted by the pressure-regulating valve, which maintains constant pressure conditions. Therefore, regardless of the cavern state of charge, as long as the same amount of mass is charged and discharged, which is the case for a given pressure swing x, the roundtrip efficiency remains the same as the designed optimum. In the case of an adiabatic cavern however, the answer to the question is not so obvious. The time dependent temperature of the discharging cavern air is carried downstream, affecting all discharge components (LTES heat exchanger, recuperator, HTES and turbine). With constant compression and expansion power, enforced throughout the paper, the roundtrip efficiency, Equation (17), is a function of the HTES power consumption, Equation (15), which is ultimately only a function of the HTES inlet temperature, T_9. The two constant temperature streams, provided by the LTES heat exchanger, T_{16}, and the recuperator, T_{11}, heat the discharging cavern air prior to their entrance into the HTES, and have the effect of drastically reducing the time dependent HTES inlet temperature variations, T_9. To demonstrate this effect, discharge temperatures are plotted as a function of time in Figure 23 for a 30bar prime pressure and a 150kg/s mass flow rate, corresponding to an optimum design given by Figure 5. In this example, the corresponding constant HTES exit temperature is T_{10}=1340K, as demonstrated by Figure 7. The constant turbine exhaust temperature is T_{11}=674K, and the constant LTES temperature is T_{16}=370.5K.

Figure 23: Transient Discharge Temperatures for an Adiabatic Cavern

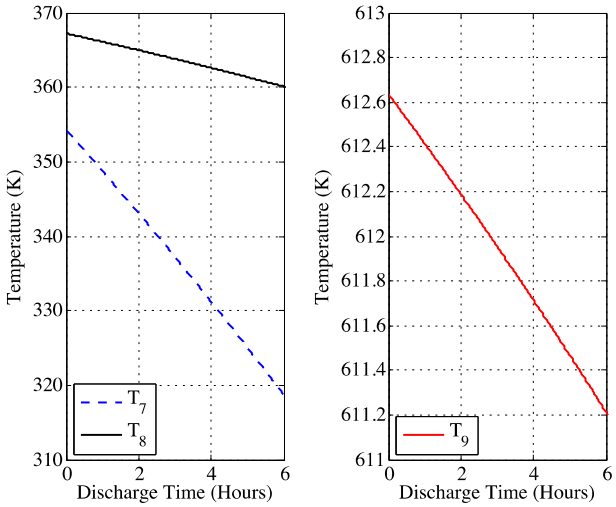

(a) (b)

Corresponding to a prime pressure of 30bar and a mass flow rate of 150kg/s

Where the HTES exit temperature is T_{10}=1340K, the turbine exhaust temperature is T_{11}=674K, and the LTES temperature is T_{16}=370.5K. T_7 is the discharging cavern air temperature, T_8 is the exit air temperature of the LTES discharge heat exchanger, and T_9 is the HTES inlet air temperature. All subscripts correspond to the process diagram points given in Figure 1.

The cavern discharge air temperature, T_7, has a relatively high temperature variation throughout the process, as shown in Figure 23(a). However, the constant temperature heating, provided by the LTES, T_{16}, reduces the temperature variations entering the recuperator, T_8, as demonstrated by the associated shallower slope in Figure 23(a). Subsequently, the constant temperature heating, provided by the recuperator, T_{11}, further reduces the temperature

transients entering the HTES, as demonstrated by T_9 in Figure 23(b). As a result, the HTES inlet temperature variations lead to a maximum temperature difference of about 1 kelvin, a negligible change. Therefore, the energy consumption of the HTES remains essentially constant throughout the cycle, and the roundtrip efficiency, again in the case of an adiabatic cavern, remains about the same as the designed optimum. The calculations performed to produce Figure 23 assumed an effectiveness of 80%, as given in Table 5. The time-dependent temperature variations, T_8 and T_9 in Figure 23, however, become identically zero at 100% heat exchanger effectiveness, where the cold exit streams become equal in temperature to the hot, and constant, inlet streams.

Another point in the analysis presented in this paper is that even though all calculations were done for a 100 MW system, the scale of utilization of the proposed HTH-CAES and the findings of the paper remain scalable and size-independent. The proposed system can be integrated with a wind or PV farm, given the local wind statistics, the solar irradiation data (TMY3, for example) and the total daily, monthly and annual energy consumption of the end users. Evidently, the farm has to be oversized to account for times of insufficient or unavailable renewable power. Since the HTES operates entirely based on resistive heating (Joule heating), the system accepts any kind of electric power signal – smooth or fluctuating. HTES therefore best lends itself to integration with the intermittently available wind and solar power. When the fluctuating electric power is below the compressor power requirement, it is entirely converted to heat and stored in the HTES. When it is above that threshold, the HTES acts as a filter that absorbs the fluctuations in the form of heat and provides the compressor with a smooth power signal for proper operation. Figure 24 illustrates the idea. A proper control system would therefore be necessary alongside the HTH-CAES system to properly distribute the intermittent input power signal between the HTES and the compressor within an HTH-CAES plant.

Figure 24: Distribution of an Intermittent Renewable Power Signal Between Thermal and Compressed Air Storage for the HTH-CAES System

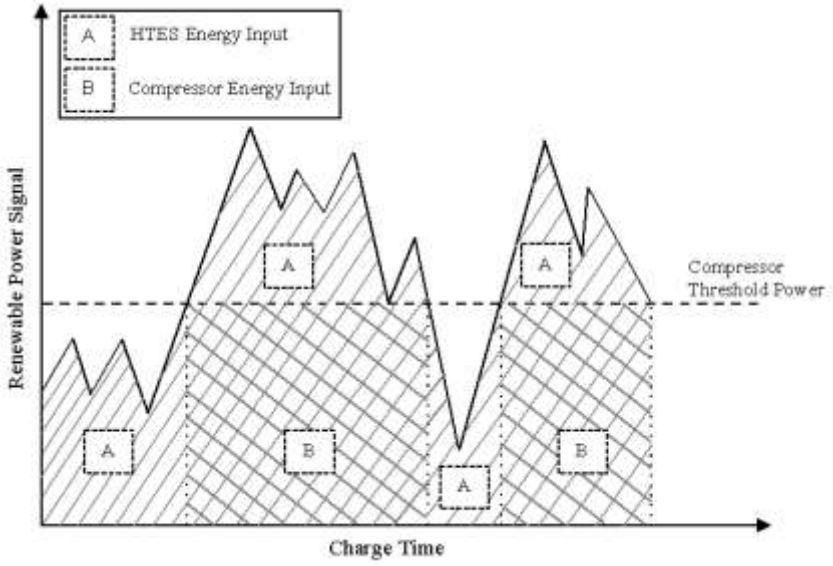

2.12 Cyclic Cavern Analysis

In this section, a brief analysis of the specific entropy, and the related cyclic variations, corresponding to an adiabatic and isochoric cavern is presented. The analysis starts by

presenting the governing equations, followed by the charge, discharge and cycle-to-cycle variations of the cavern.

2.12.1 Governing Equations

The general mass, energy and entropy balance equations together with the calorically perfect gas equations of state are given below:

$$\frac{dM}{dt} = \dot{m}_{in} - \dot{m}_{out} \qquad (A-1)$$

$$\frac{dE}{dt} = \dot{m}_{in}h_{in} - \dot{m}_{out}h_{out} + \dot{Q} \qquad (A-2)$$

$$\frac{dS}{dt} = \dot{m}_{in}s_{in} - \dot{m}_{out}s_{out} \qquad (A-3)$$

$$PV = MRT \qquad (A-4)$$

Where

$$E = Me \qquad (A-5)$$

$$S = Ms \qquad (A-6)$$

$$e = C_vT \qquad (A-7)$$

$$h = C_pT \qquad (A-8)$$

Where *e*, *h* and *s* are the specific energy, enthalpy and entropy, and *M* is the mass of air in the cavern.

Charge: ($\dot{m}_{out} = 0$)

Expanding Equation (A-3) and employing (A-1) results in the following equation for the specific entropy in the cavern:

$$M\frac{ds}{dt} = \dot{m}_{in}(s_{in} - s) \qquad (A-9)$$

with the initial condition of

$$s(t=0) = s(T_o, P_o) = s_o \qquad (A-10)$$

Where the subscript "*o*" indicates initial properties of the cavern.

Discharge: ($\dot{m}_{in} = 0$)

Similarly expanding equation (A-3) and employing (A-1), results in the following governing equation for the discharge process:

$$-\dot{m}_{out}s + M\frac{ds}{dt} = -\dot{m}_{out}s \qquad (A-11)$$

this, upon simplifying, yields

$$\frac{ds}{dt} = 0 \quad \rightarrow \quad s = constant \qquad (A-12)$$

Therefore, the specific entropy of the cavern remains constant during discharge.

2.12.2 Cyclic Variations

Coupled integration of Equations (A-1) through (A-8) along with Equations (A-9), (A-10), and (A-12) results in cycle-to-cycle variations of the isochoric cavern. The assumed constants in this analysis are provided in Table 6.

Table 6: Cyclic Cavern Assumed Constants

Constant	Value
Cavern Volume, V_{cavern}	300,000 m^3
Specific Heat of Air at Constant Pressure, C_p	1 kJ/kg.K
Specific Heat of Air at Constant Volume, C_v	0.718 kJ/kg.K
Air Gas Constant, R	0.287 kJ/kg.K
Minimum Pressure, P_{min}	5 bar
Maximum Pressure, P_{max}	20bar
Cavern Initial Temperature, T_o	300K
Cavern Inlet Temperature, T_{in}	300K
Mass Flow Rate, $\dot{m}$	200kg/s

The result, which illustrates the cyclic variations of the cavern-specific entropy, is shown in Figure 25. As shown, the specific entropy of the cavern decreases during the charge and remains constant during discharge. This trend continues until the specific entropy in the cavern during the charge process becomes isentropic, beyond which point the cavern-specific entropy does not change between cycles. As the cavern charges and discharges between the specified minimum and maximum pressures, the temperature of the cavern reaches a final range after about six cycles, under the constraints specified.

Figure 25: T-s Diagram of an Adiabatic Cavern Cyclic Process

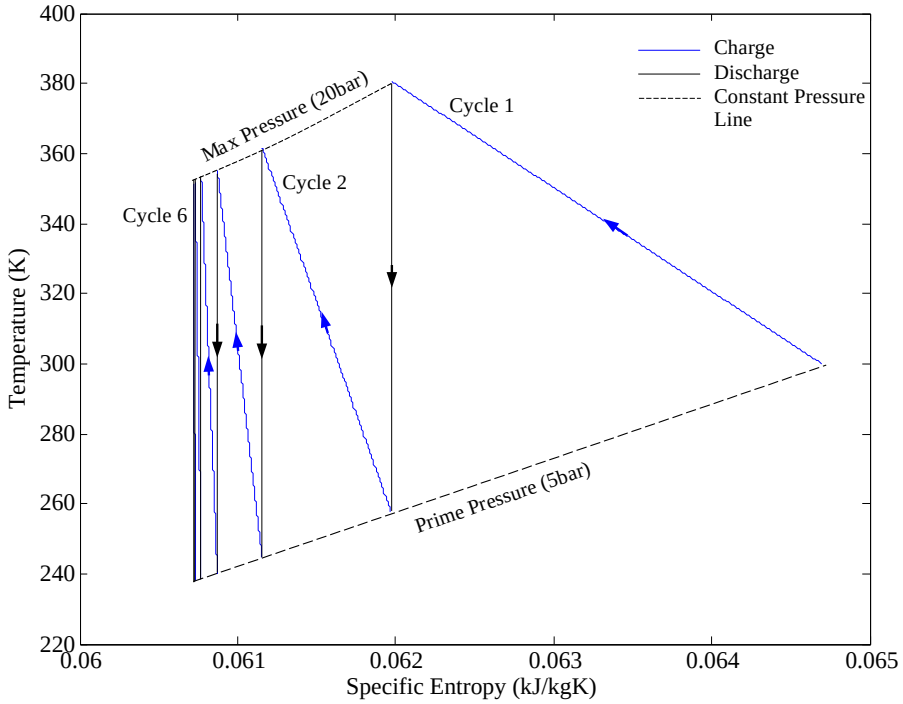

The first six cycles of the charge and discharge process are shown

2.13 Conclusion

A 100 MW output HTH-CAES system, with specified isentropic component efficiencies given by Table 6, was investigated. The sliding-pressure cavern is throttled in the discharge process to a constant pressure, that is. the prime pressure, under isothermal and adiabatic cavern conditions. The research team investigated two assumptions as the assumptions demonstrate the two possible extreme cavern conditions. Parametric studies of the prime pressure were investigated for both cavern conditions. Through the parametric study, the existence of an optimum prime pressure leading to maximum round -trip efficiency was found. For isothermal and adiabatic cavern conditions, the maximum round-trip efficiency is within the same proximity, although the associated optimum prime pressure for an adiabatic cavern is considerably higher. A 100MW AA-CAES system was also modeled as a comparison with a throttled, isothermal, sliding pressure cavern employing the same isentropic component efficiencies used for the HTH-CAES system. It was found that the roundtrip efficiency of the AA-CAES system is highly dependent on the storage temperature. In the limiting case when the heat rate capacity ratio is unity, C_r=1, i.e. when the LTES can reach the highest possible temperatures, the roundtrip efficiency for a practical yet high prime pressure of 50 bar is around 47%. The roundtrip efficiency of an HTH-CAES system with same output power of 100MW, a flow rate of 150kg/s and a prime pressure of 15bar is about 53%. The implication of this result is that even in the case of maximum LTES temperature, 725K, which is higher than what can be provided by currently available compressors, an HTH-CAES system is more efficient by 6.5%. Future works should include proper account of HTES heat losses during charge and discharge to quantify the roundtrip efficiency of thermal energy storage. In addition, future works should account for pressure losses throughout the cycle.

nomenclature

LTES	Low Temperature Thermal Energy Storage	$\dot{m}$	Air Discharge and Charge Flow Rate [kg/s]
HTES	High Temperature Thermal Energy Storage	m	Cavern Air Mass [kg]
η_c	Compressor Isentropic Efficiency	$\dot{Q}_{HTES}$	HTES Heat Input [kW]
η_t	Turbine Isentropic Efficiency	$P_{max,adiabatic}$	Maximum Adiabatic Cavern Pressure [bar]
V_{cavern}	Cavern Volume [m^3]	$P_{max,isothermal}$	Maximum Isothermal Cavern Pressure [bar]
P	Pressure [bar]	k	Ratio of Specific Heats
T	Temperature [bar]	$\dot{W}_{Output}$	Output Power [kW]
s	Specific Entropy [kJ/kgK]	$\dot{W}_c$	Compression Power [kW]
$t_{chaarge}$	Charge Time	u	Specific Internal Energy in Cavern [kJ/kg]
c_v	Specific Heat of Air at Constant Volume [kJ/kgK]	R	Specific Ideal Gas Constant of Air [kJ/kgK]
c_p	Specific Heat of Air at constant pressure [kJ/kgK]	P'	Prime Pressure [bar], Minimum Cavern Pressure and Throttling Pressure
$c_{,LTES}$	Specific heat of the LTES Heat Carrier [kJ/kgK]	$\eta_{Roundtrip}$	Round Trip Storage Efficiency
C_{LTES}	LTES Heat Capacity Rate [kW/K]	Δt	Time Step (Seconds)

2.14 Thermodynamic Performance and Cost Optimization of a Modified Hybrid Thermal-Compressed Air Energy Storage System Design

A novel hybrid thermal and compressed air energy storage (HT-CAES) configuration is presented that has the potential of eliminating the necessary combustion emissions in conventional CAES, and addressing some technical issues in the otherwise attractive CAES derivatives, such as:

1) high storage pressures,
2) large storage volumes,
3) increased complexity,
4) strict geological locations,
5) low energy density, and
6) high costs.

In HT-CAES, part of the available energy is spent on compressing the air, and the rest is directly converted to heat and stored in a high-temperature thermal energy storage (HTES) medium. The HTES can be charged either electrically from the grid, by the surplus of photovoltaic or wind electricity through Joule heating, or by a high-temperature fluid stream. The high-temperature fluid stream could also be either hot exhaust waste heat recovery or high-temperature output of a CSP plant [17-20]. Therefore the HTES eliminates the necessary combustion in conventional CAES plants and provides a means of substantially heating the air prior to expansion. The novel HT-CAES configuration presented here also includes a turbocharger, on the discharge side, which provides supplementary mass-flow rate alongside the air storage. The analysis shows the addition of a turbocharger has the potential of drastically reducing the storage volume and pressure, which reduces the system complexity and cost, in addition to eliminating the need for multistage compression and expansion.

In general, the cost of thermal storage is substantially lower than the cost of air storage, per kilowatt-hour [20]. However, a heat engine is theoretically lower in efficiency than a CAES plant. Therefore, with increased reliance on thermal storage, through the turbocharger, the HT-CAES system cost and efficiency are anticipated to decrease. This work sought to provide an efficiency and cost map of the HT-CAES system versus the operating pressure and the distribution of energy between thermal and compressed air storage. This work will illustrate and properly quantify a tradeoff that exists between storage cost and performance. Both roundtrip energy and exergy efficiencies are quantified, presented, and compared. Lastly, a local optimum line of operation, which results in a local maximum in efficiency and a local minimum in cost, is presented.

2.15 Methods

Figure 26 represents the HT-CAES thermodynamic cycle analyzed. During the charge process electricity from renewable sources or the grid is used to operate the compressor. Simultaneously or subsequently, depending on available power during the charge process, electricity is converted directly into thermal energy, through joule/resistive heating, and is stored in the high-temperature thermal energy storage (HTES) unit. The HTES unit takes advantage of the high thermal capacity of an inexpensive thermal medium to store heat that will later be used to heat the compressed air out of the air storage. Conversion of electricity to thermal energy can result in very high-temperatures and thus high energy densities when the energy is well contained. As a result, temperatures and volumetric energy densities well in excess of traditional CAES and AA-CAES can be achieved, while the size of the air storage can be reduced. The practical limit on how high a temperature can be reached in the HTES is defined by the material properties of the storage and the electric wires. With the addition of an HTES unit, the workload is shifted from pure compression to investing partially in thermal storage. This separation of energy storage between compressed air and thermal storage has the effect of expanding the energy capacity of the compressed air system without the need to increase the air pressure or air storage capacity. The HTES also allows the system to be dynamically scaled up or down as the load leveling demand changes without any structural change in system configuration.

The process pressure is herein referred to as the prime pressure. The temperature of the discharging air is then raised through three successive stages of heating before entering the expander: LTES, regenerator, and HTES. Additionally during the discharge process, a turbocharger is used which provides supplementary mass flow rate alongside the air storage. This has multiple advantages: 1) the storage system does not purely rely on the mass flow rate provided by the cavern 2) the necessary storage volume can be significantly reduced, which alleviates the restriction on geological locations 3) storage pressures can be drastically reduced, which has profound impacts on the lifetime, reliability and practicality of implementation 4) the cost of the system can be considerably reduced, as the system cost becomes leveraged by the price of thermal storage, which is typically cheaper than CAES [21].

Figure 26: Patented Hybrid Thermal and Compressed Air Energy Storage Process Diagram

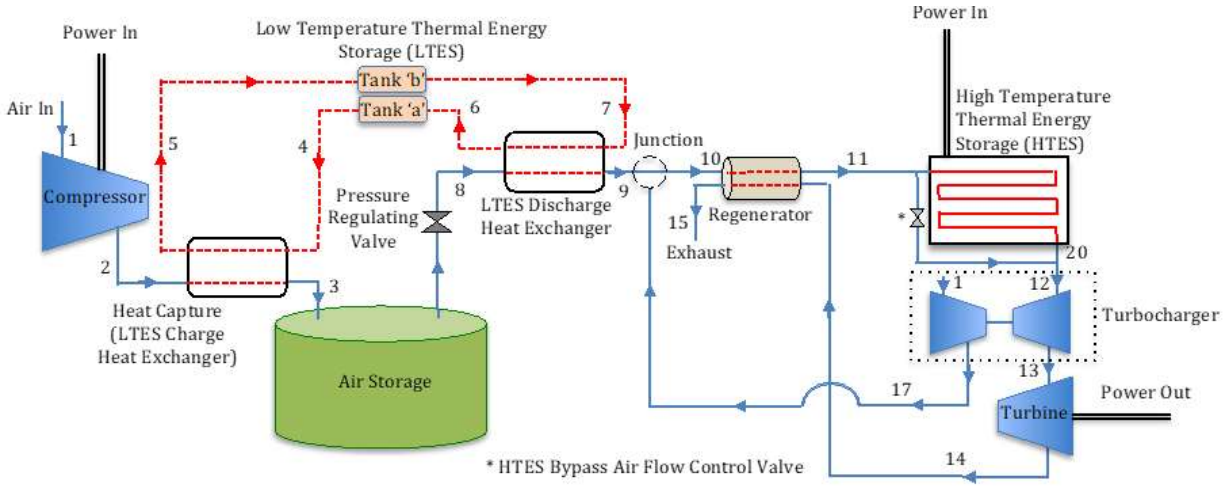

Throughout this report, the prime pressure, P_{prime}, is defined as the minimum air storage pressure and the discharge operating/process pressure, adjusted by the pressure-regulating valve. The prime pressure therefore delineates the expansion and compression ratios of the turbine and turbocharger compressor, which dictates their exhaust temperatures T_{14}, T_{17} shown in Figure 26. Therefore, the placement order of the regenerator, LTES discharge heat exchanger, and turbocharger junction on the discharge side of Figure 1 is one possible configuration. In this analysis however, depending on the chosen prime pressure, the configuration order of the LTES discharge heat exchanger, regenerator, and junction, is rearranged such that successive heating is always attained.

2.15.1 Problem Statement

As described, the novel hybrid storage system presented allows a portion of the available energy, from the grid or renewable sources, to operate a compressor and the remainder to be converted and stored directly in the form of heat by the HTES. The premise of this paper is to optimize this distribution of energy between compressed air energy storage and thermal energy storage for maximum efficiency, and for minimum cost. To properly quantify the distribution of energy between thermal and compressed air energy storage the variable β is defined, which represents the fraction of energy converted and stored in the form of heat through the HTES, Q_{HTES}, over the total amount of energy stored in the system; the energy of compression, W_{Comp}, plus electricity-to-heat conversion and storage, Q_{HTES}.

$$\beta = \frac{Q_{HTES}}{W_{Comp} + Q_{HTES}} \tag{1}$$

The optimization analysis is achieved through a parametric study of the energy allocation fraction, defined by β, and examining the effects on the performance, cost, component sizing, and various other parameters that characterize the hybrid storage system. In addition to β, the prime pressure is also investigated as the variation leads to important and conclusive design guidelines.

2.15.2 Assumptions

Pressure losses within the pipes were not taken into account and all components, besides the air storage and HTES, are assumed to operate quasi-steadily during charge and discharge. The

rational is that the residence time within these components is much shorter than charge and discharge time scales, indicated in Table 7. Also, heat capacities are assumed to be temperature independent and isentropic component efficiencies are incorporated. Table 7 summarizes the additional constants used throughout the investigation presented here.

Table 7: Thermodynamic Constants

Property	Value	Units	Description
P_1	1	Bar	Atmospheric Pressure
T_1	300	K	Atmospheric Temperature
P_2	20	Bar	Maximum Air Storage Pressure
T_4	300	K	LTES Inlet HX Temperature During Charge
T_{12}	1000	K	Turbocharger Inlet Temperature
T_{min}	1000	K	HTES Primed/Initial/Minimum Temperature
T_{max}	1600	K	HTES Maximum Temperature (End of Charge)
t_{charge}	6	Hours	Charge Time
$t_{discharge}$	6	Hours	Discharge Time
W_{output}	100	MW	Power Output Provided by the System
$\varepsilon_{d,LTES}$	0.8	-	LTES Discharge Heat Exchanger Effectiveness
$\varepsilon_{c,LTES}$	0.8	-	LTES Charge Heat Exchanger Effectiveness
η_c	0.75	-	Compressor Isentropic Efficiency
η_{Dcomp}	0.75	-	Turbocharger Compressor Isentropic Efficiency
η_t	0.8	-	Turbine Isentropic Efficiency
η_r	0.8	-	Regenerator Effectiveness
c_{HTES}	0.88	kJ/kg K	Specific Heat Capacity of HTES
R	0.287	kJ/kg K	Specific Gas Constant of Air
c_v	0.718	kJ/kg K	Specific Heat Capacity of Air at Constant Volume
c_p	1	kJ/kg K	Specific Heat Capacity of Air at Constant Pressure

It is imperative to note that the maximum air storage pressure, P_2=20bar, assumed in this analysis is considerably lower than that of conventional (~70bar) and advanced adiabatic (>70bar) compressed air energy storage systems. A detailed outline of the calculations made for

each component in the cycle is presented next; this includes all significant equations and any component specific assumptions.

2.16 Calculations

The general mass and energy balance equations together with the calorically perfect gas equations of state are given below:

$$\frac{dM}{dt} = \dot{m}_{in} - \dot{m}_{out} \tag{2}$$

$$\frac{dE}{dt} = \dot{m}_{in}h_{in} - \dot{m}_{out}h_{out} + \dot{Q} - \dot{W} \tag{3}$$

$$PV = MRT \tag{4}$$

Where

$$E = Me \tag{5}$$

$$e = c_v T \tag{6}$$

$$h = c_p T \tag{7}$$

Where e and h are the specific energy and enthalpy, and M is the mass of air. The isentropic relation, for an ideal and calorically perfect gas, relating pressure and temperature is below

$$\frac{T_2}{T_1} = \left(\frac{P_2}{P_1}\right)^{\frac{k-1}{k}} \tag{8}$$

2.16.1 Compressor

A constant compression ratio and flow rate is assumed in the compressor model. Additionally, adiabatic conditions are assumed, which result in a constant compression power with a mass flow rate given by equation (9). The compression mass flow rate, given by equation (9), is obtained by utilizing an energy balance, equation (3), and the calorically perfect and ideal gas relation given by equations (7) and (8).

$$\dot{m}_{charge} = \frac{\eta_c}{c_p T_1 \left(\left(\frac{P_2}{P_1}\right)^{\frac{k-1}{k}} - 1\right) t_{charge}} W_{comp} \tag{9}$$

Where η_c is the isentropic compressor efficiency, k is the ratio of specific heats for air, P_2 and P_1 are the maximum air storage and ambient pressures respectively, T_1 is the ambient temperature, c_p is the specific heat of air at constant pressure, and t_{charge} is the charge time. Lastly, W_{comp} is the total allocated compression energy, which is a function of β; therefore the charge mass flow rate, given by equation (9), is also a function of β. The coefficient of W_{comp} in equation (9) is a constant, the value of which can be obtained through the constants in Table 1. The compressor exhaust temperature is obtained by utilizing the isentropic compressor efficiency, defined as the ratio of isentropic work over actual work, the isentropic relation given by equation (8), and the calorically perfect gas equation (7), resulting in equation (10)

$$T_2 = \frac{T_1\left(\left(\frac{P_2}{P_1}\right)^{\frac{k-1}{k}} - 1\right)}{\eta_c} + T_1 \tag{10}$$

2.16.2 LTES

The Low Temperature Thermal Energy Storage (LTES), as explained previously, is a two-tank system containing and circulating a Heat Transfer Fluid (HTF), which collects the heat of compression during charge, and withdraws the heat during the discharge process. Tank 'a' is assumed in thermal equilibrium with the environment and tank 'b' is assumed adiabatic, shown in Figure 1. Utilizing the constant heat exchanger effectiveness, $\varepsilon_{c,LTES}$, provided by Table 1, and an energy balance, through equation (3) and (7), the inlet and exit LTES heat exchanger temperature streams, corresponding to points 3 and 5 in Figure 1, can be obtained and are given by equations (11) and (12)

$$T_3 = T_2 - \varepsilon_{c,LTES}(T_2 - T_4) \tag{11}$$

$$T_5 = \frac{\dot{m}_{charge} c_p}{\dot{m}_{c,LTES} c_{LTES}}(T_2 - T_3) + T_4 \tag{12}$$

Where $\dot{m}_{c,LTES}$ is the LTES charge mass flow rate and c_{LTES} is the specific heat of the HTF. All subscripts correspond to the process diagram in Figure 1. The heat capacity rate of the air and LTES HTF are assumed equal. Moreover, tank 'b' is assumed adiabatic, therefore T_5=T_7 in Figure 1. The temperatures in the vicinity of the LTES discharge heat exchanger and the regeneration component are calculated similarly, by applying an energy balance, assuming adiabatic conditions, and considering the heat exchanger effectiveness provided in Table. 1.

2.16.3 Air Storage

The air storage volume is calculated through an energy balance assuming an adiabatic, ideal, and calorically perfect gas. Utilizing equations (3)-(6) it can be shown that during the charge process the necessary air storage volume, which operates at a specified pressure swing, $\Delta P = P_2 - P_{prime}$, is

$$V_{Air\ Storage} = \frac{kRT_3 t_{charge}}{P_2 - P_{prime}} \dot{m}_{charge} \tag{13}$$

Where P_{prime} is the minimum storage pressure and P_2 is the maximum storage pressure, given in Table 1. The calculated results given by equations (9) and (11) are used to determine the air storage volume in equation (13). The mass flow rate, given by equation (9), is a function of the energy fraction, β, therefore the air storage volume, specified by equation (13), is also a function of β. The air storage discharge mass flow rate is determined through an energy balance assuming an adiabatic, ideal, and calorically perfect gas. Using equation (3)-(6), where M_o is the initial stored air mass determined through the ideal gas equation (4), it can be shown that

$$\dot{m}_{discharge} = \frac{M_o + t_{charge}\dot{m}_{charge}}{t_{discharge}}\left[1 - \left(\frac{P_{prime}}{P_2}\right)^{\frac{1}{k}}\right] \tag{14}$$

The air storage is initially assumed at a specified prime pressure, P_{prime}, and ambient temperature. The air storage is inherently transient therefore the time dependent temperatures and pressures must be calculated as the discharging air passes through the various

downstream components. Through the mass and energy balance, equations (2) and (3), together with the calorically perfect gas equations of state, given by equations (4)-(7), the following discretized equations are used to determine the time dependent temperature and pressure of the discharging air

$$u(t+\Delta t) = \frac{M(t)u(t)}{M(t+\Delta t)} + \frac{M(t+\Delta t) - M(t)}{M(t+\Delta t)} h(t) \tag{15}$$

$$T(t+\Delta t) = \frac{u(t+\Delta t)}{c_v} \tag{16}$$

$$P(t+\Delta t) = \rho(t+\Delta t) \cdot R \cdot T(t+\Delta t) \tag{17}$$

The initial temperature of the discharging air is found by incorporating the ideal gas law given the specified maximum pressure in Table 1, the calculated volume from equation (13), and the total stored mass. The air storage is discharged until the specified prime pressure, P_{prime}, is reached.

2.16.4 Turbocharger

The turbocharger provides supplementary mass flow rate, at the junction in Figure 26, in addition to the discharging cavern/tank flow rate. The total discharge flow rate, which enters the HTES and turbine, is therefore the sum of both discharging cavern/tank mass flow rate plus supplementary mass flow rate provided by the turbocharger. Through an energy and mass balance, on a control volume containing the turbocharger and power turbine, the total necessary discharge mass flow rate is obtained and is given by equation (18)

$$\dot{m}_t = \frac{\dot{W}_{output} - \dot{m}_{discharge} c_p (T_{17} - T_1)}{c_p (T_{12} - T_{14}) - c_p (T_{17} - T_1)} \tag{18}$$

Where $\dot{W}_{output}$, T_{12}, T_1 and c_p are constants specified by Table 1, and $\dot{m}_{discharge}$ is given by equation (14). The compressor and turbine exhaust temperatures, T_{14} and T_{17}, are obtained by employing the isentropic compressor and turbine efficiencies given in Table 1, similar to the procedure which arrived at equation (10).

2.16.5 HTES

The high-temperature thermal energy storage (HTES) is inherently a transient component. However, the HTES can be designed to deliver a constant temperature, necessary for optimal operation of a turbo-expander, through bypassing a portion of the cold inlet air with the hot flow exiting the HTES, as shown in Figure 1. Applying the energy and mass balance to the point where the bypass line mixes with the hot flow out of the HTES, the bypass mass flow rate, $\dot{m}_{bp}$(t), can be obtained as a function of $T_{20}(t)$ and T_{12}:

$$\dot{m}_{bp}(t) = \dot{m}_t \frac{T_{20}(t) - T_{12}}{T_{20}(t) - T_{11}(t)} \tag{19}$$

Where $T_{20}(t)$ is the time dependent temperature of the HTES. For simplicity, and as a first order approximation, a lumped capacitance approximation is used to model the HTES, where no temperature gradients exist within the HTES. Additionally it is assumed that at each instant of time during the discharge process the exit air temperature is equal to the instantaneous HTES temperature. The amount of energy allocated to the HTES, $Q_{\beta,HTES}$, is used to size the mass such that the maximum specified temperature is reached at the end of charge as follows

$$M_{HTES} = \frac{Q_{\beta,HTES}}{c_{HTES}(T_{max} - T_{min})} \tag{20}$$

The total energy that must be stored by the hybrid storage system, to deliver the constant energy output specified in Table 1, must be iteratively solved at each specified β. This is because the sought-after efficiency of the system is inherently a function of β as made clear by equation (21)

$$E_{input}(\beta) = \frac{E_{output}}{\eta_I(\beta)} \tag{21}$$

The first law efficiency, or equivalently the roundtrip energy efficiency, η_I, is defined as the total output energy over the total input energy, thermal plus compression. E_{input} and E_{output} are the total input and output energies. The bisection method is used to iteratively solve for the necessary input energy, such that the final HTES temperature, at the end of discharge, reaches precisely the minimum value specified in Table 1.

2.16.6 Roundtrip Energy and Exergy Efficiencies

The roundtrip energy efficiency (1st law efficiency) of the system is defined on an energy basis as the total output over total input energy as shown by equation (22).

$$\eta_I = \frac{\int \dot{W}_{output}\, dt}{\int \dot{W}_{comp} dt + \int \dot{Q}_{HTES}\, dt} \tag{22}$$

Similarly, the roundtrip exergy efficiency (2nd law efficiency) is defined as the total output over total input exergy, as shown by equation (23).

$$\eta_{II} = \frac{\int \dot{W}_{output}\, dt}{\int \dot{W}_{comp} dt + \int (1 - T_o/T_{HTES})\dot{Q}_{HTES}\, dt} \tag{23}$$

The exergy associated with compression and expansion is equivalent to their energy values, assuming adiabatic conditions. However, the exergy associated with heat transfer in the HTES is determined by the second term in the denominator of equation (23). For simplicity, assuming no temperature gradients within the HTES and a constant input electrical signal, the exergy associated with heat transfer can be calculated by first determining the HTES temperature, T_{HTES}, during the charge process using the energy balance equation (3). Performing the Integration in equation (23) and utilizing the 1st law efficiency and β definitions, through equation (22) and (1), results in equation (24)

$$\eta_{II} = \frac{\eta_I}{1 - T_o\beta \ln(1 + \delta/T_{\min})/\delta} \tag{24}$$

Where T_o is the ambient temperature, $T_{\min}$ is the minimum HTES temperature, and δ is the maximum HTES temperature difference, $\delta = T_{\max} - T_{\min}$. The 2nd law efficiency of the system, equation (24), is presented conveniently as a function of the 1st law efficiency, η_I, the energy distribution fraction, β, and the HTES periphery temperatures. By observing the 2nd law efficiency, equation (24), it becomes immediately apparent that all variables in the denominator are positive. Therefore, the 2nd law efficiency is always greater than or equal to the 1st law efficiency, $\eta_{II} \geq \eta_I$, which is consistent with the exergy efficiency of heat engines.

2.16.7 Cost Functions

The following cost functions, based on thermodynamic variables, are used to determine the purchase price of the compressors and turbines [23], [24].

$$\Xi_{\text{compressor}} = c_1 \frac{39.5\,\dot{m}}{0.9 - \eta_c} r_c \ln(r_c) \tag{25}$$

$$\Xi_{\text{turbine}} = c_1 \frac{266.3\,\dot{m}}{0.92 - \eta_t} \ln(r_e)(1 + \exp(0.036 T_{\text{inlet}} - 54.4 c_2)) \tag{26}$$

Where r_c and r_e are the compression and expansion pressure ratios and the constants, c_1=1.051 c_2=1.207, reflect costs reported by the Gas Turbine World Handbook [23], [24]. The cost of air storage through an above ground tank typically scales with volume and pressure, however, with a fixed maximum pressure throughout this study, the cost function for a tank as a function of volume, based on multiple vendors (Fjords Processing, KS Industries, Modern Custom Fabrication Inc.), is below

$$\Xi_{\text{Air Storage}} = 1000\,V_{tank} \tag{27}$$

The cavern cost function, based on volume, is shown below [5]

$$\Xi_{\text{Air Storage}} = 3.75 \times 10^7 + 62\,V_{cavern} \tag{28}$$

In this analysis the cheapest air storage architecture, based on the above cost functions, is used. Lastly, the HTES is an alumina-based refractory with a material purchase cost, based on mass and determined through various vendors (Resco Products, Harbison-Walker Refractories), given by the cost function below

$$\Xi_{\text{HTES}} = 2.2 M_{HTES} \tag{29}$$

In addition to the above cost functions, a factor of 1.25 is multiplied to account for the remaining heat exchangers, pipes, valves, LTES HTF and tanks. The total system capital cost per kilowatt-hour is given below

$$Cost\left[\frac{\$}{kWh}\right] = \frac{(\Xi_{\text{compressor}-1} + \Xi_{\text{compressor}-2} + \Xi_{\text{turbine}-1} + \Xi_{\text{turbine}-2} + \Xi_{\text{Air Storage}} + \Xi_{\text{HTES}}) \times 1.25}{E_{output}} \tag{30}$$

Where two compressor and turbine cost functions are considered, as evident by Figure 26. The denominator represents the total delivered energy, obtained by multiplying the total discharge time by the constant output power, as specified in Table 7.

2.17 Results

As stated in the Problem Statement section, the premise of this study is to investigate the performance and cost of the hybrid energy storage system as the energy distribution between thermal and compressed air energy storage is varied. The distribution of energy is quantified through the variable β, equation (1). The extreme case of β=100% results in pure thermal energy storage, as no energy is allocated towards compression, and the air storage does not receive or provide any air mass flow. Therefore, in the case where β=100% the process diagram, in Figure 26, becomes a regenerative Brayton cycle. Conversely, the case of β=0% results in pure compressed air energy storage, with no energy allocated to the HTES. In addition to analyzing

the ramifications of β on the performance and cost of the system, the prime pressure is also investigated. The prime pressure, P_{prime}, represents the minimum air storage pressure and the discharge operating pressure, which is adjusted through the pressure-regulating valve, as shown in Figure 1. The two variables under investigation β and P_{prime} are of particular interest as their variation lead to noteworthy and definitive design guidelines.

2.17.1 Roundtrip Energy and Exergy Efficiencies

The roundtrip energy efficiency (First law efficiency) map of the HT-CAES system, and the corresponding contour plot, is provided in Figure 2. As stated previously, in the extreme limit of β=100%, where the energy is stored purely in the form of heat through the HTES, the hybrid storage system becomes a regenerative Brayton cycle. Moreover, in a regenerative Brayton cycle, with a constant power output and turbine inlet temperature, there exists an optimum operating pressure (prime pressure, P_{prime}) leading to maximum energy efficiency. This is equivalent to, and validates, the profile in Figure 27 at β=100%.

Figure 27: HT-CAES Roundtrip Energy Efficiency Map

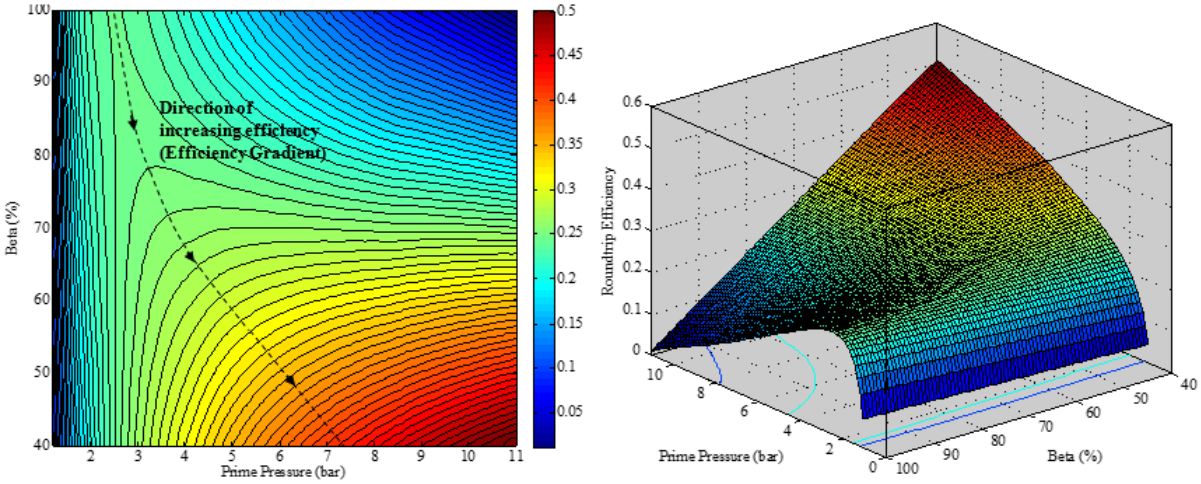

As a Function of the Energy Distribution fraction β, and the prime pressure, P_{prime}. The dotted line represents the direction of increasing efficiency (efficiency gradient, $\nabla\eta(\beta, P_{prime})$), which begins at the optimum design point of a regenerative brayton cycle (at $\beta = 100\%$).

As the operating pressure increases, at β=100%, eventually regeneration becomes ineffective as the turbine exhaust temperature falls below the turbocharger compressor exhaust temperature. At which point regeneration is disengaged and a classical Brayton cycle is employed at higher operating pressures, resulting in slightly higher efficiencies, nevertheless, eventually leading to zero efficiency. A Brayton cycle at a constant turbine inlet temperature of 1000K, power output of 100MW, and isentropic efficiencies corresponding to the constants in Table 7, reaches an efficiency of zero at an operating pressure of 11.3bar and is not operational for higher operating pressures. In general, the efficiency of the hybrid storage system increases with decreasing β; as the reliance on compressed air storage increases. This is because a hybrid CAES system is theoretically more efficient than the corresponding Brayton cycle counterpart. Additionally, CAES systems are generally not bound by the Carnot efficiency, as is the case for heat engines. Furthermore, as β increases, a larger fraction of the discharge flow rate is provided by the turbocharger, which introduces additional isentropic component efficiencies that impede the roundtrip energy efficiency of the system. The efficiency of the hybrid storage system increases with the operating pressure at the lower end of the β spectrum, corresponding

to higher compressed air storage dependence, as illustrated in Figure 2. The reason behind the monotonic increase in efficiency with operating pressure, at lower β values, stems from the accompanying decrease in throttling losses and exhaust temperatures.

At β values below 40%, the amount of energy allocated towards the HTES becomes too low for proper operation. This is because the HTES mass, which is calculated based on the specified temperature swing in Table 1, decreases with decreasing β; as the energy allocated for thermal storage decreases. Eventually, the HTES mass becomes too low and drops below the minimum specified temperature at the end of discharge, and therefore cannot bear the total discharging flow rate. Hence, β values below 40% are not investigated. Beginning with the optimum prime pressure of a regenerative Brayton cycle, at β=100% in Figure 2, and moving along the direction of increasing efficiency or efficiency gradient, results in the dotted line shown. Any perpendicular deviation along this efficiency gradient results in a lower efficiency than otherwise achievable. The significance of this efficiency gradient curve will be demonstrated and revisited when discussing the capital cost of the system.

The roundtrip exergy efficiency (2nd law efficiency) contour map of the HT-CAES system is provided in Figure 28.

Figure 28: HT-CAES Roundtrip Energy Efficiency Contour Map – Energy Distribution Fraction, β, and the Prime Pressure

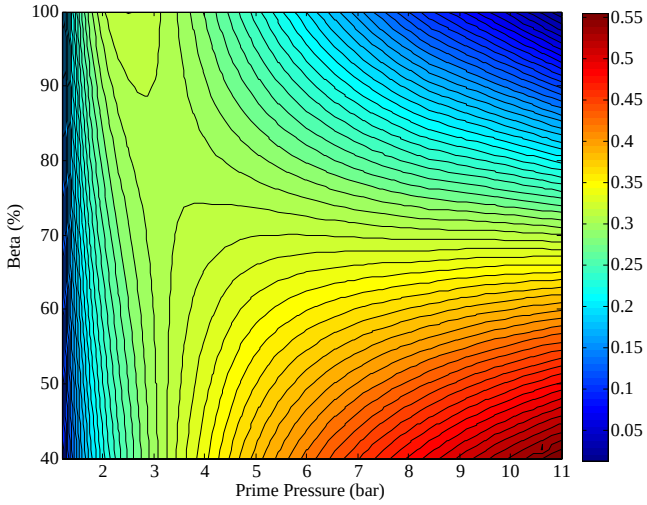

The HT-CAES exergy efficiency is always greater than the energy efficiency, a result that is consistent with heat engines. The energy and exergy efficiencies become coincident in the limiting case of a very large HTES temperature swing, $\delta = T_{max} - T_{min}$, as indicated by equation (31).

$$\lim_{\delta \to \infty} \eta_{II} = \eta_I \tag{31}$$

Therefore, the minimum exergy efficiency is equal to the corresponding energy efficiency, $\eta_{II,min} = \eta_I$. This is due to the increase in internal irreversibilities associated with mixing losses in the HTES at a high-temperature swing; a result that is undetected through the first law analysis and efficiency. Conversely, the largest difference in 1st and 2nd law efficiencies (in other words, the maximum exergy efficiency for a given energy efficiency) occurs in the limit of a very low HTES temperature difference, where internal irreversibility associated with mixing losses are eliminated, as shown by equation (32)

$$\lim_{\delta \to 0} \eta_{II} = \frac{\eta_I}{1 - \beta \frac{T_o}{T_{\min}}} \tag{32}$$

Further increase in their difference occurs for 1) high β values, and 2) as the HTES minimum temperature approaches the ambient temperature, $T_{min} \to T_o$. This is because for low β values, the system becomes weakly dependent on thermal energy storage and both energy and exergy efficiencies, equation (22) and (23), become equivalent. Furthermore, in the limit that $\delta = T_{max} - T_{min} = 0$, by definition this means $T_{min} = T_{max} = T_{HTES}$. Therefore, the additional limit $T_{min} \to T_o$ leads to $T_{HTES} = T_0$, meaning the HTES remains at ambient temperature. As a mathematical consequence, the second term in the denominator of equation (23) is lost, leading to maximum exergy efficiency for a given energy efficiency. However, physically this means no external irreversibility associated with heat transfer in the HTES.

2.17.2 Component Sizing

The various mass flow rates of the system, the air storage volume, and the thermal storage mass are presented in this section. The charge and discharge mass flow rates into and out of the cavern/tank are plotted, in Figure 4, as functions of the prime pressure and the energy distribution fraction. The charging mass flow rate, into the air storage, is identically zero at β=100% as no energy is allocated and stored in the form of compression, Figure 29. In general, the charge mass flow rate increases with decreasing β as more energy is allocated towards compressing and storing air. In addition, at higher roundtrip efficiencies the amount of output power per kilogram of air is also higher; meaning, for a constant power output the necessary mass flow rate is lower. Consequently, at the lower end of the β spectrum, the charge mass flow rate decreases with prime pressure, as a result of the increase in efficiency, as evident by Figure 27 and 28. The discharging mass flow rate provided by the air storage is nearly identical to the charge mass flow rate, as the air storage is assumed adiabatic. Therefore, the trends of the discharging mass flow rate, as a function of β and the prime pressure, are the same as those described previously for the charging flow rate. The analysis performed here is of the first cycle, however after several cycles the air storage no longer experience cyclic variations, at which point the charge and discharge mass flow rates become identical.

Figure 29: HT-CAES Air Storage, Charge and Discharge, Mass Flow Rates

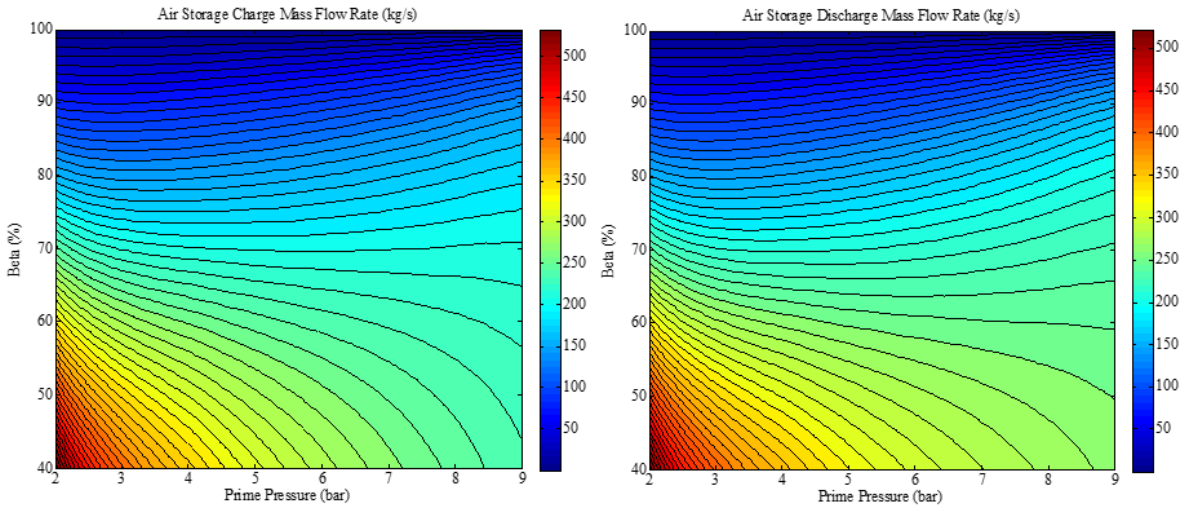

As a function of the energy distribution, β, and the prime pressure

The turbine and turbocharger mass flow rates are plotted in Figure 30as functions of the energy distribution fraction and the prime pressure. As depicted by Figure 30, the turbine mass flow rate generally decreases with decreasing β. Moreover, the turbine mass flow rate, at the higher β spectrum, reaches a minimum value as a function of the prime pressure and decreases with increasing prime pressure at the lower β spectrum. The turbine mass flow rate resembles the opposite trend depicted by the roundtrip efficiency. This is because the total and necessary mass flow rate through the turbine is largely influenced by the roundtrip efficiency of the system. The total mass flow rate is inversely proportional to the roundtrip storage efficiency, since the total power output per kilogram of air is higher at regions of higher efficiency, which for a constant power output results in lower mass flow rates. Conversely, the total power output per kilogram is lower at regions of lower efficiency, which for a constant power output results in higher necessary mass flow rates.

Figure 30: HT-CAES Turbine and Turbocharger, Mass Flow Rates

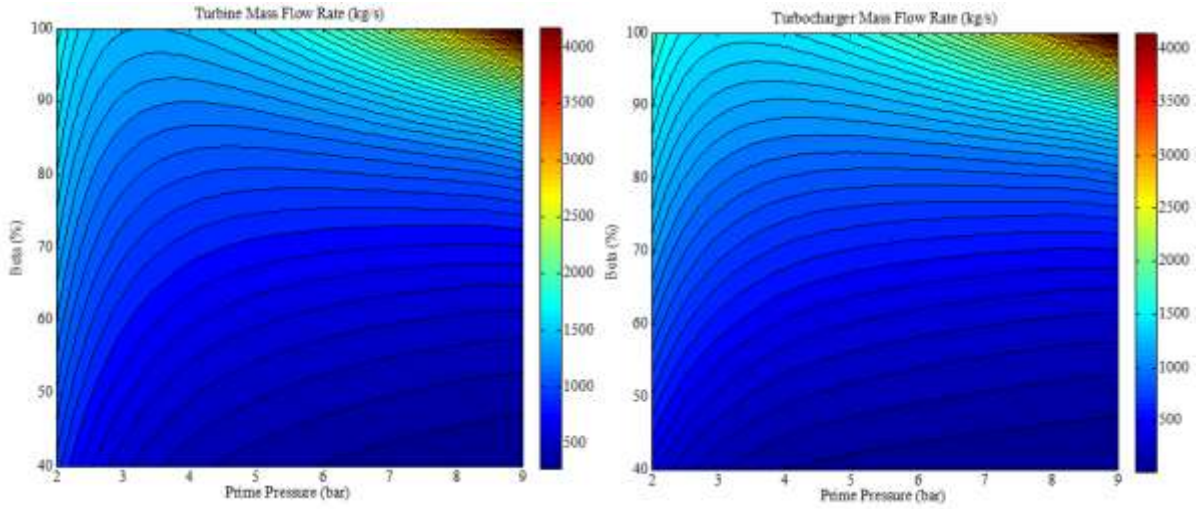

As a function of the energy distribution, β, and the prime pressure

The necessary turbocharger mass flow rate, in general, decreases with decreasing β values. By definition, as β decreases the reliance of the flow rate on the turbocharger decreases as the air storage provides a larger fraction of the total flow rate. The turbocharger mass flow rate map is largely influenced by the total turbine mass flow rate, as it is defined as the difference between the total and the stored air discharge mass flow rate.

The air storage volume, Figure 31, generally increases with decreasing β; this is because the reliance on the compression energy increases with decreasing β. At β=100%, the air storage volume is identically zero, as the system evolves into a regenerative Brayton cycle. As β values decrease from 100%, the volume increases with the prime pressure and the total compression energy, as depicted by equation (13). The compression energy, for a fixed β value, is inversely proportional to the roundtrip efficiency of the system. Therefore the air storage volume, at constant β, is proportional to the prime pressure and inversely proportional to the roundtrip efficiency of the system. The competition between the efficiency of the system and the prime pressure leads to a minimum air storage volume illustrated in Figure 30, for a fixed β value, particularly at the lower β spectrum.

Figure 31: HT-CAES Air Storage Volume and Thermal Storage Mass

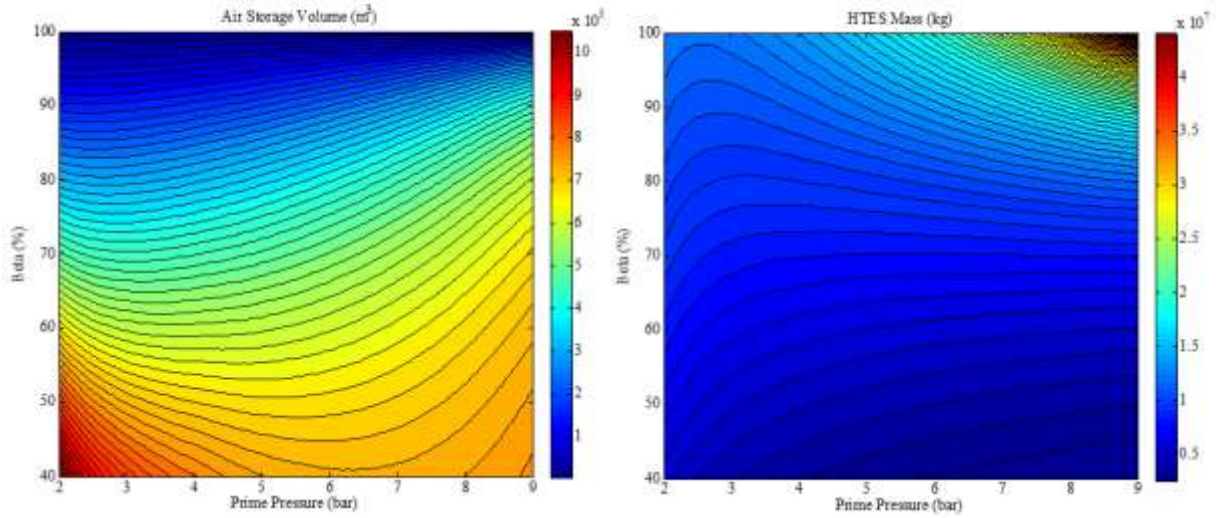

As a function of the energy distribution, β, and the prime pressure.

The HTES mass is plotted in Figure 31 as functions of the prime pressure and β. More energy is allocated towards thermal storage with increasing β. Therefore in general, the HTES mass increases with β to achieve the specified and constant HTES temperature swing in each cycle, as shown in Figure 31. For a fixed value of β, at the higher end of the spectrum, the HTES mass given in Figure 31 reaches a minimum as a function of the prime pressure. The prime pressure leading to a minimum HTES mass coincides with that of maximum efficiency. As the prime pressure increases, the HTES mass also increases due to the decrease in system efficiency; therefore more energy must be stored as higher turbine mass flow rates are employed to obtain the constant output energy during each cycle. Inversely, at the lower end of the β spectrum, the efficiency of the system increases with prime pressure, therefore the total discharge flow rate and the total necessary HTES mass decrease with increasing prime pressure.

2.17.3 Capital Cost

The total cost of the storage system per unit of delivered energy, equation (27), is shown in Figure 32. The roundtrip efficiency and air storage price have a dominant influence on the system capital cost, as the air storage price per unit volume is much higher than the HTES cost per unit mass, and the efficiency dictates the necessary storage sizes. Therefore in general, the cost increases with decreasing efficiency and increasing storage volume. At β=100%, where the air storage volume is identically zero, the cost is purely that of the HTES and the corresponding machinery cost per kilowatt-hour. As the system efficiency decreases, with increasing prime pressure at β=100%, the necessary HTES mass and flow rates, Figures 28 & 29, increase drastically resulting in higher cost. As β decreases, the air storage price begins to influence the system cost as the necessary volume increases. At β values very near 100%, a tank is more cost effective than a cavern, however caverns become more cost effective very quickly as β is decreased from 100%.

Figure 32: HT-CAES Cost ($/kWh), Equation (27)

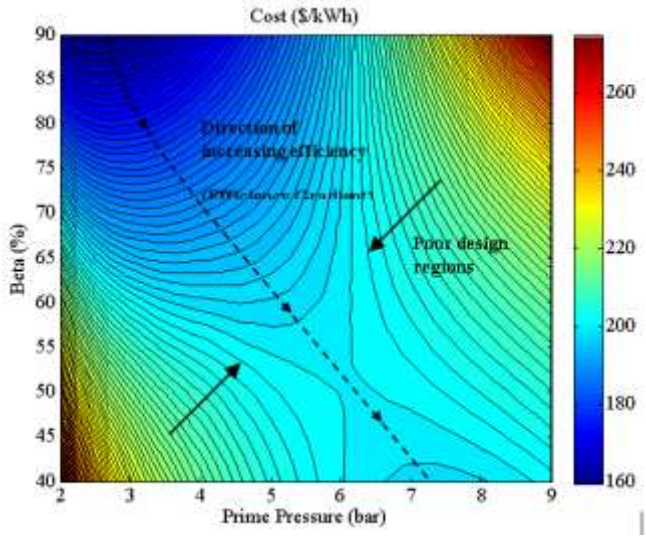

As a function of the energy distribution, β, and the prime pressure. The dotted line represents the direction of increasing efficiency (given in Figure 2), which begins at the optimum prime pressure of a regenerative Brayton cycle (at $\beta = 100\%$).

Revisiting the efficiency gradient in Figure 27, and overlapping the efficiency gradient on the cost map results in the dotted line, labeled “Efficiency gradient”. As demonstrated, any perpendicular deviation from this efficiency gradient results in a lower efficiency than otherwise achievable. Additionally however, the cost map demonstrates that perpendicular deviations from this efficiency gradient also result in a higher cost. Therefore, the efficiency gradient provides a local optimum design region resulting in maximum efficiency and minimum cost. Any deviation perpendicular to the efficiency gradient line results in a higher cost and lower efficiency than otherwise achievable, therefore areas away from this line can be regarded as poor design regions that should be avoided.

In general, the cost of the hybrid storage system increases along the efficiency gradient, or along the local optimum line of operation. In other words, as the reliance on thermal energy storage is increased the cost of the system is decreased, as the system cost becomes leveraged by the cheap thermal energy storage cost. The addition of the turbocharger provides a means of heavily relying on thermal storage, as the additional mass flow rate reduces the reliance on the air storage. Therefore, there exists an inherent trade-off in the hybrid storage cost and efficiency as a function of the energy distribution. The desired point of operation along the efficiency gradient, or the local optimum line of operation, depends on the specific energy application, which the hybrid storage system must integrate with. Energy application priorities are not unique; these priorities may include cost, efficiency and footprint. The efficiency gradient line provides a means of adjusting the system characteristics to meet various application priorities without a change in system capacity. However, tradeoffs between efficiency, cost, and footprint are inherent in the system and quantified through the efficiency, size, and cost maps provided. A lower system cost and footprint results in a lower efficiency, corresponding to higher thermal energy storage allocation (large β values). On the contrary, higher system efficiency requires a higher capital cost and a larger footprint, corresponding to higher compressed air energy storage allocation (lower β values).

It is imperative to note the existence of a local minimum and maximum in cost along the efficiency gradient, at the lower end of the β spectrum. This is caused by the local minimum in

storage volume, shown in Figure 5, as a function of the prime pressure at lower β values. The slopes in the vicinity of the local minimum and maximum in cost are quite gradual. Additionally, any further increase in efficiency at β=40%, at the lower end of the efficiency gradient would require an increase in the prime pressure which would further increase the cost of the system. Therefore, the optimal global maximum and minimum in cost and efficiency reside at the ends of the local optimum line of operation.

2.18 Discussion

The capital costs of various grid-scale energy storage systems are widely available in the literature. Table.8 provides a summary of the minimum, average, and maximum reported capital cost values of various available grid-scale energy storage technologies, along with the calculated HT-CAES system cost for comparison.

Table 8: Reported Capital Costs of Various Grid-scale Energy Storage Systems

Energy Storage Technology	Capital cost, per unit of storage capacity ($/kWh)		
	Minimum	Average	Maximum
CAES	249	312	330
Flywheel	2,201	5,701	29,808
Li-ion battery	546	649	666
Supercapacitors	822	910	1,018
Hydrogen	474	642	927
HT-CAES	**65**	**-**	**200**

From the literature [25]

The minimum hybrid thermal-compressed air energy storage (HT-CAES) system capital cost, in Table 8, corresponds to β=100%, which results in pure thermal storage. The maximum HT-CAES capital cost value corresponds to β=40%, where the turbocharger is essentially turned off and the system resembles that of a conventional CAES design. Moreover, the performance of a conventional CAES system is identical to that of an HT-CAES system at β=40%, assuming a similar storage pressure and turbine inlet temperature. As evident through Table 2, the HT-CAES system is reasonably competitive from a capital cost perspective, as the HT-CAES system cost is leveraged by the cheap thermal storage. The CAES capital cost range is that of a conventional design. The cost of an advanced adiabatic CAES system is typically higher than that of a conventional system because of the need for multistage compression and expansion [26]. Additionally, the performance of an AA-CAES is typically lower in efficiency than that of hybrid system, assuming throttling losses exist, due to its strong dependence on the temperatures captured by the generated heat of compression. Realistic AA-CAES efficiencies range from 28%-47% depending on the temperature limit provided by the generated and stored heat of compression [26]. Therefore, the HT-CAES system provides a competitive design compared to conventional CAES systems and its advanced adiabatic derivative. Moreover, HT-CAES provides a means of adjusting to various footprint and cost requirements, without compromising the storage capacity. Further performance improvements in the HT-CAES system are possible. The HT-CAES system cost is dominated by the air storage price. Therefore,

incorporating intercooling and reheating components can reduce the necessary compression power and increase the potential for regeneration. Thereby improving the performance of the HT-CAES system without a substantial increase in the capital cost per unit of storage capacity.

Although batteries, flywheels, and supercapacitors generally have higher energy efficiencies, their costs are substantially higher than CAES systems. In addition, their lifetime, energy capacity and discharge times are typically lower than CAES systems. These parameters, among others, play a key role in determining the suitable applications that an energy storage technology may provide within the electrical grid. With their unique strengths and weaknesses, it is unlikely that a sole energy storage technology will provide a universal solution. On the contrary, each available energy storage technology may provide an exclusive solution to a specific grid/renewable-integration application. A good metric for comparing various forms of energy storage is the levelized cost of electricity (LCOE), as it considers the energy efficiency, lifetime, capital cost, and maintenance cost of the system. Therefore, in future work, further insight can be gained by comparing the HT-CAES system with various other forms of energy storage from an LCOE perspective.

2.19 Conclusion

A novel hybrid thermal and compressed air energy storage configuration is developed which has the potential of eliminating combustion emissions and drastically reducing the storage pressure, volume, and cost as compared with conventional CAES and the respective derivatives. The addition of thermal energy storage and a turbocharger have the effect of significantly leveraging the cost of the system, as supplementary mass flow rate is provided alongside the stored air, and the cost of thermal storage is considerably cheaper than air storage. The reduced system cost, however, comes at the expense of a reduced efficiency, as the performance of heat engines are bound by the Carnot limit and compressed air energy storage, theoretically, has no such constraint. The hybrid system provides the flexibility of adjusting to a myriad of storage volumes based on available geological restrictions. In addition, the hybrid storage system performs best at low storage pressures, which reduces the complexity as it alleviates the need for multistage compression and expansion. The thermodynamic optimization results provide the operational efficiency, cost and storage sizing (thermal and air volume) maps, which can be used as a reference in future development endeavors. In addition all mass flow rate maps are provided, which dictate the necessary machinery sizes. The operational flexibility of HT-CAES is particularly useful as the priorities of various energy applications are not unique, these priorities may include cost, efficiency, and footprint. The hybrid CAES system possesses a wide range of possible operations, without a compromise in the storage capacity, which may prove useful towards a sustainable future.

Nomenclature

HT-CAES	Hybrid Thermal Compressed Air Energy Storage	LTES	Low Temperature Thermal Energy Storage
HTES	High Temperature Thermal Energy Storage	HTF	LTES Heat Transfer Fluid
r_e	Expansion Pressure Ratio	r_c	Compression Pressure Ratio
β	Energy Distribution (equation 1)	η	Component Efficiency
W	Energy of Compression or	ε	Heat Exchanger Effectiveness

	Expansion		
$\dot{W}$	Power of Compression or Expansion	k	Ratio of Specific Heat of Air
Q	Heat Energy	V	Volume
$\dot{Q}$	Heat Power	R	Ideal Gas Constant of Air
P	Pressure	E	Energy
T	Temperature	e	Specific Energy
ρ	Density	h	Specific Enthalpy
M	Mass	u	Specific Internal Energy
$\dot{m}$	Mass Flow Rate	Ξ	Component Cost Function
t	Time of Charge or Discharge	c_p	Specific Heat of Air at Constant Pressure
c_v	Specific Heat of Air at Constant Volume	c_{HTES}	Specific Heat of the HTES
c_{LTES}	Specific Heat of the LTES HTF	t	Charge or Discharge Time
η_I	Roundtrip Energy Efficiency (1st Law Efficiency)	η_{II}	Roundtrip Exergy Efficiency (2nd Law Efficiency)

2.20 Performance of the Hybrid Thermal-Compressed Air Energy Storage System at Minimum Entropy Generation

The optimization of a hybrid thermal-compressed air energy storage system, unlike heat engines, has not been devoted any attention. Conversely, the optimization of heat engines is an old subject of thermodynamics. Various optimization objectives have been examined to investigate the performance of standard power cycles such as Brayton, Otto, Diesel, Atkinson, Millar and Dual cycles. However such analysis has not been employed on a hybrid thermal-compressed air energy storage system. The most common optimization criteria examined in the literature for power cycles are maximum efficiency, maximum work output, minimum entropy generation, and maximum ecological function (defined as the output power minus the entropy generation rate, multiplied by the environmental temperature). According to the Gouy-Stodola theorem, maximum output power and minimum entropy production rate are equivalent, however this equivalence in heat engines was later shown to be limited to certain design conditions. For heat engines, the maximum thermal efficiency and maximum work output do not necessarily coincide. For example, in a regenerative Brayton cycle maximum work and maximum thermal efficiency coincide only at a regenerator effectiveness of 50%. Whether the optimization objective should be performed based on maximum power or maximum efficiency is dependent on the application of use. In general however, the operational regime should be between the maximum efficiency and maximum output power design points.

The main objective of this paper is to investigate the performance of an isobaric hybrid thermal and compressed air energy storage system at the point of minimum entropy generation, which to the best of the team's knowledge has not been formerly reported. The energy and exergy efficiencies are examined and the optimum design points leading to their maxima is compared

with the design point corresponding to minimum entropy generation. The premise is to determine whether minimization of entropy production may lead to definitive design guidelines. Additionally, a discussion is provided that demonstrates the criterion at which the maximum energy efficiency and maximum exergy efficiency become coincident with the design point of minimum entropy generation. Throughout the analysis, it is assumed that external irreversibility's are present. The effects of both internally reversible and irreversible processes are examined and compared. Additionally, the thermal energy storage efficiency is taken into consideration and the effects on the optimum design points, leading to maximum energy efficiency, maximum exergy efficiency, and minimum entropy generation, are examined.

2.21 HT-CAES Thermodynamic Cycles

Figure 33 represents the HT-CAES thermodynamic cycles that are analyzed here. During the charge process electricity from renewable sources, or the gird, is used to operate the compressor. Simultaneously or subsequently, depending on available power during the charge process, electricity is converted directly into thermal energy, through joule/resistive heating, and is stored in the Thermal Energy Storage (TES) unit. The TES unit takes advantage of the high thermal capacity of an inexpensive thermal medium to store heat that will later be used to heat up the compressed air out of the air storage. Conversion of electricity to thermal energy can result in very high temperatures and thus high energy densities when the energy is well contained. As a result, temperatures and volumetric energy densities well in excess of traditional CAES and AA-CAES can be achieved, while the size of the air storage can be reduced. The practical limit on how high a temperature can be reached in the TES is defined by the material properties of the storage and the electric wires. Alumina-based refractory provides service temperatures in excess of 1700C and Nichrome wires can have a continuously operating temperature of ~ 1680C. With the addition of a TES unit, the workload is shifted from pure compression to investing partially in thermal storage. This separation of energy storage between compressed air and thermal storage has the effect of expanding the energy capacity of the compressed air system without the need to increase the air pressure or air storage capacity. The TES also allows the system to be dynamically scaled up or down as the load leveling demand changes without any structural change in system configuration.

The thermodynamic models assume an adiabatic and constant pressure air storage, which can be either underwater air storage or a cavern constructed in underground rock formation with a water-equalizing pit, to maintain isobaric conditions [29]. The air storage under this assumption remains isothermal, therefore reduces to just a delay time in the operation of the plant. Figures 33 and 34 show the described HT-CAES system with and without regeneration.

Figure 33: HT-CAES Thermodynamic Cycle Configuration Without Regeneration

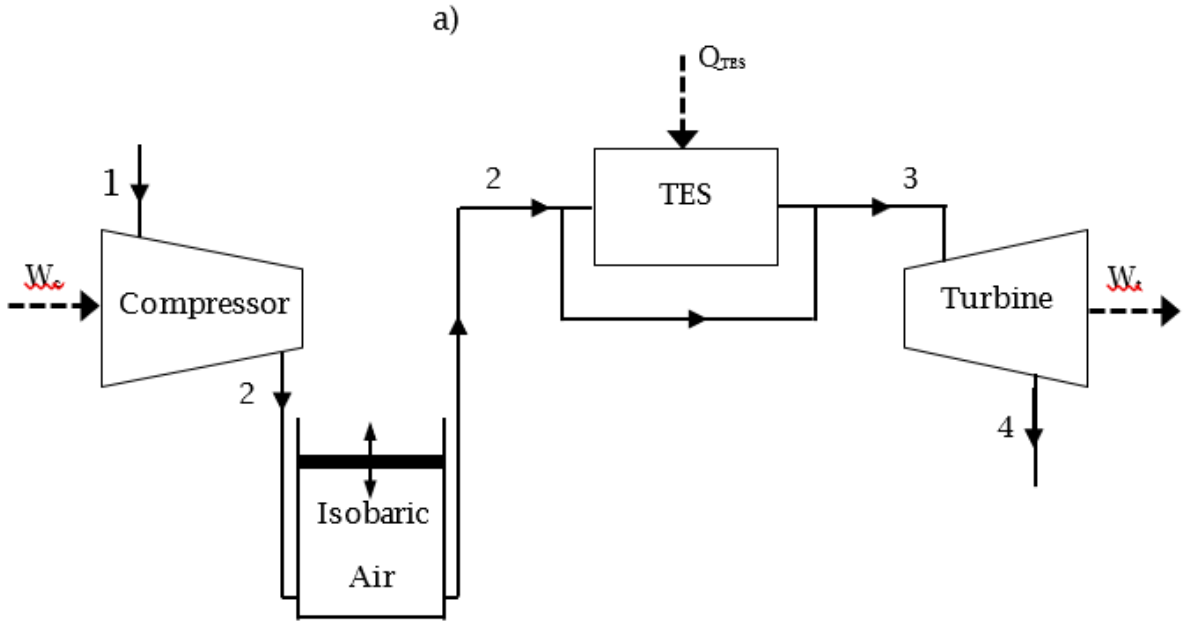

Figure 34: HT-CAES Thermodynamic Cycle Configuration With Regeneration

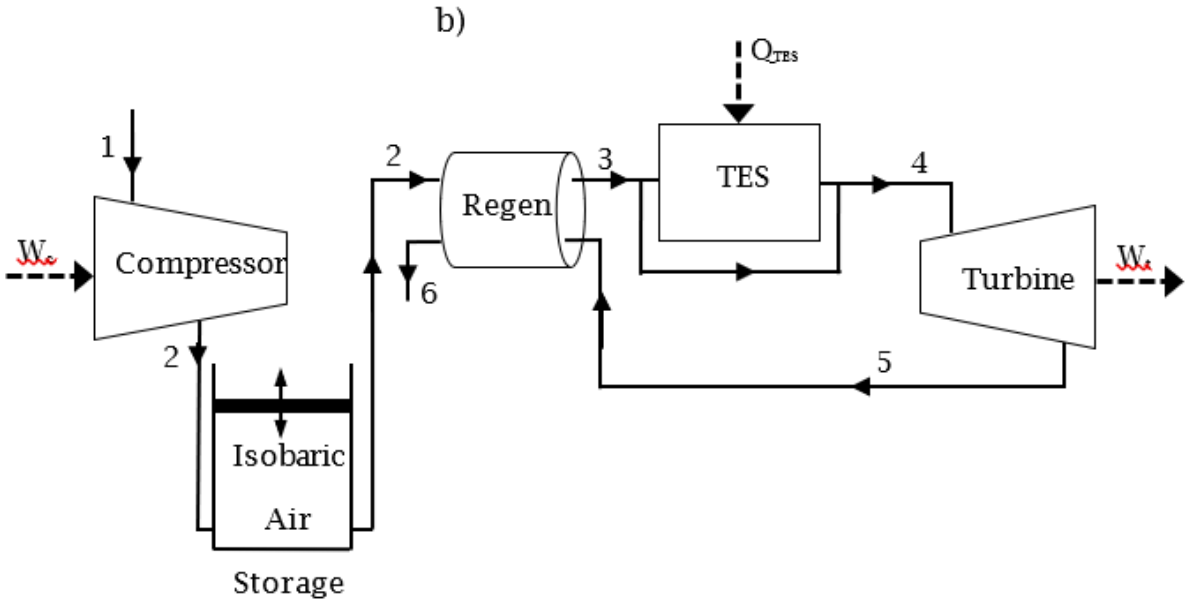

The sensible thermal energy storage unit, shown in Fig. 1, is inherently a transient component. However, the TES can be designed to deliver a constant temperature, necessary for optimal operation of an expander, through bypassing a portion of the cold inlet air with the hot flow exiting the TES, as demonstrated by Figure 33. Throughout the analysis it is assumed that the TES has a minimum temperature, T_{min}, which is equivalent to the constant turbine inlet temperature ($T_{min} = T_3$ in the case without regeneration in Figure 33, and $T_{min} = T_4$ with regeneration in Fig. 1(b)) at the beginning of charge and end of discharge. The TES maximum

temperature, T_{max}, is reached at the end of the charge process and beginning of the discharge process, which must be set larger than the turbine inlet temperature. A zero order model of the TES is assumed, in which no temperature gradients within the TES exist during the charge or discharge process. However, thermal storage efficiency is taken into consideration and the value represents the percentage of irretrievable energy loss within a full cycle. Additionally, the following analysis is based on the simplifying assumptions of a calorically perfect gas, ideal gas, and negligible pressure drops.

2.22 Internally Reversible HT-CAES

First consider the internally reversible HT-CAES system without regeneration, followed by a similar analysis of an internally reversible HT-CASES system with regeneration. In this section it is also assumed that the thermal energy storage is 100% energy efficient. The thermal energy storage efficiency and the internal irreversibilities are analyzed. The following analysis is composed of a calculation of the energy efficiency, exergy efficiency and the entropy generation as the pressure ratio is varied. The pressure ratio is defined as the maximum to minimum pressure ratio in the system ($r = P_2/P_1 = P_4/P_5$).

2.22.1 HT-CAES Without Regeneration

2.22.1.1 First Law Efficiency

The roundtrip energy storage efficiency of the HT-CAES system, defined as the output power over the total input power, is given by equation (1)

$$\eta_I = \frac{\dot{W}_t}{\dot{W}_C + \dot{Q}_{TES}} \tag{1}$$

Assuming constant specific heats for air, isentropic compressor and turbine, and constant inlet turbine temperature, T_3, the energy efficiency can be rewritten to equation (2).

$$\eta_I = \frac{1 - T_1/T_2}{1 - T_1/T_3} = \frac{1 - r^{-\alpha}}{1 - r_T^{-1}} \tag{2}$$

Where, $\propto = (\gamma - 1)/\gamma$, γ is the ratio of specific heats for air, and r_T is the maximum to minimum temperature ratio in the cycle, $r_T = \frac{T_3}{T_1}$. By examining equation (2), and considering a Brayton cycle with a heat source provided by the TES, it becomes evident that the numerator represents the Brayton cycle efficiency, in the case of pure thermal energy storage and no air storage. Similarly, the denominator of equation (2) represents the Carnot efficiency of the associated Brayton cycle. Therefore, equation (2) can be written as shown in equation (3)

$$\eta_I = \frac{\eta_{Brayton}}{\eta_{Carnot}} \tag{3}$$

Equation (3) provides an interesting result, which illustrates that the process is 100% efficient when there is no heat addition provided by the thermal storage, $T_3 = T_2$, and the compression and expansion processes are along the same isentropic line. The addition of heat through the thermal storage takes the process off the compression isentrope and introduces the Carnot limit into the cycle. In the extreme of very high temperatures of thermal storage, i.e. when the balance between heat and isentropic work of compression shifts predominantly toward heat, the cycle is dominated by the Brayton cycle as the Carnot efficiency approaches unity. In another extreme where the energy allocated into thermal energy storage approaches zero and $T_3 = T_2$, HT-CAES reduces to an advanced adiabatic system with a theoretical round-trip

efficiency of unity, as evident from equation (3). In this limit, where advanced adiabatic CAES aims to operate, the expansion isentrope coincides with the compression isentrope. When there is economic and technological justification, this limit is theoretically the most desirable zone of operation for energy storage/retrieval. It can be concluded that the efficiency of a non-regenerative HT-CAES cycle is 1) always greater than the efficiency of the corresponding Brayton cycle, in the case of pure thermal energy storage, and 2) is not bound by the Carnot efficiency.

2.22.1.2 Second Law Efficiency

The roundtrip exergy efficiency of the HT-CAES system, which is defined as the total output exergy over the total input exergy, is given by equation (4)

$$\eta_{II} = \frac{\int \dot{W}_t \, dt}{\int \dot{W}_c \, dt + \int (1 - T_1/T_{TES}) \dot{Q}_{TES} \, dt} \tag{4}$$

Where $\dot{Q}_{TES}$ is the TES input joule heating power. The total energy stored in the TES is calculated through an energy balance which results in: Q_{TES}=$\dot{Q}_{TES}t = Mc(T_{max} - T_{min}) = Mc(T_{max} - T_3) = \dot{m}c_p t(T_3 - T_2)$, where $M, c, \dot{m}$ and c_p are the TES mass, TES specific heat, air mass flow rate, and specific heat of air at constant pressure, respectively. Lastly, the instantaneous temperature of the TES during the charge process is calculated through an energy balance, which results in $T_{TES} = \frac{\dot{Q}_{TES}}{Mc} t + T_{min}$, where $T_{min} = T_3$. Evaluating the integrals in equation (4) results in equation (5)

$$\eta_{II} = \frac{T_3 - T_4}{T_2 - T_1 + \frac{Mc}{\dot{m}c_P t}(T_{\max} - T_3) - T_1 \frac{Mc}{\dot{m}c_P t} \ln\left(\frac{T_{max}}{T_3}\right)} \tag{5}$$

Further simplification of equation (5), while substituting temperature ratios, $r_T = \frac{T_3}{T_1}$ and $r_H = \frac{T_{max}}{T_3}$, leads to equation (6)

$$\eta_{II} = \frac{\eta_{Brayton}}{\eta_{Carnot} - r_T^{-1}(1 - r_T^{-1} r^{\alpha}) \frac{\ln(r_H)}{(r_H - 1)}} \tag{6}$$

Equation (6) reveals that the exergy efficiency of the HT-CAES system is always higher than the energy efficiency given by equation (3), provided the TES increases the temperature of the discharging air, $T_2 < T_3$. This result is consistent with heat engines, in which their exergy efficiencies are generally higher than their associated energy efficiencies.

2.22.1.3 Entropy Generation

The total entropy generation associated with the operation of the HT-CAES system is evaluated through an entropy balance and is given in equation (7)

$$S_{gen} = \int \frac{\dot{Q}_{out}}{T_{out}} dt - \int \frac{\dot{Q}_{in}}{T_{in}} dt \tag{7}$$

The second integral in equation (7), associated with the TES heat input, is calculated through a similar approach that arrived at equation (5), resulting in the following expression

$$S_{gen} = \frac{\dot{m}c_P t(T_4 - T_1)}{T_1} - Mcln\left(\frac{T_{max}}{T_3}\right) \tag{8}$$

Normalizing the entropy generation with the total stored air mass times its specific heat, $\dot{m}c_P t$, and relating temperature ratios with pressure ratios through isentropic relations, results in equation (9)

$$\frac{S_{gen}}{\dot{m}c_P t} = (r_T r^{-\alpha} - 1) + (r_T^{-1} r^{\alpha} - 1)\frac{\ln(r_H)}{r_H - 1} \tag{9}$$

Plotting the energy efficiency, exergy efficiency, and the normalized entropy generation given by equations (3), (6) and (9) respectively results in Figure 35.

Figure 35: Energy Efficiency, Exergy Efficiency and Normalized Entropy Generation of the Internal Reversible TES, HT-CAES System Without Regeneration

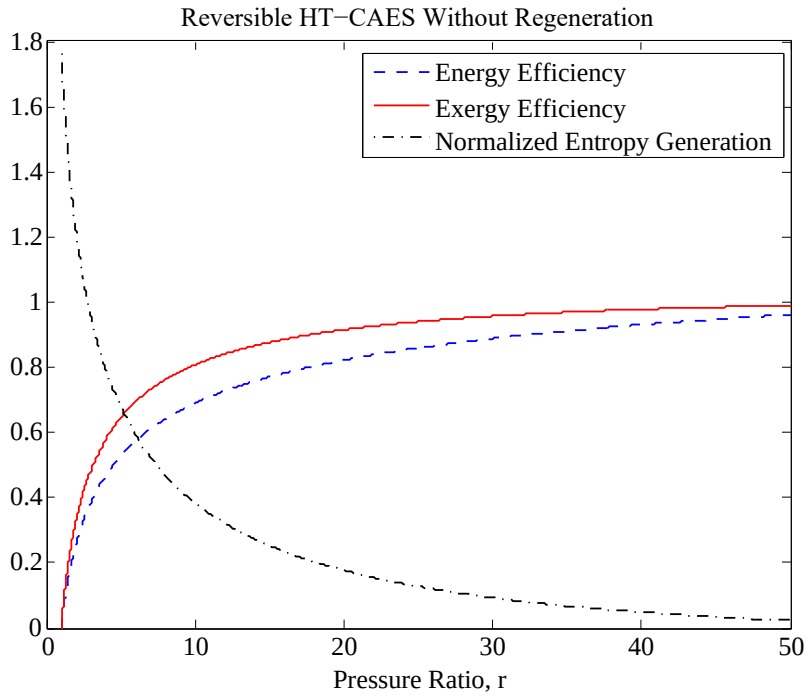

Without regeneration as a function of the pressure ratio, r.

For an internally reversible HT-CAES system without regeneration, all performance indices monotonically improve with increasing operating pressure, as shown by Figure 35. Therefore, in this specific case, an increase in the energy and exergy efficiency does in fact correlate with a decrease in entropy generation. It is also imperative to note that in an HT-CAES system the output power increases with the pressure ratio, as the turbine and compressor are decupled in contrast to a Brayton cycle. Therefore, a decrease in entropy generation also correlates with an increase in output power. It will be shown that this is not necessarily the case in the presence of internal irreversibility's, and a discussion explaining the reason behind the phenomenon is provided in section 5.

2.22.2 With Regeneration

A similar procedure to arrive at the energy efficiency, exergy efficiency, and entropy generation in the case of internally reversible HT-CAES system is undertaken, however including regeneration, Figure 35. Similarly, the pressure ratio is varied, and the performance indices are

examined and compared to determine whether minimization of entropy production may lead to conclusive design guidelines.

2.22.2.1 First Law Efficiency

The energy efficiency, as defined in equation (1) and assuming constant specific heat, leads to equation (10).

$$\eta_I = \frac{T_4 - T_5}{T_2 - T_1 + T_4 - T_3} \tag{10}$$

Rearranging equation (10) and relating temperature ratios to pressure ratios through isentropic relations leads to equation (11)

$$\eta_I = \frac{1}{2 - \eta_{Brayton,R}} \tag{11}$$

Where $\eta_{Brayton,R}$ is the energy efficiency of the corresponding regenerative Brayton cycle, in the case of pure thermal energy storage and no air storage. Equation (11) is analogous to equation (3), however including regeneration. The regenerative Brayton cycle efficiency is given by equation (12)

$$\eta_{Brayton,R} = 1 - r_T^{-1} r^{\alpha} \tag{12}$$

The temperature ratios $r_T = \frac{T_4}{T_1}$ and $r_H = \frac{T_{max}}{T_4}$ are defined as the maximum to minimum temperature ratios that the air and TES experience in the regenerative cycle. Equation (11) illustrates that the 1st law efficiency of a regenerative HT-CAES system is always higher than its Brayton cycle counterpart, as was the case in the non-regenerative system shown by equation (3).

2.22.2.2 Second Law Efficiency

The second law efficiency of the HT-CAES system with regeneration, Figure 35 is obtained through a similar procedure, which arrived at the exergy efficiency without regeneration, given by equation (6). The result is given by equation (13)

$$\eta_{II} = \frac{\eta_I}{1 - \eta_I \frac{\ln(r_H)}{r_T(r_H - 1)}} \tag{13}$$

Where η_I is the first law efficiency given by equation (11). Through an energy balance, the following relation given by equation (14) was used to relate the mass and specific heats of the air and TES with their temperature differences

$$\frac{Mc}{\dot{m} c_P t} = \frac{T_4 - T_3}{T_{max} - T_4} = \frac{(1 - r^{-\alpha})}{r_H - 1} \tag{14}$$

Again, notice that the second law efficiency of the HT-CAES system, given by equation (13), is always higher than the first law efficiency. The gap between the energy and exergy efficiency increases with increasing energy efficiency and decreasing temperature ratios (r_T and r_H). Meaning it is more effective, exergetically, to reduce the TES temperature swing and air temperature swing throughout the cycle, as a result of the associated decrease in mixing irreversibility's.

2.22.2.3 Entropy Generation

The normalized entropy generation associated with the operation of a regenerative HT-CAES system, Figure 34, is evaluated through an entropy balance, equation (7), undertaking a similar procedure which arrived at equation (9), the result is given in equation (15).

$$\frac{S_{gen}}{\dot{m}c_P t} = (r^{\alpha} - 1) + (r^{-\alpha} - 1)\frac{\ln(r_H)}{r_H - 1} \tag{15}$$

Plotting the energy efficiency, exergy efficiency, and the normalized entropy generation given by equations (11), (13) and (15) respectively results in Figure 36.

Figure 36: Energy Efficiency, Exergy Efficiency and Normalized Entropy Generation of the Internal Reversible TES, HT-CAES System With Regeneration

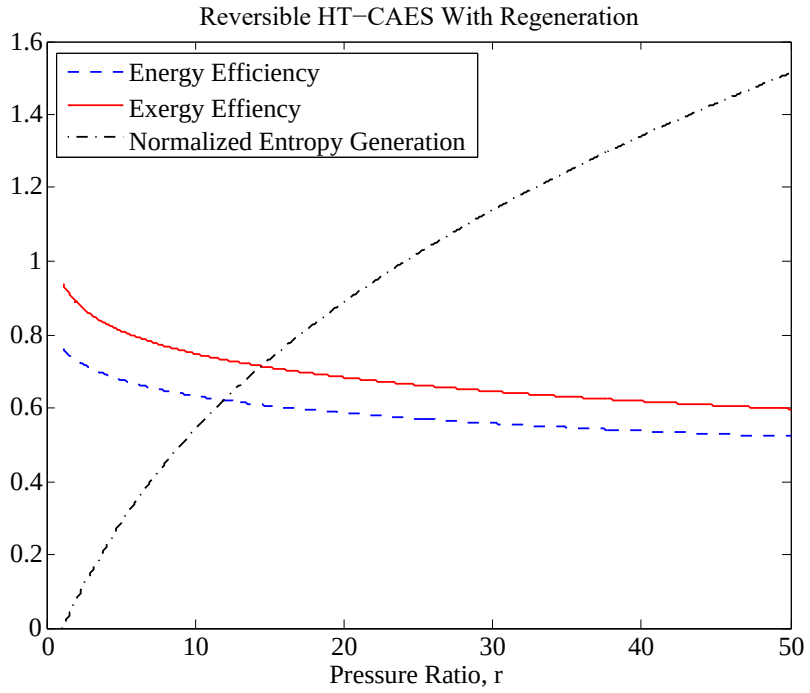

With regeneration as a function of the pressure ratio, r.

For an internally reversible HT-CAES system with regeneration, the optimum operating pressure occurs at unity, as measured by the maximum energy and exergy efficiencies along with the coincident minimum entropy generation. However, at a pressure ratio of unity the power output is zero. Therefore to achieve finite time processes, and for the system to become operational, entropy must be generated. This contradicts the Gouy-Stodola theorem of heat engines, which demonstrates that maximum output power correlates with minimum entropy generation. In section 4.4, internal irreversibility's and thermal energy storage efficiencies are taken into consideration to determine whether minimization of entropy generation may lead to conclusive design guidelines in a real system.

2.23 Internally Irreversible HT-CAES With Regeneration

Consider the regenerative HT-CAES system, Figure 34, with internal irreversibilies and TES inefficiencies. The analysis is similar to the procedures involved in the reversible case. However,

the temperatures, T_2, T_5, T_3, and T_6 must be determined as functions of other operating parameters. Using isentropic component efficiencies, regenerator effectiveness, and an energy balance of the regenerator, results in the following temperatures corresponding to Figure 34.

$$T_2 = T_1\left(1 + \frac{1}{\eta_c}(r^{\alpha} - 1)\right) \tag{16}$$

$$T_5 = T_4\left(1 - \eta_T(1 - r^{-\alpha})\right) \tag{17}$$

$$T_3 = T_2 + (T_5 - T_2)\eta_R \tag{18}$$

$$T_6 = T_5 + T_2 - T_3 \tag{19}$$

Where η_c, η_T and η_R are the compressor, turbine and regenerator efficiencies, respectively.

2.23.1 First Law Efficiency

Starting with equation (1) and undertaking a similar procedure, which arrived at equation (3) and (11), results in equation (20), where η_H is the TES retrieval efficiency.

$$\eta_I = \frac{T_4 - T_5}{T_2 - T_1 + (T_4 - T_3)/\eta_H} \tag{20}$$

Using temperatures (16) through (19) results in equation (21)

$$\eta_I = \frac{\eta_T\eta_H\eta_C(1 - r^{-\alpha})}{(\eta_H + \eta_R - 1)\, r_T^{-1}(r^{\alpha} - 1) + \eta_C\eta_R\eta_T(1 - r^{-\alpha}) + \eta_{Carnot}\eta_C(1 - \eta_R)} \tag{21}$$

Where η_{Carnot} is the Carnot efficiency of the corresponding Brayton cycle, analogous to the HT-CAES cycle of Fig. 1(b), and is given by equation (22)

$$\eta_{Carnot} = 1 - \frac{T_1}{T_4} = 1 - r_T^{-1} \tag{22}$$

An optimum compression ratio can be found, which would result in a maximum energy efficiency by applying $(\partial\eta_I/\partial r) = 0$ whose solution gives

$$r_{opt}(\eta_{I,max}) = \left(1 + \sqrt{\frac{r_T\eta_C(1 - \eta_R)\eta_{Carnot}}{(\eta_R + \eta_H - 1)}}\right)^{\frac{1}{\alpha}} \tag{23}$$

Interestingly, the optimum pressure ratio, which leads to maximum energy efficiency, is independent of the turbine isentropic efficiency. In addition, when the regenerator effectiveness is unity, the optimum pressure ratio is also unity, matching that of Fig. 3.

2.23.2 Second Law Efficiency

Starting with equation (4) and undertaking a similar procedure that arrived at equations (6) and (13), results in equation (24)

$$\eta_{II} = \frac{T_4 - T_5}{T_2 - T_1 + \frac{Mc}{\dot{m}c_p t}(T_{max} - T_4) - T_1\frac{Mc}{\dot{m}c_p t}\ln\left(\frac{T_{max}}{T_4}\right)} \tag{24}$$

Where the mass and specific heats of the air and TES medium are related by equation (25)

$$\frac{Mc}{\dot{m}c_P t} = \frac{T_4 - T_3}{\eta_H (T_{max} - T_4)} \tag{25}$$

Substituting equations (16) through (19) and equation (25) into equation (24) and simplifying results in equation (26)

$$\eta_{II} = \frac{\eta_T \eta_H \eta_C (1 - r^{-\alpha})}{(r^{\alpha} - 1) r_T^{-1} (\eta_H - A + A\eta_R) + A\eta_T \eta_C \eta_R (1 - r^{-\alpha}) + \eta_{Carnot} A \eta_C (1 - \eta_R)} \tag{26}$$

Where

$$A = 1 - \frac{\ln(r_H)}{r_T (r_H - 1)} \tag{27}$$

An optimum compression ratio can be found, which would result in a maximum exergy efficiency by applying $(\partial \eta_{II}/\partial r) = 0$ whose solution gives

$$r_{opt}(\eta_{II,max}) = \left(1 + \sqrt{\frac{\eta_C (1 - \eta_R) \eta_{Carnot} [r_T (r_H - 1) - \ln(r_H)]}{(r_H - 1)(\eta_R + \eta_H - 1) + (1 - \eta_R) r_T^{-1} \ln(r_H)}} \right)^{\frac{1}{\alpha}} \tag{28}$$

Similar to the optimum pressure ratio leading to maximum energy efficiency, equation (23), the optimum pressure ratio, which leads to maximum exergy efficiency, is independent of the turbine isentropic efficiency. In addition, when the regenerator effectiveness is unity, the optimum pressure ratio is also unity, matching that of Figure 36.

2.23.3 Entropy Generation

Starting with equation (7), and undertaking a similar procedure, which arrived at equations (9) and (15), however with an additional heat loss term associated with the TES irretrievable energy efficiency, results in equation (29).

$$\frac{S_{gen}}{\dot{m}c_p t} = \left(\frac{T_6}{T_1} - 1 \right) - \frac{T_4 - T_3}{\eta_H (T_{max} - T_4)} \ln \left(\frac{T_{max}}{T_4} \right) + \frac{2(T_4 - T_3)(1 - \eta_H)/\eta_H}{T_{max}(1 + \eta_H) + T_4 (1 - \eta_H)} \tag{29}$$

Using the temperatures in equations (16) through (19) and finding an optimum compression ratio, which would result in minimum entropy generation by applying $(\partial S_{gen}/\partial r) = 0$, results in equation (30) as the solution

$$r_{opt}(S_{gen,min}) = \left(\frac{\eta_T \eta_H \eta_C (1 - \eta_R) r_T + \eta_C \eta_T \eta_R B}{\eta_R \eta_H + r_T^{-1} (1 - \eta_R) B} \right)^{\frac{1}{2\alpha}} \tag{30}$$

Where

$$B = \frac{\ln(r_H)}{r_H - 1} - \frac{2}{r_H \frac{(1 + \eta_H)}{(1 - \eta_H)} + 1} \tag{31}$$

Typical trends of the energy efficiency, exergy efficiency and normalized entropy generation as functions of the pressure ratio, given by equations (21), (26) and (29), are illustrated in Figure 37

Figure 37: Energy Efficiency, Exergy Efficiency and Normalized Entropy Generation of the Regenerative HT-CAES Cycle

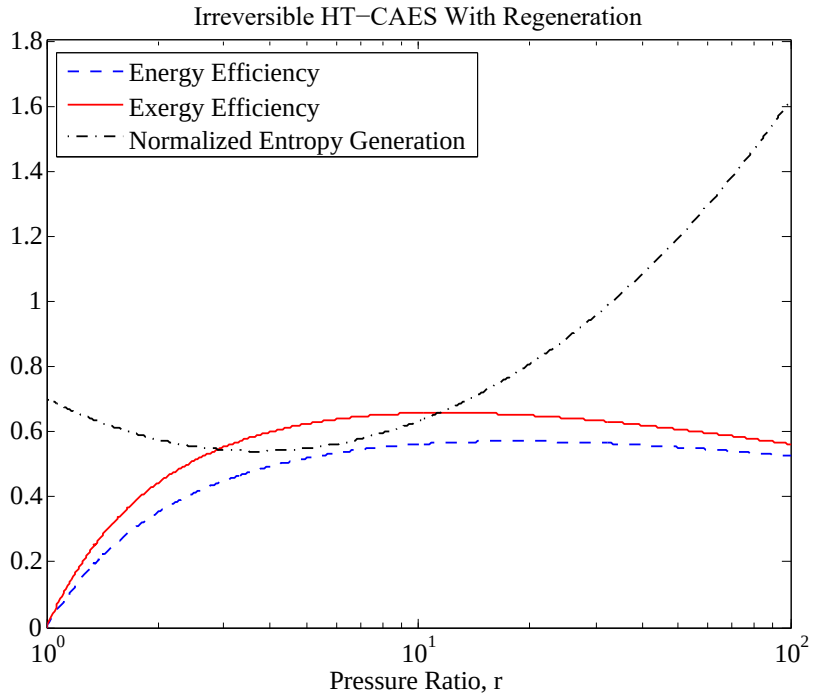

With $\eta_R = 0.6, \eta_c = \eta_T = \eta_H = 0.9, r_T = 3.33$, and $r_H = 1.5$

The results provided in Figure 37 are for $\eta_R = 0.6, \eta_c = \eta_T = \eta_H = 0.9$, $r_T = 3.33$, and $r_H = 1.5$. Since the HT-CAES system is essentially a broken Brayton cycle, where the compressor is decoupled from the turbine, the turbine power is entirely available for useful work. Therefore, the power output increases monotonically with increasing pressure ratio. Consequently, Figure 37 offers a design region in terms of the pressure ratio: the pressure ratio of a real HT-CAES system must be larger than $r(\eta_{I,max})$. The rational being that the system efficiency should only be compromised for a higher output power, depending on the specific applications of use and their priorities i.e., cost, size, performance, etc. Figure 37 reveals that the operational regime at minimum entropy generation is different from that at maximum exergy efficiency, maximum energy efficiency, and maximum work output. Indicating that a real HT-CAES system designed based on a minimum entropy generation criterion, in general, would not operate at maximum work output, maximum energy efficiency, or maximum exergy efficiency. It will be further shown, in a forthcoming discussion, that in an HT-CAES system, the regime of minimum entropy generation may become equivalent to the regime of maximum energy and exergy efficiency only under certain conditions.

The optimum pressure ratios corresponding to the maximum energy efficiency, exergy efficiency and minimum entropy generation, given by equations (23), (28) and (30), are plotted as a function of the regenerator effectiveness, in Figure 38. These results are plotted assuming $\eta_c = \eta_T = \eta_H = 0.9$, $r_T = 3.33$, and $r_H = 1.5$ and reveal the design regime corresponding to minimum entropy generation occurs at a lower pressure ratio than that which corresponds to maximum energy efficiency and/or maximum exergy efficiency, more specifically $r(S_{gen,min}) < r(\eta_{II,max}) < r(\eta_{I,max})$. In addition, as the regenerator effectiveness decreases the optimum pressure ratios, corresponding to all performance indices, increase and the gaps between them also increase. As evident by equations (23), (28) and their plots in Fig. 5, the optimum pressure

ratio leading to maximum energy and exergy efficiencies, at a regenerator effectiveness of unity, is unity. Moreover, the optimum pressure ratio corresponding to minimum entropy generation, at $\eta_R = 1$ and as given by equation (30), leads to a calculated value of 0.49, which is a nonoperational value. However, restricting the pressure ratios to values above unity, results in an optimum of unity. Therefore, at a regenerator effectiveness of unity, all optimum design conditions converge, which is in agreement with the reversible case, as given by Fig. 3. In contrast, a regenerator effectiveness of 0.5 leads to a convergence in the optimum pressure ratios leading to maximum output power, maximum energy efficiency, and minimum entropy generation, in a Brayton cycle [28].

Figure 38: Optimum Pressure Ratios Corresponding to the Maximum Energy Efficiency, Exergy Efficiency and Minimum Entropy Generation

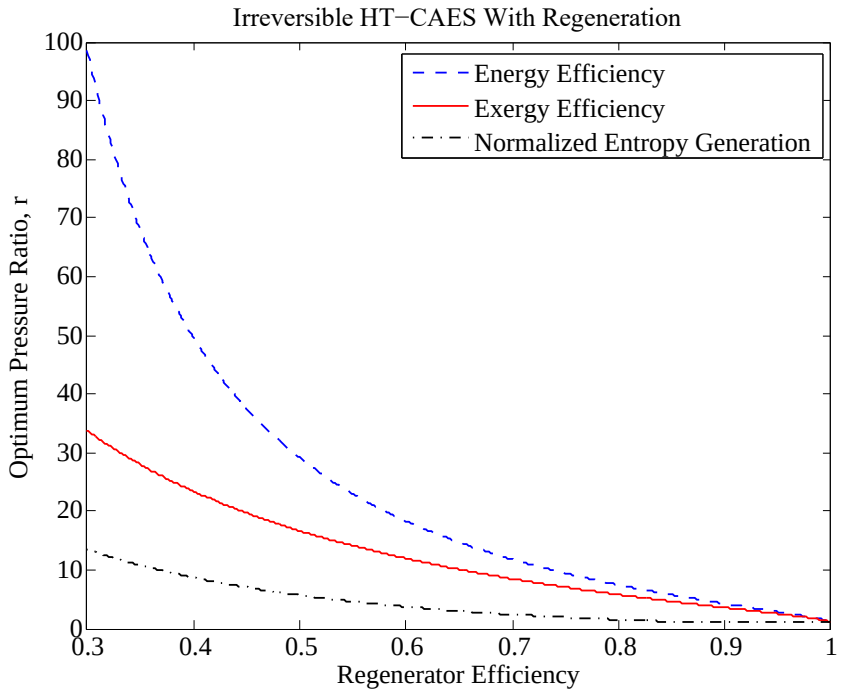

Are plotted as a function of the regenerator effectiveness

A plot of the optimum pressure ratios as a function of the temperature ratio, r_T, is given in Figure 39. The result was plotted for $\eta_R = \eta_c = \eta_T = \eta_H = 0.9$, and $r_H = 1.5$ and further demonstrate that optimum design criterions do not necessarily coincide. More specifically, as in the case with varying regenerator effectiveness, $r(S_{gen,min}) < r(\eta_{II,max}) < r(\eta_{I,max})$.

Figure 39: Optimum Pressure Ratios as a Function of the Temperature Ratio, r_T

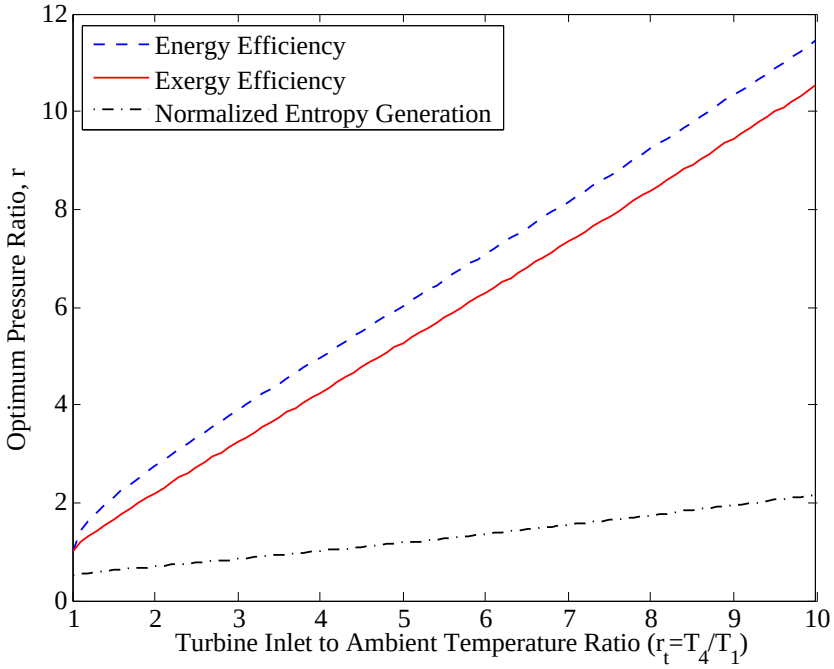

The effect of the thermal energy storage efficiency on the optimum pressure ratio design is illustrated by Figure 40, assuming $\eta_R = \eta_c = \eta_T = 0.9$, $r_H = 1.5$, and $r_T = 3.33$, for all performance indices given by equations (23), (28) and (30). The optimum pressure ratios for all indices increase with decreasing thermal storage efficiency. Additionally, Figure 39 reveals that the optimum pressure is again observed in the same order, $r(S_{gen,min}) < r(\eta_{II,max}) < r(\eta_{I,max})$, as that in Figure 38 and 39. Equation (30) is unbiased to the pressure ratio range, therefore although the optimum pressure ratio values corresponding to minimum entropy generation, at thermal storage energy efficiencies greater than 0.5, are below unity, this indicates that the actual optimum and realistic value, although non-operational, is in fact unity.

Lastly, the compressor isentropic efficiency is varied, and the effects on the optimal pressure ratios are investigated, as shown in Figure 41, assuming $\eta_R = \eta_H = \eta_T$, $r_H = 1.5$ and, $r_T = 3.33$. The trends exhibited by the optimal pressure ratios, as the compressor isentropic efficiency is decreased in Figure 41, are quite the opposite as those observed when the thermal energy storage efficiency is decreased, Figure 40. Nonetheless, the optimal pressure ratio range ranking remains consistent, namely, $r(S_{gen,min}) < r(\eta_{II,max}) < r(\eta_{I,max})$. Equation (30) is unbiased to the pressure ratio range. Therefore, although the optimum pressure ratio values corresponding to minimum entropy generation are below unity, at compressor isentropic efficiencies less than 0.95, this indicates that the actual optimum and realistic value, although non-operational, is in fact unity.

Figure 40: Optimum Pressure Ratios Corresponding to Maximum Energy and Exergy Efficiency and Minimum Normalized Entropy Generation

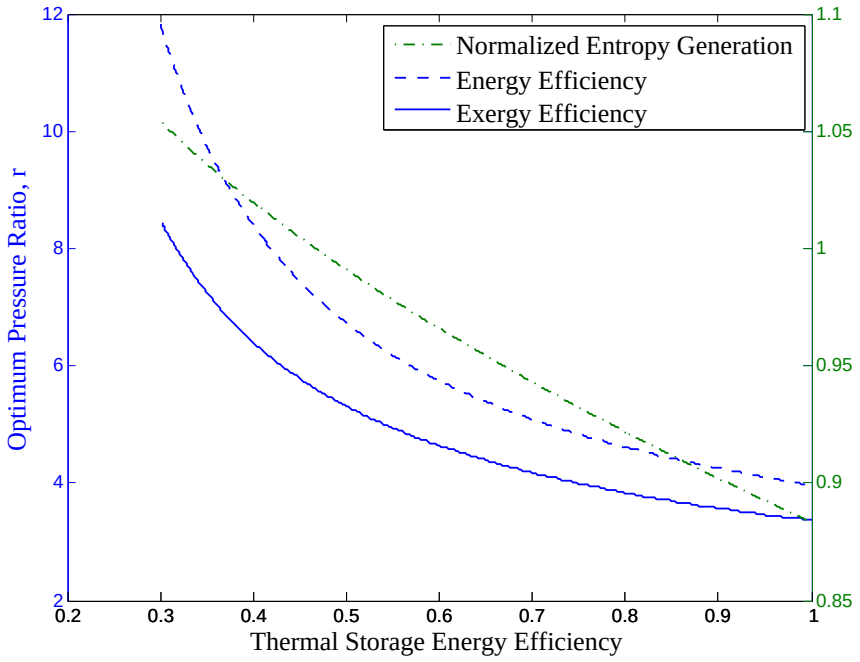

Figure 41: Optimum Pressure Ratios Corresponding to Maximum Energy and Exergy Efficiency and Minimum Normalized Entropy Generation (Varied Compressor Isentropic Efficiency)

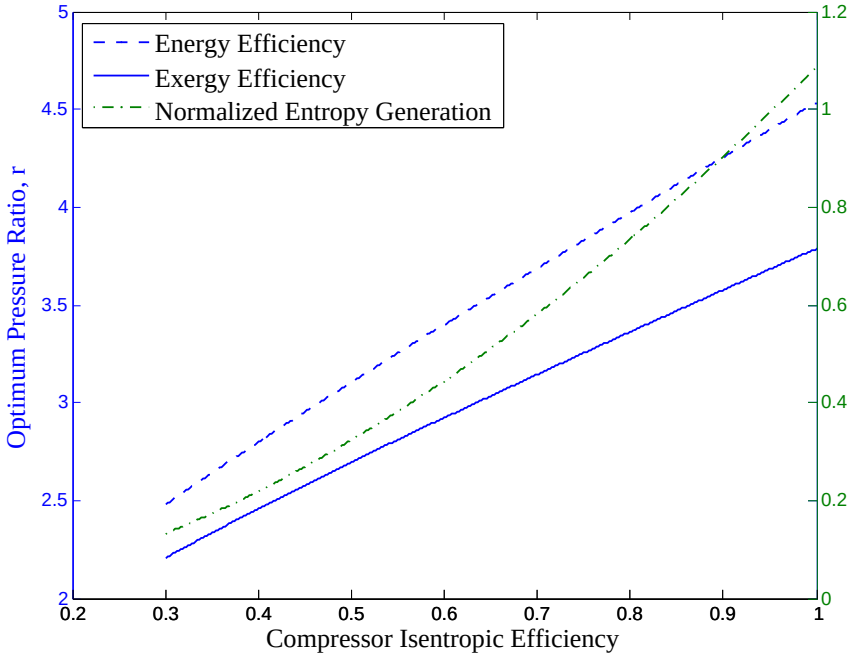

2.24 Discussion

The results of this work illustrate that it is inaccurate to generally interpret the generation of entropy as a measure of the losses in a hybrid thermal and compressed air energy storage system. The reason being, as was demonstrated, the minimization of entropy generation neither

correlates with the maximization of energy efficiency, exergy efficiency, or output power. As in the case for heat engines, it seems that the physical meaning of entropy generation is best described as a measure of the dispersal of energy, or the tendency of energy to spread out in space [28]. Therefore, the application of the second law of thermodynamics for the design of hybrid compressed air energy storage systems may not necessarily provide definitive design guidelines.

It's important, however, to note that in certain conditions the minimization of entropy generation may correlate with the maximization of energy efficiency, exergy efficiency, and power output. This was demonstrated in the case of an internally reversible and non-regenerative HT-CAES system. In the case of an internally reversible regenerative HT-CAES system, the maximum energy and exergy efficiencies did correlate with minimum entropy generation, however, this was not the case for the maximum output power. In practical applications it is almost unavoidable to neglect internal irreversibility's, and the additional energy retrieval benefit provided by a regenerator far outweighs the cost. Therefore, the more realistic results are those provided by the regenerative HT-CAES cycle with internal irreversibility's. It was observed, for a regenerative HT-CAES system with internally irreversibilies, that only in the case of a regenerative effectiveness of 100% did the minimum entropy generation correlate with maximum energy and exergy efficiencies, however not with maximum output power. In contrast to heat engines, where optimum design condition become coincident at a regenerator effectiveness of 50% [28]. It was also observed that the optimum pressure ratio corresponding to minimum entropy generation occurs at generally lower values than those corresponding to maximum exergy and energy efficiencies. Furthermore, the optimum pressure ratio corresponding to maximum energy efficiency was generally the largest. More specifically, the following order, $r(S_{gen,min}) < r(\eta_{II,max}) < r(\eta_{I,max})$, was a consistent trend throughout the analysis.

Combining the first and second laws of thermodynamics can provide further useful insights on the criterions necessary for coincident optimal design conditions. The turbine output energy is given simply by equation (32)

$$W_T = W_C + Q_{in} - Q_{out} \tag{32}$$

Eliminating Q_{out} from equations (7) and (32) and dividing by the total input energy, E_{input}, results in equation (33)

$$\eta_I = 1 - \frac{T_1}{E_{input}}\left[Mcln(r_h) + S_{gen}\right] \tag{33}$$

Similarly, eliminating Q_{out} from equations (7) and (32) and dividing by the total input exergy, $\mathbf{E}_{input}$, results in equation (34)

$$\eta_{II} = 1 - \frac{T_1}{\mathbf{E}_{input}} S_{gen} \tag{34}$$

The first and second law efficiencies, given by equations (33) and (34), reveal the specific conditions upon which the minimum generation of entropy becomes coincident with the maximization of the energy and exergy efficiencies. Only in the particular case where the input energy, thermal energy storage mass, specific heat, and maximum to minimum temperature ratio, r_h, are a constant does the minimum entropy generation coincide with maximum energy efficiency. Similarly, only the specific case where the total input exergy is a constant, does the minimum entropy generation coincide with maximum exergy efficiency. Otherwise, the entire

term in the vicinity of the entropy generation variable, S_{gen}, must reach a minimum for the energy and exergy efficiencies to reach a maximum, in equation (33) and (34). This is precisely the reason why optimal conditions corresponding to minimum entropy generation did not correlate with maximum energy or maximum exergy efficiencies in the irreversible hybrid thermal and compressed air energy storage system examined in this report.

2.25 Conclusion

A regenerative and non-regenerative hybrid thermal and compressed air energy storage system is designed based on the objective of minimum entropy generation. The cases of both internally reversible and irreversible conditions were investigated. It is shown that a hybrid compressed air energy storage system designed based on this criteria may operate at an energy and exergy efficiency which is lower than the maximum possible achievable. The main conclusion being that minimization of entropy generation does not necessarily correlate with minimization of energy losses in a real hybrid compressed air energy storage system. Only under certain circumstance does the minimum entropy generation coincide with maximum energy and exergy efficiencies. Moreover it was generally observed that the optimum operating pressure conditions based on maximum energy efficiency, maximum exergy efficiency, and minimum entropy generation can be ordered in the following manner: $r(S_{gen,min}) < r(\eta_{II,max}) < r(\eta_{I,max})$.

Nomenclature

CAES	Compressed Air Energy Storage	TES	Thermal Energy Storage
HT-CAES	Hybrid Thermal - CAES	AA-CAES	Advanced Adiabatic - CAES
r	Pressure Ratio	r_H	Maximum TES Temperature Ratio
r_T	Maximum Cycle Temperature Ratio	η_c	Compressor Isentropic Efficiency
$\dot{W}_t$	Turbine Output Power	η_R	Regenerator Effectiveness
$\dot{W}_c$	Compressor Input Power	η_T	Turbine Isentropic Efficiency
$\dot{Q}_{TES}$	TES Power/Heat input	η_H	TES Efficiency
W_c	Compression Energy	$\eta_{Brayton}$	Brayton Cycle Efficiency
Q_{TES}	TES Energy Input	$\eta_{Brayton,R}$	Regenerative Brayton Cycle Efficiency
W_t	Turbine Energy Output	η_{Carnot}	Carnot Efficiency
P	Pressure	S_{gen}	Entropy Generation
T	Temperature	r_{opt}	Optimum Pressure Ratio
γ	Ratio of Specific Heat for Air	E_{input}	Input Energy
M	TES Mass	$\mathbf{E}_{input}$	Input Exergy
$\dot{m}$	Mass Flow Rate	Q_{in}	Input Heat
R	Ideal Gas Constant of Air	Q_{out}	Output Heat
c_v	Specific Heat of Air at Constant Volume	c_p	Specific Heat of Air at Constant Pressure

c	TES Specific Heat	t	Total Charge or Discharge Time
η_I	HT-CAES Roundtrip Energy Efficiency (1^{st} Law Efficiency)	η_{II}	HT-CAES Roundtrip Exergy Efficiency (2^{nd} Law Efficiency)

CHAPTER 3:
Process Design

3.1 Basis of Design – Process Description

The HTH-CAES (High Temperature Hybrid Compressed Air Energy Storage) process can be described in two, distinct stages – charging and discharging.

During the charging phase, electricity provided by the grid is used to simultaneously power an air screw compressor, which loads a 100 cubic meter air storage vessel with compressed air, and electrically heat the HTES (High Temperature Energy Storage), a solid state thermal energy storage composed of refractory cement, to 2450 F via joule heating. The air screw compressor is a 30 HP Kaeser compressor that delivers 100 SCFM FAD (~0.058 kg/s) at 232 psia. The compressor charges the air storage tank from approximately 58 psia (the process' priming pressure) to 232 psia. The air screw compressor includes the HRS (Heat Recovery System) option to transfer heat captured by the oil lubrication system to a water circulation system during compression. This water circulation system is known as the LTES (Low Temperature Energy Storage). Ambient temperature water is pumped at 1.4 GPM and near atmospheric conditions from a polyethylene cold water tank and enters the compressor's HRS and exits at approximately 160 F. The heated water is then stored in an insulated, polypropylene hot water tank until the discharge cycle begins. The charge phase takes approximately six hours to complete.

During the start of the discharge cycle, the Ingersoll-Rand (IR) 70 kW PowerWorks unit has a hydraulic starter located in the gas generator turbine assembly. A high pressure coolant jet from a dedicated starter pump directs coolant at a drive turbine (sometimes called a Pelton wheel) on the gas generator shaft. This drive turbine accelerates the gas generator turbine and compressor to about 6,000 RPM to allow the compressor to provide enough air for start-up. The ramp-up time for this equipment is on the order of 1-2 minutes. The IR unit functions to introduce supplemental, compressed air to the process during discharge, and to provide a turbine to expand the compressed air and generate power. Supplementing the mass flow during the discharge phase, although this takes a large hit on the overall efficiency of the pilot plant, allows for less air storage volume, which lowers the $/kWh of the plant. Also during the discharge phase, compressed air is simultaneously discharged from the air storage tank. The mass flow rate of the discharging air is dependent on the test being conducted; multiple mass flow rates being relieved from the tank will be explored (e.g., 0.8 kg/s, 0.2 kg/s, and 0.058 kg/s). The discharging mass flow rate from the tank will be controlled via a mass flow controller. There is also a temperature controller that will stop the discharge process if the surface temperature of the air storage tank reaches below -30 F (the MDMT of the vessel). This is measured by a temperature probe near the outlet of the vessel. As air is being discharged, the air in the tank expands, and subsequently cools. Although the tank's surroundings are expected to contribute heat to the tank during discharge, the team still anticipates the discharging air to reach cold temperatures within the tank for some of the tests conducted.

The compressed air from the air storage tank, depending on the mass flow rate, may either be heated by the hot water stored in the charge phase via an air-to-water heat exchanger (the LTES HEX), or bypass the LTES HEX. Water flows through this HEX at 1.4 GPM, entering the HEX at approximately 120 F (a drop from 160 F due to predicted heat losses to the environment) and

exiting at approximately 100 F. The LTES HEX is only sized for small air mass flow rates (0.058 kg/s), and is designed to handle compressed air temperatures as low as -30 F. The pressure drop across this HEX is nearly negligible. The exiting air temperature is expected to be at least 70 F. For tests where this mass flow rate is exceeded, the air will bypass the LTES HEX. This allows the LTES to be used only for the six-hour discharge test. After being pre-heated by the LTES (or bypassing this cycle), the compressed air from the IR unit intermixes at the junction. The design pressure ratio, mass flow rate, and discharge temperature of the IR compressor varies widely depending on ambient conditions (Table 9).

Table 9: IR Compressor Design Pressure Ratio, Mass Flow Rate, and Discharge Temperature for Various Ambient Conditions

Ambient Temperature (F)	Pressure Ratio	Mass Flow Rate (kg/s)	Discharge Temperature (F)
0	4.22	0.86	340
60	3.71	0.74	403
120	3.15	0.61	447

The design combined mass flow rate is approximately 0.8 kg/s. The operating pressure of the process will be dictated by the pressure ratio of the IR compressor. This operating pressure will consequently determine the priming pressure of the tank (the minimum pressure to be maintained in the air storage tank that is achieved at the very end of discharge). After this air intermixes, the compressed air then enters an air-to-air recuperator, where it is further heated by a crossflow of the power turbine exhaust. This recuperator was salvaged from the IR unit. This exhaust air enters the recuperator at approximately 1000 F and 17 psia, and heats the compressed air to approximately 750 F. The pressure drop across this recuperator is approximately 1.8 psia. The inlet and exiting air temperature will depend largely on the test being conducted, ambient conditions, and the recuperator's effectiveness while operating slightly off-design. The heated, compressed air is then split between the HTES, where the air is heated to temperatures up to 2450 F, and the HTES bypass. Initially this ratio is 1:1. Heat stored in the refractory cement during the charge phase is transferred to the compressed air flowing through the HTES's void space. A temperature control valve on the HTES bypass controls the mass flow rate entering the bypass, and consequently controls the final inlet temperature of 1300 F to the IR unit. The temperature control valve is also on power control to ensure that the power generation limits of the IR are not exceeded, and to control the target power generated during testing. As air continuously flows through the HTES, the overall temperature of the HTES gradually decreases during discharge, therefore forcing more mass flow to enter the HTES and less through the bypass. At the very end of discharge, this entire mass flow goes through the HTES.

The compressed air, after being heated by the HTES, then enters the IR unit. The heated, compressed air is expanded first through the gasifier turbine, which generates the power to run the IR compressor. The exhaust from the gasifier turbine then enters the power turbine, where anywhere from 35-92 kW can be typically generated. The power output will depend largely on the efficiency of the process and the final inlet temperature, pressure, and mass flow rate. The exhaust air from the power turbine then enters the air-to-air recuperator used to pre-heat the compressed air prior to the HTES. A high level process flow diagram is shown in Figure 42 which is complemented by a detailed Piping and Instrumentation Diagram (P&ID) in Figure 43.

Figure 42: Process Flow Diagram of the System

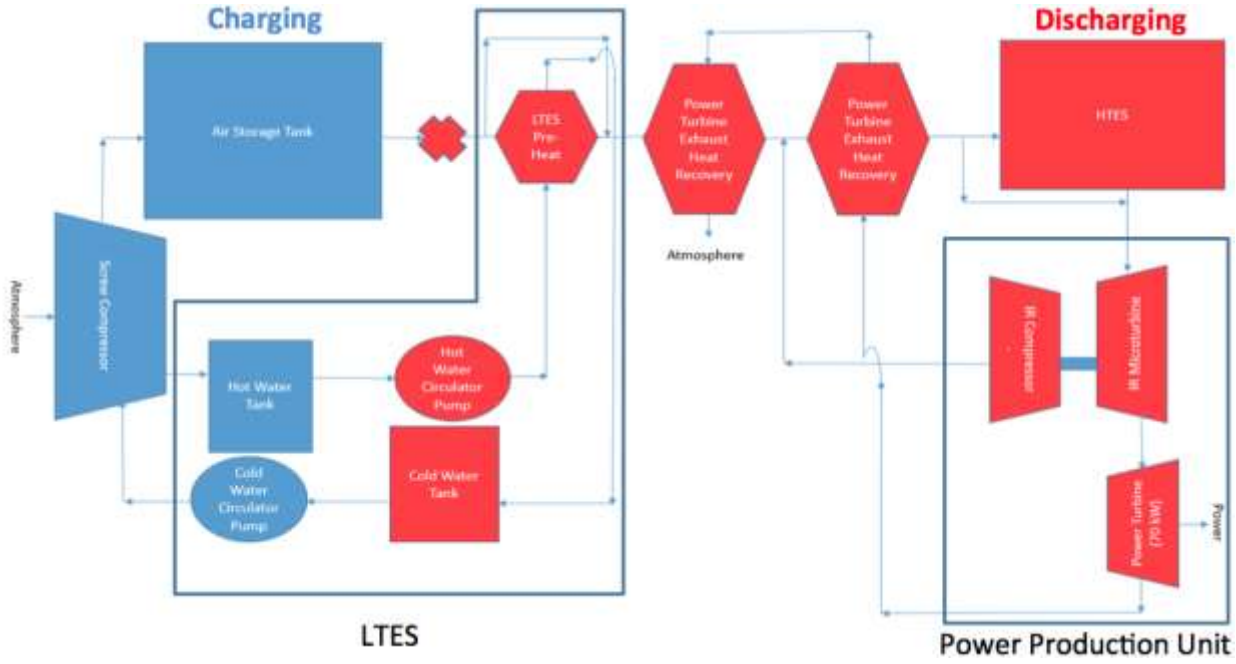

Figure 43: Piping and Instrumentation Diagram (P&ID)

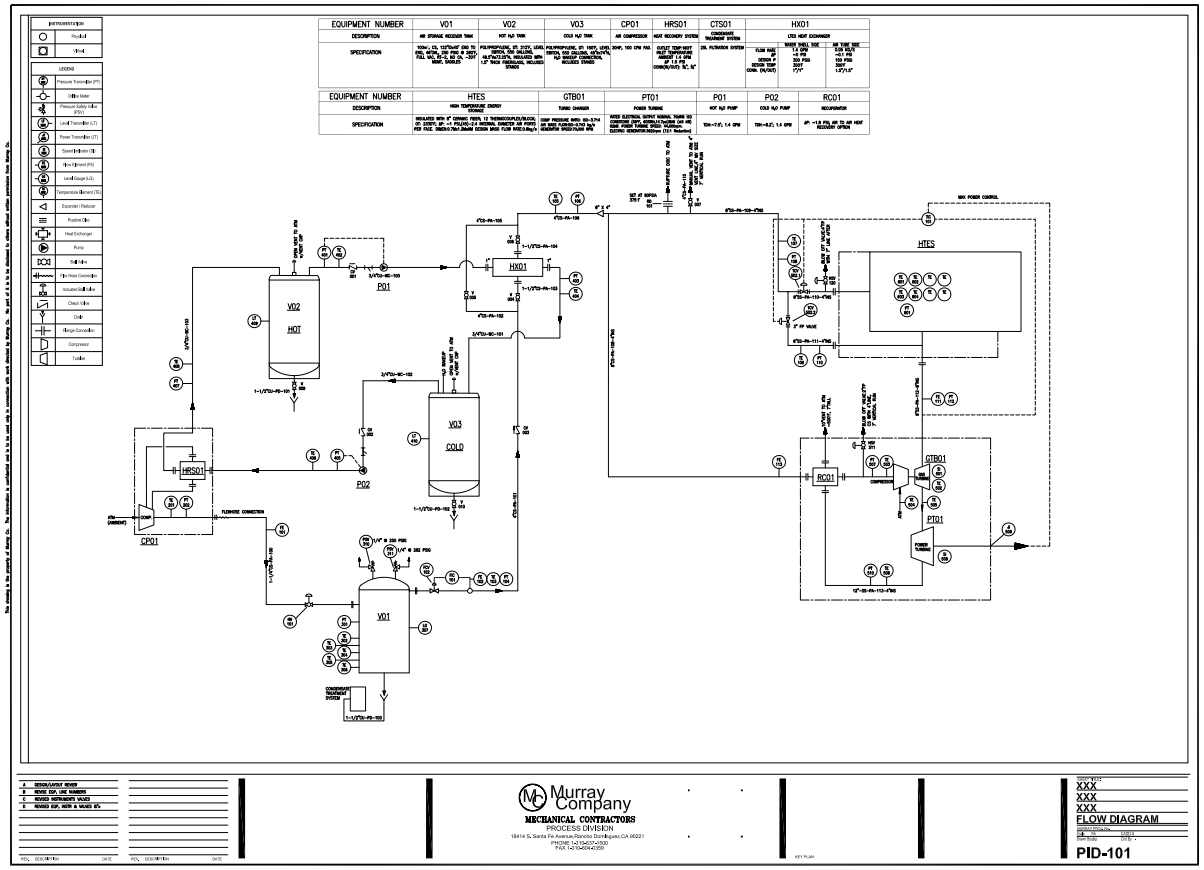

3.2 Mechanical Layout

The mechanical layout of the plant is an extremely compact design to minimize pressure drops due to bends and long runs, and hence maximize efficiency. Having a compact design also saves on material costs for the plant, and demonstrates the CAES product as more appealing due to the condensed footprint. Appendix C for 3-D renderings of the mechanical layout.

3.3 Process Development and History

3.3.1 Tank Storage Volume

The original intent for this pilot plant was to depend solely on compressed air directly from storage, such as tanks or an underground cavern. To satisfy the power generation target of ~74 kW (100 HP), it was calculated that 500 cubic meters of compressed air, stored at 217 psig, is necessary to discharge 0.2 kg/s over a six-hour period, and still maintain 58 psia (the prime pressure) within the tank at the end of discharge. It is important to note that the 74 kW power output would only be achieved with the assistance of a turbocharger which would supplement the additional 0.6 kg/s mass flow of compressed air, and the high-temperature energy storage which would heat the compressed air to the inlet design temperature of 1600 F. However, because of budgetary reasons, the original 500 cubic meter air storage volume was not considered feasible (five carbon steel tanks, each 100 cubic meters, quoted for $500,000). Therefore, it was determined that only one 100 cubic meter vessel can be purchased (quoted for $100,000). Because of this reduced storage volume, the mass flow rate from the tank must be proportionally reduced to maintain six hours of discharge, and therefore, the process relies more heavily on supplemental compressed air from turbocharger to make up for this reduction in mass flow rate. The mass flow rate from the tank is approximately 0.058 kg/s for a six-hour discharge period from 100 cubic meters of storage. It was also determined to not pursue priming the tank with paint (quoted for $4,638), as this was purely cosmetic.

3.3.2 Tank Material Selection

It was determined that carbon steel was the appropriate material choice for the air storage tanks for budgetary reasons. Given the minimum temperature limits of carbon steel, the process controls will maintain a minimum vessel surface temperature of -30 F (the MDMT of the vessel). Stainless steel is not a necessary material for compressed air, especially for a plant designed for a two-year service life.

3.3.3 Tank Insulation and Heating Strategies

Dynamic modeling shows that heat dissipated to the environment and internal convection strongly influences the internal temperature of the vessel during the charge and discharge phase. During charging, the thermodynamic modeling predicts that the heat of compression largely dissipates, and the vessel temperature will not rise 10 F above ambient temperature. The team explored using insulation, however, determined this would ultimately be counterproductive. Insulation would retain the heat of compression, and although there would be hotter, compressed air, less mass was stored, and would therefore have to further reduce the mass flow rate from the tank to meet the goal of a six-hour discharge. The team wanted the heat generated from compression within the tank to dissipate to the environment so the maximum possible mass can be stored for the tank volume. Also, during the discharge phase, there would not be a mechanism to counteract the low temperatures possible during expansion. With insulation, the environment could not contribute heat to the tank to counteract these lower temperatures. The research team explored other possibilities to heat the tank during the

discharge phase, such as attaching fins (both retractable and stationary), heating jackets, and internal piping for a hot medium. Ultimately, none of these options were pursued because of budget, however the research team believes the large surface area of the tank would have a tremendous influence on the internal temperature of the tank. The only test of concern is during the 0.8 kg/s test, where the tank would be entirely discharged, and the discharge period will happen quickly so there would not be enough time to absorb heat from the environment. The team expected low temperatures to be reached during this test, and would potentially discharge for a 10-minute period.

3.3.4 High Pressure vs. Low Pressure Tanks

The team explored the concept of larger, lower pressure tanks and smaller, higher pressure tanks. It was determined it was more economical to pursue smaller, high pressure tanks for a given mass of air.

3.3.5 Multiple Tanks for Multiple Pressures

The research team explored using multiple tanks at multiple pressure ranges. This had no measurable benefit to this process performance based on the modeling, besides increased surface area from having multiple tanks, hence more help from your environment to maintain the internal temperature of the vessel to ambient conditions. The team also explored using multiple tanks at a single pressure, however this had no measurable benefit besides increased surface area.

3.4 Single vs. Multiple Tanks at Single Pressure

It was determined that a single tank would be more economical than multiple tanks for the same given volume. Although there will be increased surface area for multiple tanks, this pilot plant is very cost-motivated, so a single, large tank at a single pressure was pursued.

3.5 Tank Instrumentation

The original design for vessel instrumentation called for 13 temperature indicators and 1 pressure indicator. A CFD analysis determined that temperature will vary vertically, and an adiabatic core will not form during discharge. At approximately $350 per probe, it was determined to limit the number of temperature indicators in the vessel for a more cost-effective design. It was decided that 14 indicators were an overdesign for this project. Instead, only 5 temperature indicators and 1 pressure indicator was implemented. This will measure temperature stratification in both the horizontal and vertical directions, and measure temperature at the coldest predicted point, adjacent to the outlet during discharge. The temperature indicator near the tank outlet will be used to as temperature control to ensure the vessel surface temperature stays above the MDMT of -30 F.

3.6 Tank Vessel Drains

To drain the vessel condensate directly to the surroundings and avoid costly waste haul-off, the vessel drains were designed to be routed to the screw air compressor's condensate treatment system. This was done via attaching the vessel drain directly to a manifold on the condensate treatment system (manifold quoted for $310).

3.7 Air Compressor Selection

Originally a 125 HP Kaeser screw compressor was selected (quoted for $44,944) with a mass flow rate of ~0.23 kg/s and FAD of 399 SCFM to satisfy a charge time of six hours for 500 cubic meters of air storage volume. Based on the specification selection of around six hours for charging, the 125 HP compressor was determined to be oversized for this process after it was determined that there will be only 100 cubic meters of air storage volume. A 30 HP Kaeser screw compressor (quotes for $16,745) with a mass flow rate of ~0.058 kg/s and FAD of 100 SCFM was therefore selected (a little more than 1/5 of the mass flow rate for 1/5 of the previously designated compressed air storage volume). A heat recovery option was also selected as part of the LTES process, an option that was not considered previously.

3.8 Ingersoll-Rand Powerworks Equipment

To save on power turbine costs and to introduce supplementary mass flow to the process through a turbocharger, a used, 70 kW Ingersoll-Rand Powerworks was acquired for this project. System specifications were subsequently catered to the operating limits and design parameters of this equipment. Although the system efficiency is drastically reduced, the addition of a turbocharger effectively lowered the plant's $/kWh due to the savings from forgoing purchasing additional air storage volume.

3.9 LTES Process

Originally, a compression heat recovery system utilizing Therminol 72 was proposed. This proposal was unrealistic for the screw compressor the team intended to purchase. The heat of compression is absorbed by the circulating lubricating oil injected at the inlet of the compressor, and the heat absorbed by the lubricating oil is removed by either an optional heat recovery system or an air fan. The cooled, lubricating oil is then recirculated to the inlet of the compressor. The LTES because the lubricating oil was determined to be very capital intensive (quoted for $77,000 for 1,100 gallons of Therminol 72). The pressurized air discharged from the screw compressor is further cooled by an air fan, reducing the temperature to near isothermal conditions. The optional heat recovery system in the process was determined to replace the originally proposed LTES. The heat recovery system works by using water or a water-glycol mixture to absorb the heat of compression that was first transferred to the lubricating oil – this simultaneously heats the LTES medium (water) and cools the lubricating oil to be recirculated within the compressor. The heated water is stored in an insulated hot water tank, and is later discharged during the discharge process to pre-heat the compressed air prior to the power turbine heat recovery and HTES.

3.10 HTES Re-Heating

Re-heating the gasifier turbine exhaust via re-routing the compressed air to the HTES was explored. Since there is a maximum power output that the Ingersoll-Rand equipment can generate, this was determined to not be a feasible idea for the pilot plant. Also, this would add to the overall capital cost and complexity of the pilot plant. It was determined this was an option that will be explored further for future plants.

3.11 LTES Optimization Considerations

We explored a variety of ways to improve the LTES process. One possibility explored the concept of reheating the LTES medium during the discharge phase by utilizing the power turbine exhaust heat prior to being discharged to atmosphere. This heat recovery using the

LTES medium may be before or after additional heat recovery processes take place with the power turbine exhaust heat before the compressed air is discharged to atmosphere. The most logical place to return this heat to the system would be prior to any other heating of the discharging compressed air. The LTES thermal storage medium may then be vaporized after heat is transferred from the power turbine exhaust, and then expanded through a power production unit to generate additional power to supplement the CAES plant power production. Or, the process may be designed so that the LTES medium is either a gas or liquid, and sent to a heat exchanger where the LTES medium transfers heat to the discharging compressed air to pre-heat the compressed air. None of these options were pursued for the pilot plant due to the limited impact on the overall efficiency of the plant.

3.12 Chilling Inlet Air to Compressor

To minimize the increase in temperature of the compressed air relative to the environment, the team proposed cooling the incoming air before compression using a cross flow of a cooled thermal fluid medium. Cooling the incoming air before compression also improves the overall efficiency of the compressor. Cooling the incoming air reduces the volume of the incoming air, increasing its density, and therefore allowing the work done by the compressor to be less, and hence the required power input to be reduced. This pre-cooling may also occur to improve the efficiency of a compressor in a turbocharger. This process improvement will have the effect of reducing the required work needed to compress the air to a desired pressure while also producing compressed air that is at a lower temperature so that it loses less energy to the environment. This process will concurrently warm the thermal fluid medium to room temperature which will be useful in the discharge phase of the process. During the discharge cycle of this process, when the compressed air expands to generate energy, the air is cooled during expansion. As the air is cooled during the discharge cycle, the heat captured in the cooling medium is used, now at room temperature, during the charge phase, to heat this cooled air to temperatures near room temperature. This increases the amount of energy the warmed air can produce. Because the heat added to the air came from incoming room temperature air, this additional energy comes at no thermodynamic cost. Also, because the expanding air reaches cold temperatures, the thermal fluid medium is cooled to very low temperatures by this process. This cooled thermal fluid medium is what is used in the first step to cool the incoming room temperature air. Thus, a two-step cycle is created thereby the incoming air to be compressed is cooled by the air expanding to produce energy with the thermal fluid medium transferring the energy in between. However, it was determined that this process will not be implemented in the pilot plant and pursued further in future plants.

3.13 Single-Speed vs. VFD for Compressor

The option of pursuing a variable frequency drive on the air compressor was explored. However, because of the added cost of additional equipment, the near-negligible improvement to the overall efficiency of the plant at this scale, and the limited pressure range that the compressor could operate at, it was determined that it will not be pursued for the pilot plant, and option to look into further as the project is scaled up. A single-speed VFD compressor was purchased.

3.14 Compressor Type Selection

A few compressor options were explored centrifugal, reciprocating, and screw compressors. It was determined that an air screw compressor would be the best fit and most economical for this process based on the pressure specifications and mass flow rate requirements.

3.15 Multiple Compressors

Using multiple compressors, discharging at incrementally increasing pressures, was explored briefly. It was determined that this modification would be too capital intensive for the pilot plant, and provides little long-term benefit for this scale. It was determined that this option may provide some long-term economic benefit to plant operating and maintenance costs as plants continue to scale up.

3.16 Single vs. Dual LTES Pump Design

To come up with a more cost-effective LTES design, two pump designs were explored – the use of dual vs. single water circulation pumps for the LTES. It was determined that dual pumps would ultimately be more cost effective and simplistic than the single pump design at this scale. Small, water circulation pumps are inexpensive ($100), and a single pump design would require multiple actuated ball valves to implement. The overall cost of the dual pump design was determined to be less than the single pump design. This idea will be explored further as the pilot plant scales.

3.17 LTES Heat Exchanger and Bypass

To meet the budget for the LTES heat exchanger, the team decided to size this heat exchanger for only the six-hour discharge case (when process experiences the least amount of mass flow coming from the tank, and hence through the LTES heat exchanger). Static and dynamic modeling shows that the LTES is rather ineffective in improving efficiency, especially as the mass flow rate from the tank increases, and the fixed flow rate of heated water raises the compressed air temperature only slightly. Therefore, the team planned to operate this process in the LTES HEX bypass for the majority of the tests when there is a high mass flow rates from the tank. The LTES HEX was selected and sized for this small flow of 0.058 kg/s (quoted for $634). The team received quotes for the tests for entirely discharging from the tank at 0.8 kg/s (quoted for $7,200) and it was determined this was not a worthwhile option to pursue for this process at this scale.

3.18 LTES Water Tanks

Metallic tanks were looked into for the water tanks (both hot and cold water tanks quoted at $21,000 total). It was determined that the LTES water would not be stored under any pressure, and he water temperatures are manageable (between 60 F and 160 F), therefore polypropylene for the hot water tank (quoted for $2,600) and polyethylene for the cold water tank (quoted for $1,700) was selected. Not pursuing metallic tanks resulted in considerable cost savings. In addition, further cost savings were realized by having an open vent to atmosphere vs. the installation of pressure relieving devices in the instance of an overpressure event. Although this may result in some heat loss to the environment, it was determined that this heat loss would be negligible.

3.19 LTES Piping Material Selection

Multiple piping materials were explored for the low pressure, water circulation system within the LTES, including PVC, carbon steel, copper, santoprene, and additional thermoplastic materials. It was ultimately determined that copper will be pursued as the most cost effective option. Santoprene, although the material is more cost effective per linear foot compared to copper, requires the use of cable trays which makes this a less cost-effective option than copper pipe. It was also determined that the majority of PVC pipe is unable to handle the

operating conditions, and higher temperature rated PVC piping were not as cost competitive. Copper is also a superior corrosion resistant material compared to carbon steel. The team decided to not select carbon steel due to the possibility of stagnant water remaining in the piping for long durations of time, since the plant is not intended to be operated continuously.

3.20 Compressed Air Piping Material Selection and Sizing

Carbon steel and 304L stainless steel were selected for the majority of the piping for compressed air, while 304H stainless steel was selected for the high temperature combined flow discharge from the HTES for its superior thermal resistance. Piping was sized for velocity and minimizing pressure drops to maintain the efficiency of the system. HTES manifold was designed to insulate temperature exposure to upstream piping and valves, which are not rated for high temperatures. Insulating gaskets were also used to prevent high temperature exposure to upstream equipment.

3.21 HTES Discharge Piping Material Selection

Multiple material options were explored for the high-temperature HTES discharge piping. With an initial combined flow temperature specification requirement of 1600 F, and operating pressures of approximately 4 barometric, Inconel appeared to be the best-suited material for piping and valves downstream of the HTES. At approximately $2,000 per foot, 8" Inconel piping was determined to be uneconomical to pursue for this project. The team lowered the combined flow temperature specification to 1300 F to use 304H stainless steel, effectively lowering the material cost by a more than factor of five (quoted at $450 per foot). Lowering this temperature specification led to more economical options for hot valves. Inconel valves were quoted at $310,000 – making this process unfeasible. Instead, only stainless steel valves were pursued for the high temperature processes. There is a concern of generating enough power in the power turbine at these lower temperatures, since there is a chance that most of the energy will be used to power the turbocharger, leaving a low energy compressed air stream entering the power turbine. This is a risk the team was willing to take to meet the project budget.

3.22 Power Turbine Heat Exhaust Recovery Placement

Several options were explored for how to best recover heat from the power turbine exhaust. Such options included pre-heating the turbocharger compressor discharge directly, pre-heating the compressed air prior to the turbocharger compressor junction, and multiple recuperators in series. Through static modeling and efficiency calculations for all of the options explored, it was determined that the most ideal placement of this recuperator would be downstream of the turbocharger junction, so that the combined stream compressed air stream, prior to being further heated within the HTES, would be heated directly by the power turbine exhaust. After heating the compressed air through this single recuperator, the lower temperature power turbine exhaust is relieved to atmosphere.

3.23 Power Turbine Heat Exhaust Recovery Exchangers

While exploring the possibility of multiple air-to-air heat exchangers for pre-heating the compressed air with the power turbine exhaust, the search became laborious. The majority of the vendors contacted did not have an off-the-shelf recuperator that fit the needs of the project. The air-to-air heat exchangers for the specifications required for the process therefore resulted in a custom design, and was therefore very capital intensive, heat exchangers. It was determined instead to use the existing recuperator within the Ingersoll-Rand equipment. This

recuperator is only slightly off-design for this process specification, and added no additional equipment cost for the pilot plant.

3.24 Hot Valve Placement and Loss of Load Considerations

Multiple options for hot valve placement were explored to adequately isolate the upstream piping and equipment from the downstream, high temperature process, and also protect the downstream equipment from a loss of load scenario. After receiving the quotes for multiple valve configurations, it was determined that these options were uneconomical to protect the downstream equipment during a loss of load. The team determined there is a potential risk of sacrificing the power turbine during a loss of load. The potential cost of replacement is drastically less than the cost of the piping and valves required to protect form this process scenario. Only a single hot valve was purchased to insulate the upstream piping, valves, and equipment, and prevent backflow into the HTES bypass during a sudden pressure drop upstream.

3.25 HTES Bypass Line Operation and Plumbing

The HTES bypass line is used to maintain a target combined compressed air temperature to the inlet of the Ingersoll-Rand Powerworks equipment. During normal operations, this line starts off with half of the mass flow rate, and as the temperature of the HTES drops during discharge as more heat is transferred to the compressed air, the mass flow through the bypass line also decreases, and more flow is sent through the HTES to reach the target combined temperature. The outlet of the bypass line ties directly to the manifold of the HTES to drop the temperature of the air discharging the HTES to the target temperature of 1300 F. Tying the bypass line directly to the manifold drops the design temperature of the discharge piping leaving the HTES, permitting the use of stainless steel versus a more capital-intensive alloy, such as Inconel, that is able to handle the much higher temperature air discharging directly from the HTES. The bypass line is sized and designed to handle the full mass flow rate during emergency situations where the HTES must be entirely bypassed. There is a swing check valve, also sized to handle full flow, located downstream of the temperature control valve to insulate the piping upstream from the high temperature process downstream of the HTES and bypass line.

3.26 Aspen HYSYS: Simulation and design

Aspen HYSYS, the energy industry's leading process simulation, was integral to the process simulation and design of this system. HYSYS proved to be a robust process optimization tool and was used for steady state simulations in this project. The company also granted the team access to an extensive property database that helped optimize this process at every design desired point in. The rapid process simulation that was enabled by using HYSYS allowed for a feasibility analysis of the entire plant where the team could model all the processes, size the equipment, identify the flow characteristics and run rapid iterations. Snapshots from the HYSYS software are presented in Appendix D.

Below is a list of examples of processes where HYSYS was instrumental:

- Steady state charging and discharging processes, various ambient conditions and mass flows
- Tank charging and discharging dynamics
- LTES design – pumps, tanks, heat exchanger and efficiency contribution
- HTES pressure drop and bypass control valve modeling
- Roundtrip efficiency calculations and predicted power outputs

- Process specification selection and identification
- Power turbine exhaust heat recovery recuperate placement and sizing
- Equipment sizing: piping, control and blow off valves, tank and compressor, etc.

CHAPTER 4:
Thermal Energy Storage

4.1 Principle of Operation

This chapter focuses on the design and analysis of one of the main components of the plant that is high-temperature energy storage (HTES). The principle of operation of HTES, as also explained briefly in Chapter 2, is to convert the surplus of electricity directly to heat through Joule Heating. The thermal energy is then stored in a well-insulated solid material that is capable of withstanding high temperatures. When the electric power is needed, usually during the peak demand period, air is run through HTES and is heated up to the desired temperature. The hot air then goes to an expander, either reciprocating or turbo, and turns a shaft that is connected to a generator. The discharge air comes either from the storage tank or is generated online via turbocharger. The HTES, as a result, is an unsteady heat exchanger that absorbed the energy during the charge phase and returns it during the discharge phase. The ratio of the energy returned during the discharge phase to the energy absorbed during the charge phase measures the roundtrip efficiency of the thermal energy storage. The main loss component is usually associated to energy losses through insulation during the shift time between the charge and discharge. The loss obviously depends on the insulation thickness, and is usually in the range of 5%-10%. Figure 43 depicts the bare storage body of one of the modules of the HTES.

Figure 43: One Bare Storage Module of HTES

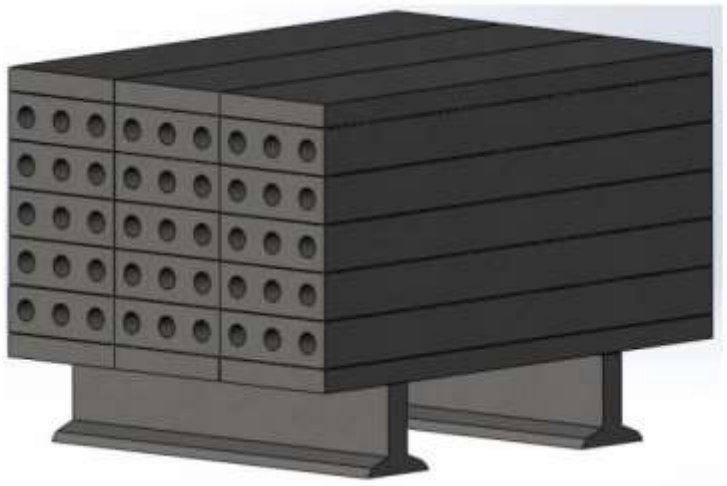

4.2 Design Flow Chart of HTES

The design concept of the HTES is shown in Figure 44. There are two main criteria that must be met for the design to be considered acceptable. Stress criteria states that the maximum hoop stresses developed under internal pressure during the discharge phase must not at any time exceed a maximum tensile stress. The maximum tensile stress is obtained by building a safety factor of three into the maximum tensile stress of the refractory, which itself is obtained based on the minimum hot modulus of rupture of the material at the service temperature. The thermal criteria require that:

- the maximum temperature of the block must always remain below the maximum continuously operating temperature of the electric wires (1680K),
- the temperature distribution within the concrete during the charge phase should be acceptably uniform, say to within 20 K,
- Given the wait time between charge and discharge, the design must be such that the energy deposited in the refractory during the charge phase should be retrievable during the discharge phase for maximal roundtrip efficiency even for a fully adiabatic thermal storage. This constraint imposes a length scale for spacing of the air holes that should be smaller than thermal diffusion length scale over the charge and wait time.

Figure 44: Conceptual System Design of the High-Temperature Energy Storage (HTES)

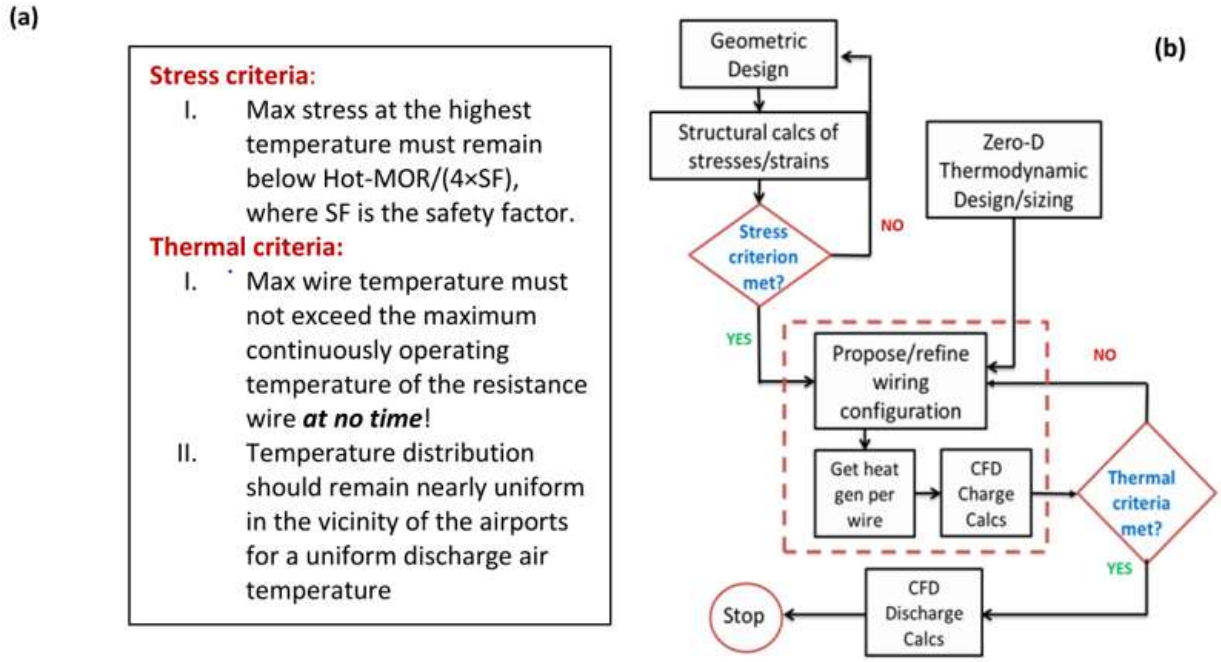

4.3. Thermodynamic Modeling and Sizing

The sizing of HTES is done based on the discharge phase. Knowing how much energy is to be deployed to the end user and for how long coupled with thermodynamic efficiency of thermal-to-electricity conversion enables sizing of HTES. In doing so, the energy density per volume is imposed by the mass density and heat capacity of the storage material. The higher these properties, the more compact the storage and the higher the energy density per unit mass and volume. This generally makes the storage more attractive since real estate could be prohibitively expensive at certain locations. It also lowers the $/kWh of thermal energy stored. To size the HTES, the total energy absorbed by air during the discharge phase is calculated. That energy has to be stored in HTES. The equality of the two energies determines the volume of the storage medium, which together with the mass density of refractory determines the total mass of storage. The required energy balances are as follows:

*Power absorbed by **the air stream**:*

$$\dot{Q}_{abs,air} = \dot{m}_{air}(T_{\max} - T_{\min}) \quad (1)$$

*Energy absorbed by **the air stream**:*

$$Q_{abs,air,total} = \dot{Q}_{abs} \times t_{\text{discharge}} \quad (2)$$

The energy absorbed by the air has to be stored in storage medium, refractory concrete:

$$Q_{concrete} = Q_{abs,air,total} \quad (3)$$

Also,

$$Q_{concrete} = M_{conc} C_{p,conc} \left(T_{\max,\text{conc}} - T_{\min,\text{conc}}\right), M_{conc} = \rho_{conc} V_{conc} \quad (4)$$

Where M_{conc} is the mass of storage and ρ_{conc} and V_{conc} are also the density and volume of storage material. $C_{p,conc}$ is also the heat capacity of the refractory concrete which depends on the composition and is given. Figure 45 contains technical data of the refractory material used in this research. The expender purchased for this project has the design inlet temperature of 1144K with an isentropic efficiency of 83%. Thermodynamic calculations of the plant also reveal that the air temperature into HTES, after recuperator, is 720K. As a result, the energy absorbed by air over six hours of operation can be calculated from equation (2). The service temperature of the refractory, as shown in Figure 45, is 3200F = 2033K. Therefore, to increase the energy density of the refractory and lower the storage mass, and hence reduce the $/kWh of thermal energy stored, it is desirable to heat up the refractory to the highest possible temperature. Nonetheless a thermal design requirement of HTES is that the storage temperature should not exceed the maximum continuously operating temperature of the electric wires. The electric wires are Kanthal A (a mixture of Chromium, Iron and Aluminum) with the service temperature of 1680K. HTES was sized and designed for a maximum temperature of 1550K. It was done in consideration of the brittleness of Kanthal wires after multiple heating/cooling cycles.

Given that the turbo-expander has to be fed with a steady flow while HTES is an unsteady component in nature, a control strategy is required to satisfy this condition. A calculated fraction of the cold air into HTES is bypassed around it and is then mixed with the remaining portion that goes through HTES to moderates the temperature of the combined air stream down to the expander inlet air temperature, 1144K. Figure 46 schematically shows this setup. The setup is general and is an intelligent way to increase the energy density of the HTES and lower the $/kWh of thermal energy stored in HTES.

Given the output constraints of the plant, that is deploying 74kW for six hours, the result of thermodynamic analysis, equations (1) – (4), show that a volume of 6.5 m3 is required. Multiple rounds of refinements to meet the design criteria, stress and thermo-fluids, has resulted in the specs for HTES shown in Table 10. The thermo-mechanical analysis of this design will be presented later in this chapter.

Table 10: Geometric Specification of an Acceptable HTES Design

Length	9.6 m
Cross section (height × width)	0.79m × 1.18m
Number of holes	45
Hole diameter	0.061 m = 2.4 inch
Hole spacing (center to center)	0.131 m = 5.2 inch
Number of holes per row	9
Number of columns of holes	5

Figure 45: Technical Data Sheet of HTES Storage Medium Refractory

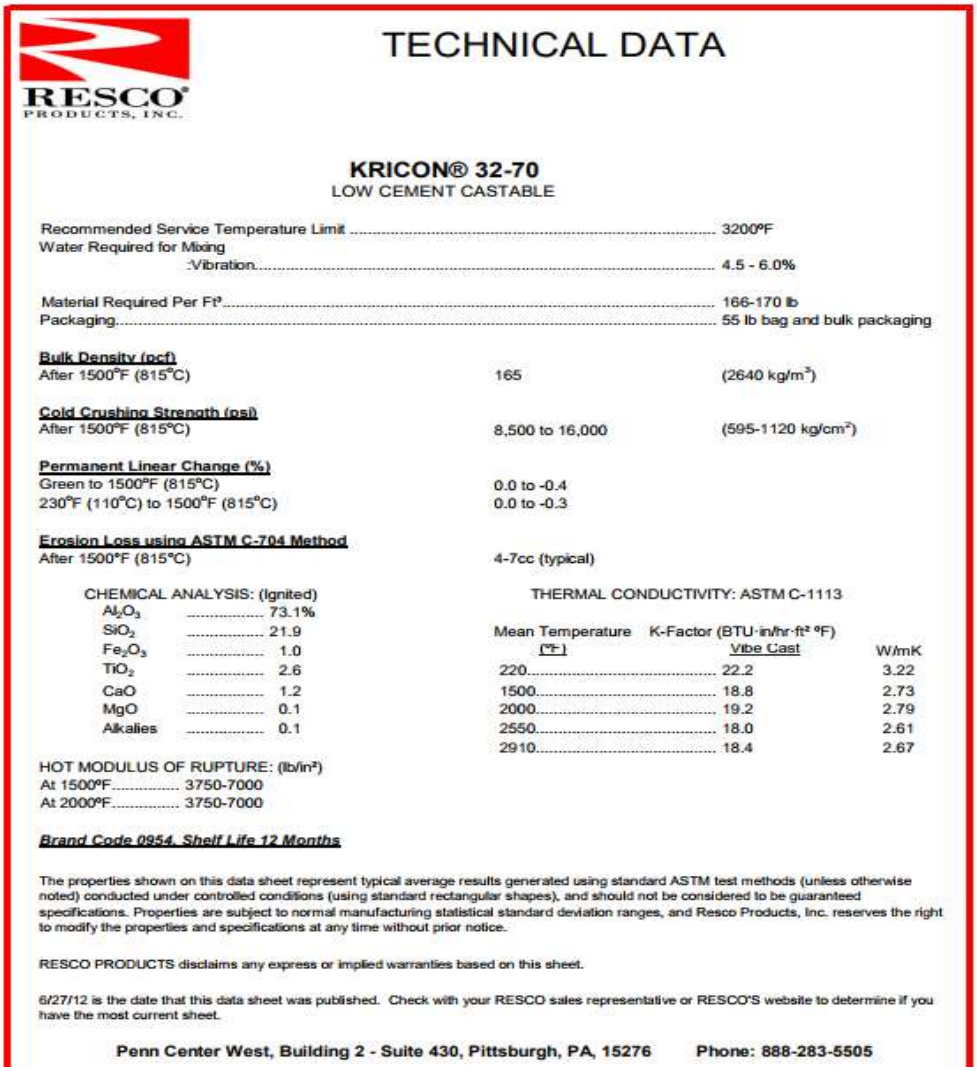

RESCO PRODUCTS, INC.

TECHNICAL DATA

KRICON® 32-70
LOW CEMENT CASTABLE

Recommended Service Temperature Limit		3200ºF
Water Required for Mixing :Vibration		4.5 - 6.0%
Material Required Per Ft³		166-170 lb
Packaging		55 lb bag and bulk packaging
Bulk Density (pcf) After 1500ºF (815ºC)	165	(2640 kg/m³)
Cold Crushing Strength (psi) After 1500ºF (815ºC)	8,500 to 16,000	(595-1120 kg/cm²)
Permanent Linear Change (%) Green to 1500ºF (815ºC)	0.0 to -0.4	
230ºF (110ºC) to 1500ºF (815ºC)	0.0 to -0.3	
Erosion Loss using ASTM C-704 Method After 1500°F (815°C)	4-7cc (typical)	

CHEMICAL ANALYSIS: (Ignited)

Al_2O_3	73.1%
SiO_2	21.9
Fe_2O_3	1.0
TiO_2	2.6
CaO	1.2
MgO	0.1
Alkalies	0.1

THERMAL CONDUCTIVITY: ASTM C-1113

Mean Temperature (ºF)	K-Factor (BTU·in/hr·ft²·ºF) Vibe Cast	W/mK
220	22.2	3.22
1500	18.8	2.73
2000	19.2	2.79
2550	18.0	2.61
2910	18.4	2.67

HOT MODULUS OF RUPTURE: (lb/in²)
At 1500ºF..... 3750-7000
At 2000ºF..... 3750-7000

Brand Code 0954, Shelf Life 12 Months

The properties shown on this data sheet represent typical average results generated using standard ASTM test methods (unless otherwise noted) conducted under controlled conditions (using standard rectangular shapes), and should not be considered to be guaranteed specifications. Properties are subject to normal manufacturing statistical standard deviation ranges, and Resco Products, Inc. reserves the right to modify the properties and specifications at any time without prior notice.

RESCO PRODUCTS disclaims any express or implied warranties based on this sheet.

6/27/12 is the date that this data sheet was published. Check with your RESCO sales representative or RESCO'S website to determine if you have the most current sheet.

Penn Center West, Building 2 - Suite 430, Pittsburgh, PA, 15276 **Phone: 888-283-5505**

Figure 46: Control Strategy to Keep the Air Temperature Out of the HTES Constant

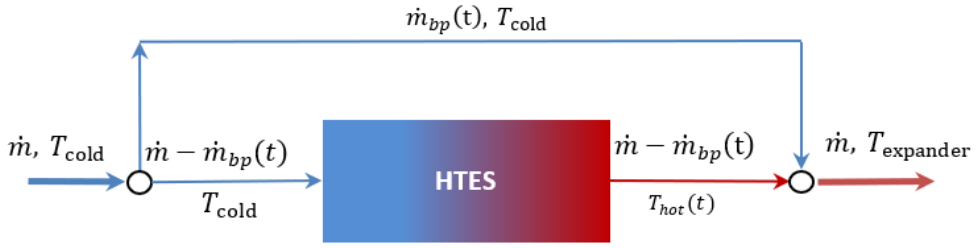

A safety factor of three has been considered in dimensioning the hole spacing (center to center) for mechanical stresses. Figure 47 shows one row of holes in HTES. A stack of five of these modules on top of each other constitutes the face of HTES.

Figure 47: One Row of the Face of HTES

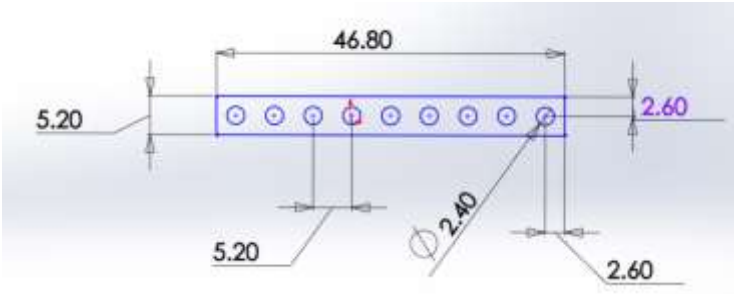

4.4 Structural Analysis

The HTES design process went through multiple iterations, mainly in an effort to both reduce the complexity of design and the cost of storage, hence a reduced $/kWh of stored thermal energy. Given the relatively low thermal conductivity of refractory concrete, the first round of design involved insertion of two components inside refractory: a) metallic fins to distribute the thermal energy uniformly within refractory, and b) air pipes (designed to ASME B31.3 code) to withstand the internal air pressure. Nonetheless, the cost was prohibitively high while the performance enhancement was minimal. As a result, both fins and the pipes were removed through multiple revision of the design. The final design therefore, entailed no metallic components, except the electric wires. An immediate advantage of this design was to allow very high temperatures in the body of storage for maximal energy density and minimal $/kWh of stored thermal energy. This section briefly presents the structural calculation that demonstrates the structural integrity of the current design under internal pressure and at high temperatures.

4.4.1 Mechanical Properties of Concrete

A reliable design of HTES entails a maximal Von-Misses stress that is always below a critical stress. The critical stress is determined by building a safety factor into the tensile yield stress of refractory. After consulting with multiple firms and experts, it became apparent that the tensile strength of refractory is empirically related to the Hot Modulus of Rupture (HMoR) of the material. The relationship is such that the tensile yield stress is roughly fourth of the HMoR. Choosing the minimum HMoR and considering a safety factor of 3, the maximum allowed stress that could be realized in the design is therefore ~25 bar.

Figure 48 shows the computational setup for one hole along with the predicted stress distribution around the hole. As shown the maximum Von-Misses hoop stress imposed under an internal pressure of four bar (the process pressure) is 7.25 bar. This is so that the maximum allowable tensile stress is 25 bar. Therefore, the design is acceptable with a build-in safety factor of more than six. Calculations were performed under initial temperature of 1600K and all mechanical properties, modulus of elasticity, tensile yield stress, thermal expansion coefficient, etc., were imposed at that temperature.

Figure 48: Finite Element Analysis of HTES Storage Design

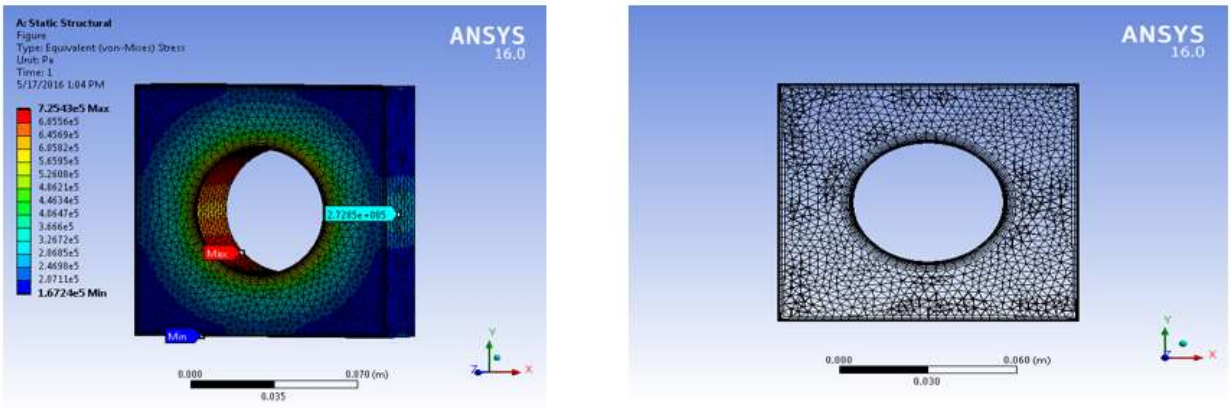

It should be noted that when the weight of the whole stack of HTES is considered, the stress distribution is even better since the weight of the structure counteracts the internal pressure. Therefore, the unit module, as considered in Figure 48, represents the outermost holes as the worst-case scenario.

4.4.2. Thermo-Fluids Design

After making sure that the design is structurally reliable under the process pressure at peak temperature, the next step is to do thermo-fluids performance calculations during charge and discharge. The charge design requirement is that the available energy has to be distributed within the refractory such that the temperature distribution is nearly uniform. This translates into an acceptable range for spacing of the electric wires along the length of the HTES. The rate of power deposited in each wire is calculated by dividing the total available electric power by the total number of wires. Generally speaking, one should be interested in a rate of heat generation, low enough to avoid thermal shock, given low thermal conductivity of refractory. The discharge design requirement, on the other hand, is that the air temperature out of HTES, after mixing with the bypass line, must always be equal to the expander inlet design temperature, in this case 1144K.

4.4.3 Charge Phase

To decide the wire spacing along the length of HTES to meet the uniform temperature distribution constraint during the charge phase an iterative process must be employed. One starts with a guess for wire spacing, calculates the number of wires required, determines the rate of heat generation per wire given the total power, and conducts simulations. If the spacing is larger than required, there will be a temperature gradient within the concrete –higher near the wire location and lower farther away. Any spacing less than required will result in minimal temperature gradient. Obviously, however, the ease of manufacturing and handling the wires should set a lower bound on how close the spacing should be. Several iterations resulted in a wire spacing of 2.8 cm, which is manufactural and results in an acceptable temperature field within HTES. Figure 49 shows the front face of the HTES. Figure 50 involves the result of computations after six hours of continuous charging along with the side view of the computational module. The depth of the module is 2.8cm, the same as the wire spacing. Given the periodicity of this configuration along the length of HTES, one module is sufficient to conduct the simulations.

Figure 49: A Front Face of HTES for Charge Calculations

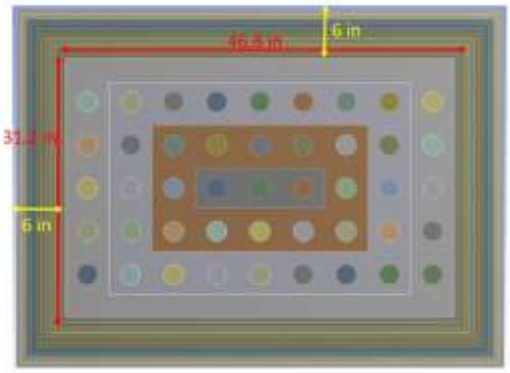

The 6-inch outer layer is the ceramic fiber insulation.

The insulation around the module, where the maximum temperature gradient is observed is six inches thick and the outer boundary condition is a winter time for maximum heat losses. It should be noted that during the charge phase the air pressure within the holes is atmospheric and there is no flow of air going through HTES.

Figure 51 shows the volume average temperature within refractory after charging for six hours. The bulk temperature is below the design temperature of 1550 Kelvin because of convective heat losses on the external boundary.

Figure 50: The Charge Phase Calculations

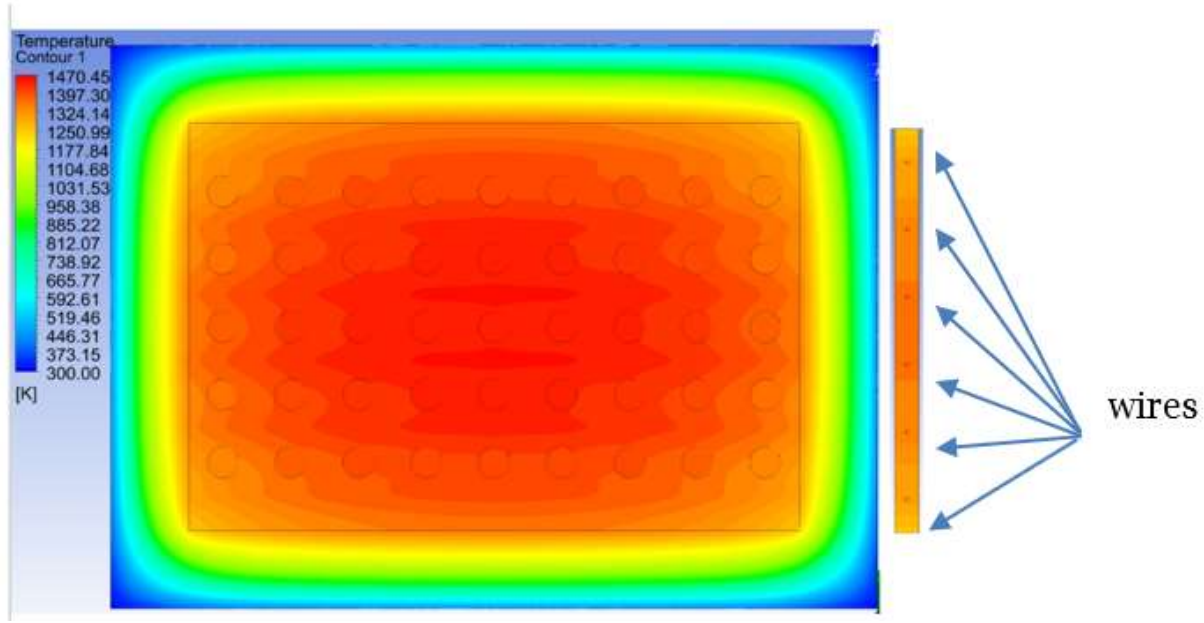

With the side view of the wires for one computational module of the charge phase

Figure 51: Volume Average Temperature in Refractory After Six Hours of Charging

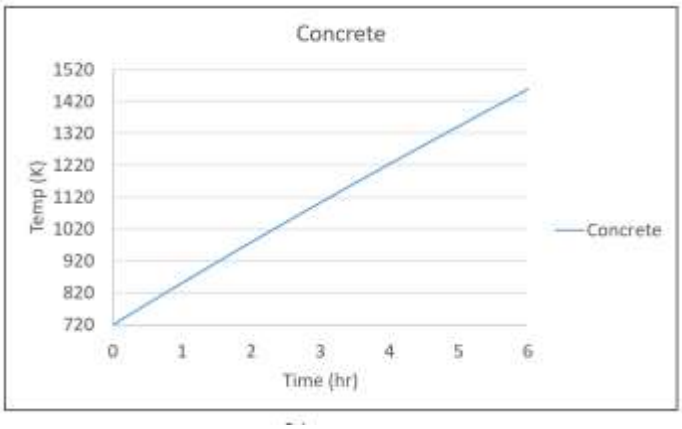

Also, as shown in Figures 52 and 53, considering different directions to quantify the temperature gradients within refractory during the charge phase, it is apparent that the current design produces an acceptable uniformity of temperature distribution in six hours.

Figure 52: Quantification of Temperature Distribution in Refractory During the Charge Phase

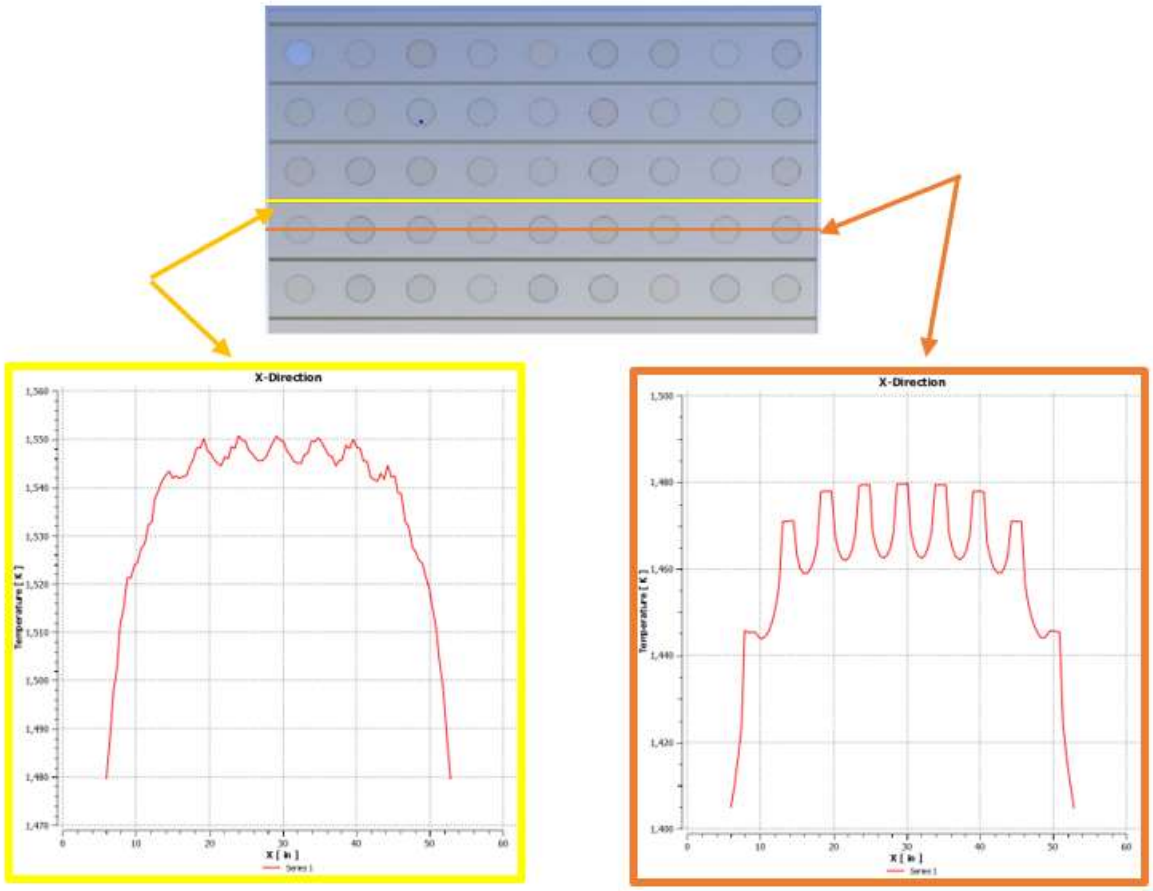

Figure 53: Quantification of Temperature Distribution in Refractory During the Charge Phase

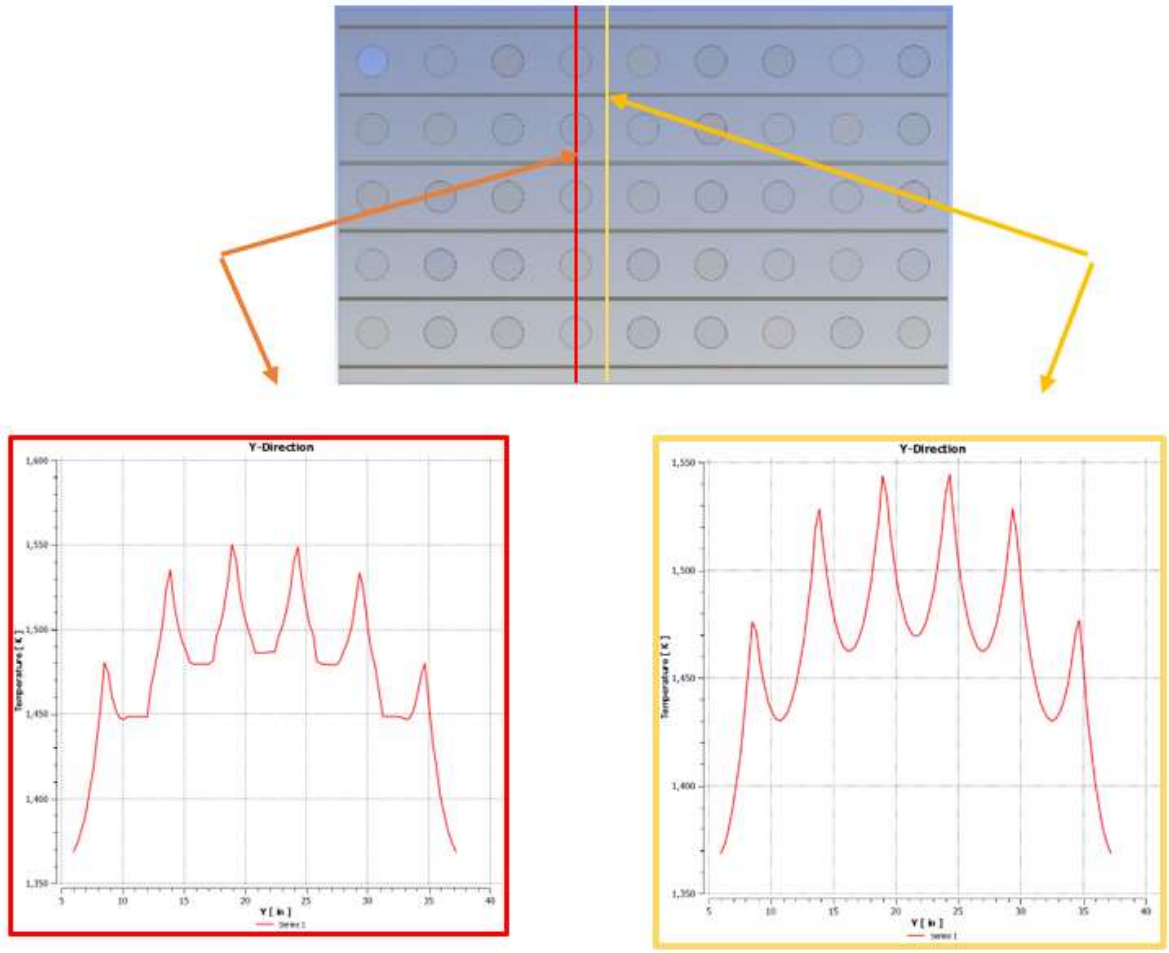

4.4.4 Discharge Phase

The discharge phase requires the entire length of the HTES to be considered. Nonetheless, since there are two axes of symmetry involved in the design, only 1/4th of the model is considered. Figure 54 shows the computational model.

Figure 54: Quarter Model of HTES

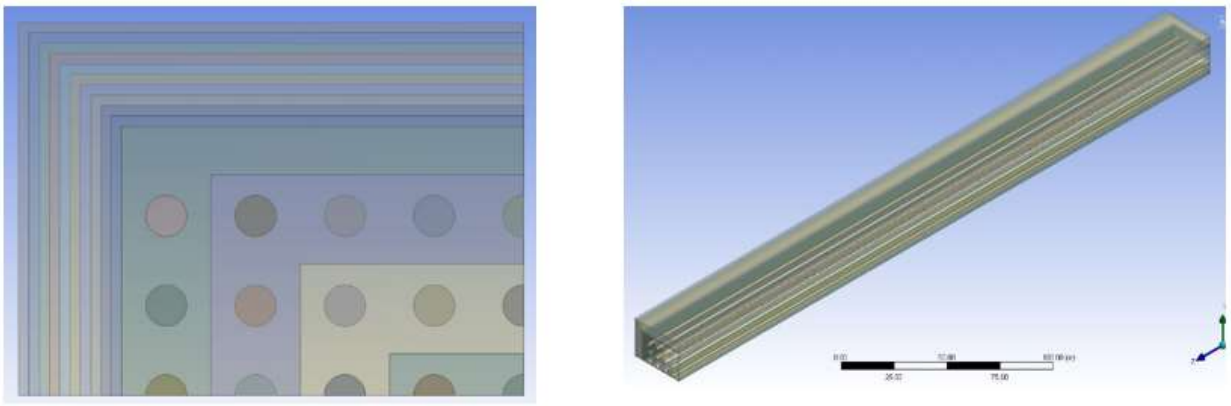

Front face and the side view of the whole HTES.

Figures 55 and 56 show the results of computations for the discharge phase. The average temperature over the whole 15 holes was also calculated at any given time. The time variation of the average exit temperature is shown in Figure 57.

Figure 55: Computational Results Corresponding to the End of Discharge Phase

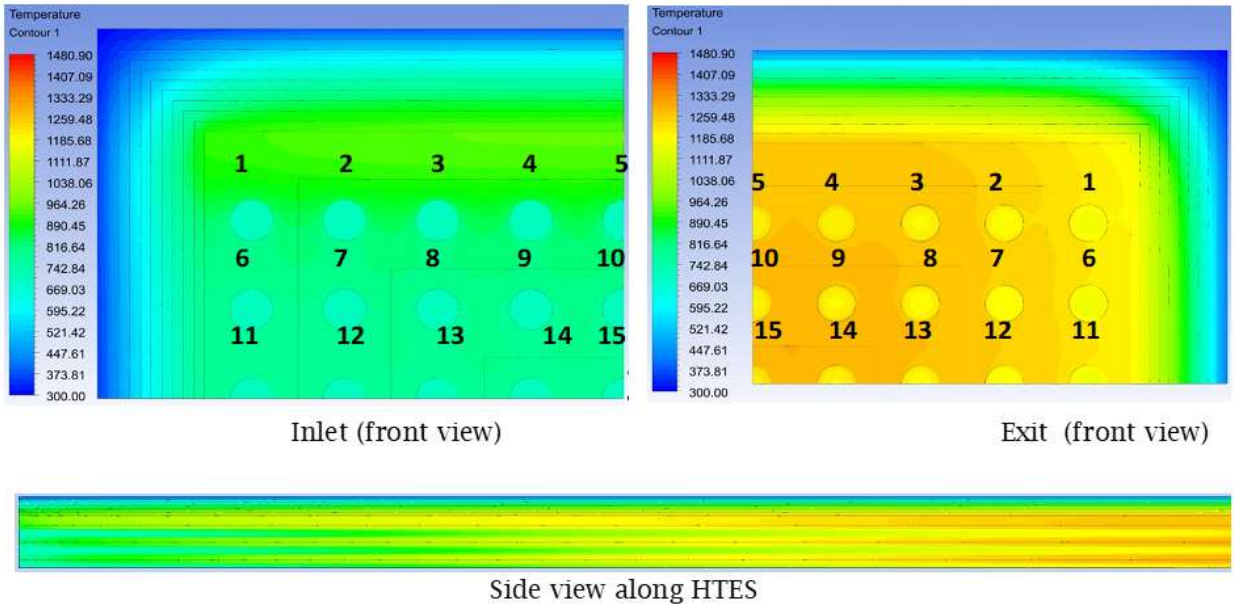

Figure 56: Average Air Temperature at the Exit Plane of HTES During Six Hours of Discharge

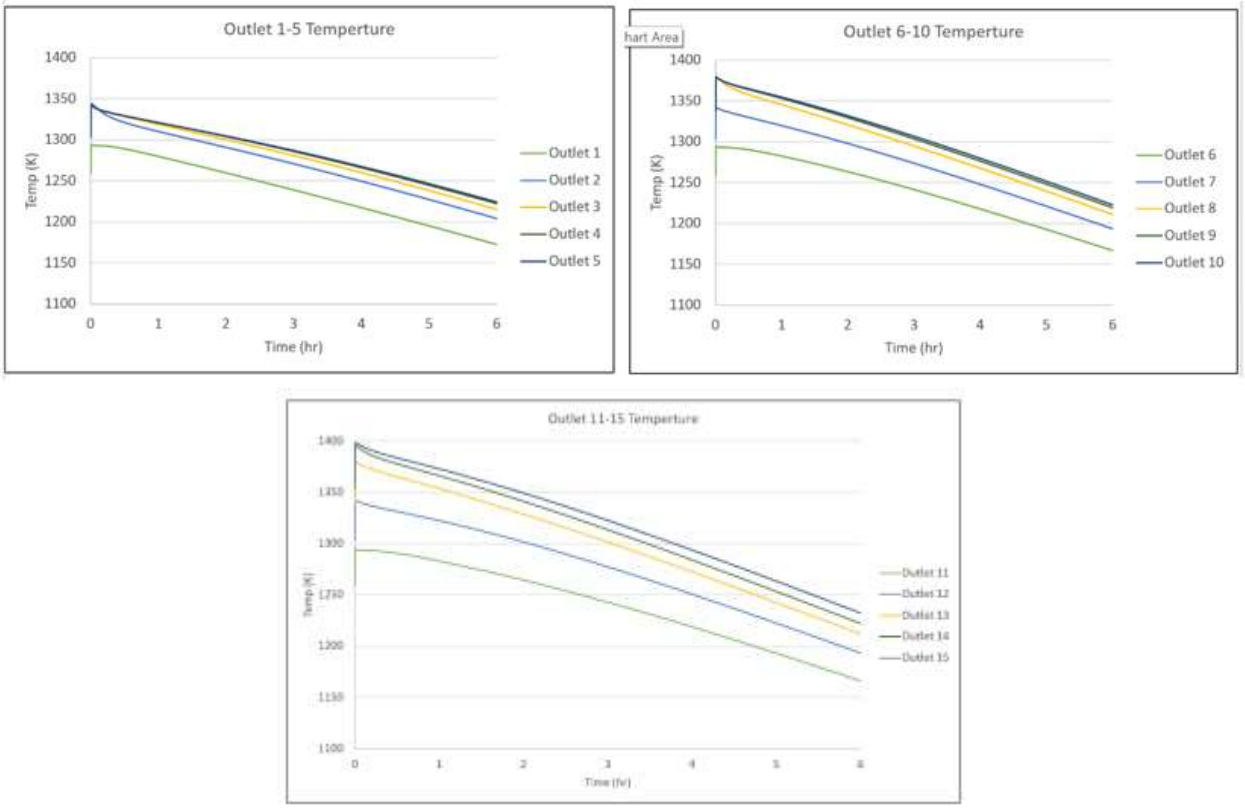

Figure 57: Average HTES Exit Air Temperature

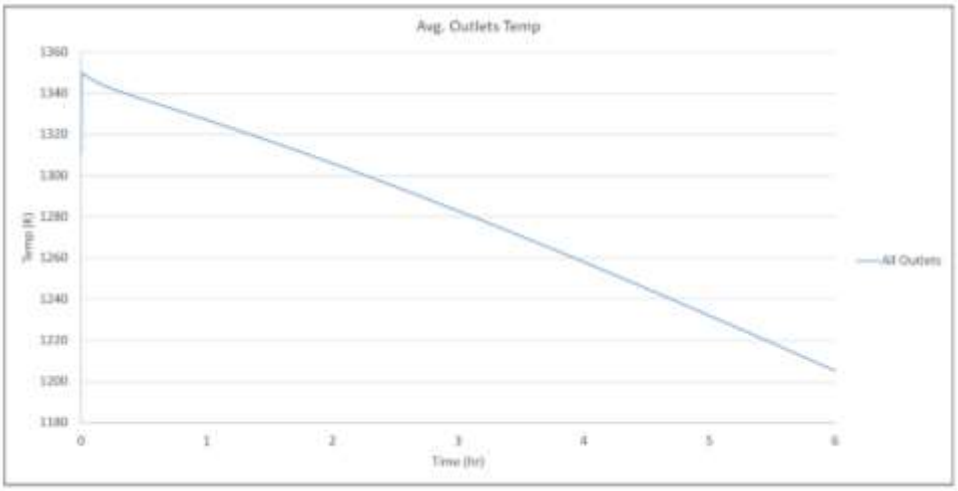

As shown in Figure 57, the main design requirement of the discharge phase is always met, i.e. the air temperature at the HTES exit plane is always above the expander inlet design temperature if 1144K. This means that there is always a non-zero bypass air flow to moderate the hot air temperature down to 1144K. Note that the discharge calculations were conducted under the entire mass flow rate through HTES as the worst-case scenario.

4.4.5. Energy Leak into Foundation

The issues related to heat leak into Portland-Cement foundation were investigated. Heating the concrete to high temperatures could cause the following problems:

1. The moisture in the composition boils and generates steam, which in turn raises the pressure inside the foundation. At high enough temperatures, the high steam vapor pressure might exceed the tensile yield strength of the concrete and cause explosion. This could happen particularly near the surface where the concrete is most prone to cracking due to thermal expansion.
2. The loss of strength in reinforcement rebar at high temperatures.

To investigate this problem a 2D and 3D model were created The HTES was heated up to its design temperature in 22 hours. It was then left alone for long enough to examine the variation of temperature within the foundation. When useful mechanical power is generated, thermal leak into foundation is less pronounced. Figure 58 shows the designed foundation of the HTES.

Figure 58: Schematic of the Foundation of HTES

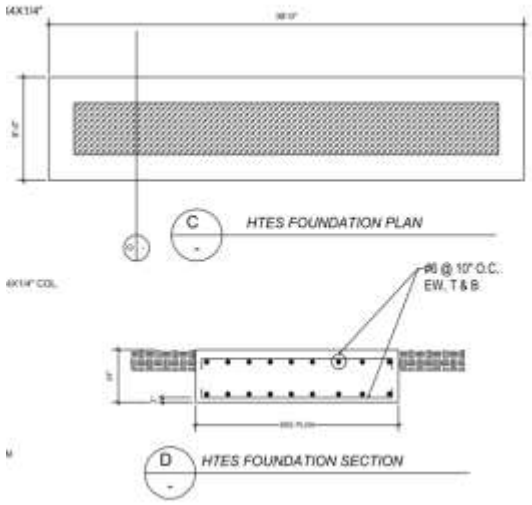

4.4.6 2D Modeling of HTES and Foundation

The 2D simulation represents the worst-case scenario due to one less degree of freedom. The insulation boundary condition was enforced wherever the foundation comes into contact with soil to contain the heat, also as the worst case scenario. The free convection boundary condition was enforced to the exposed surface. Figure 59 shows the computational model and Figure 60 shows the result along the line of symmetry (centerline), as the most critical line.

Figure 59: The 2D Model of the HTES-Foundation Setup

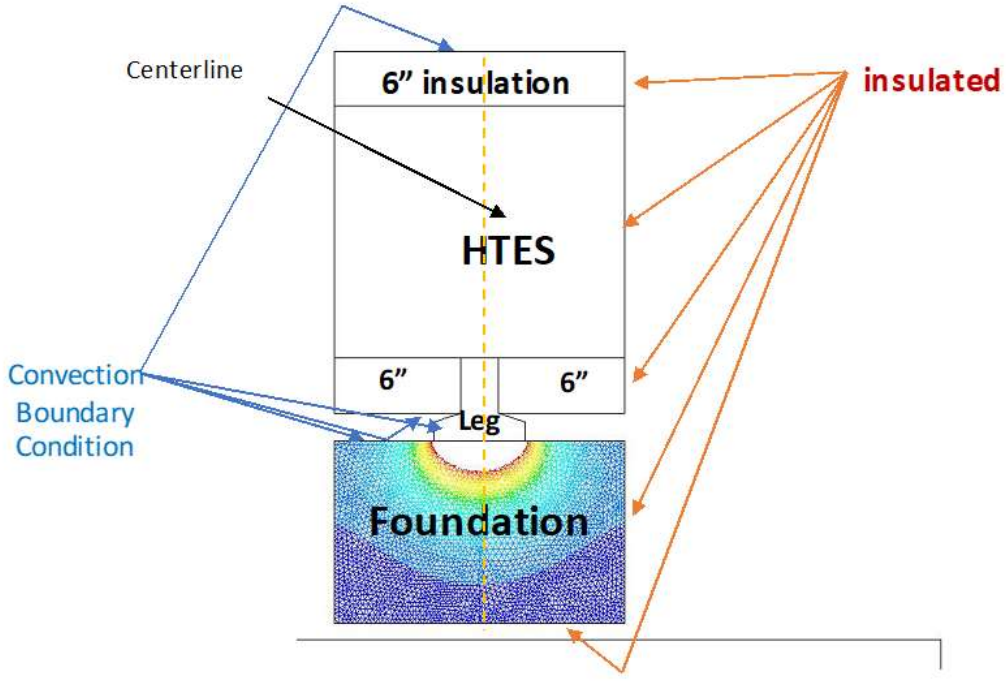

Figure 60: Temperature History Along the Centerline of the Model

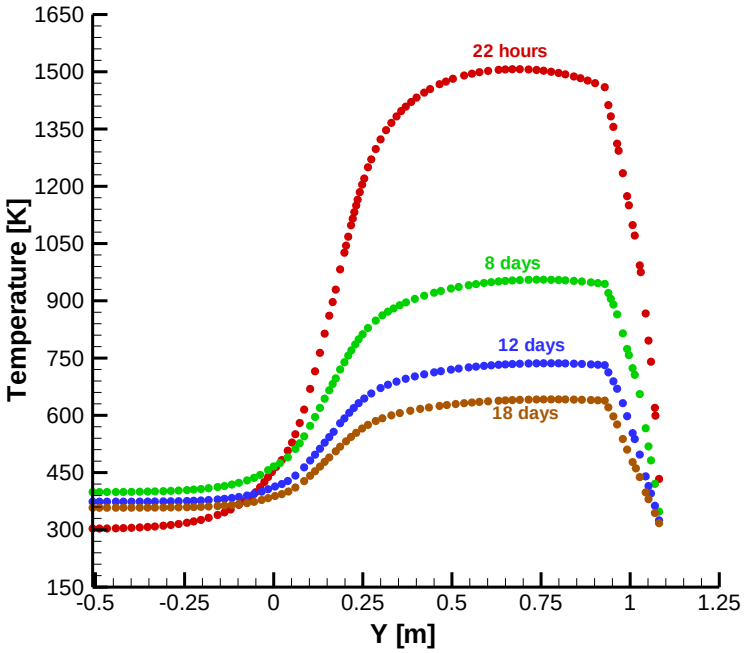

4.4.7 3D Modeling of HTES and Foundation

Obviously, the 3D modeling has an extra dimension over the 2D case which results in the relieving effect and the less pronounced thermal effect. Nonetheless, calculations were conducted to capture the thermal transients. Figures 61 and 62 represent such calculation.

Figure 61: The 3D Geometry of the HTES-Foundation Assembly

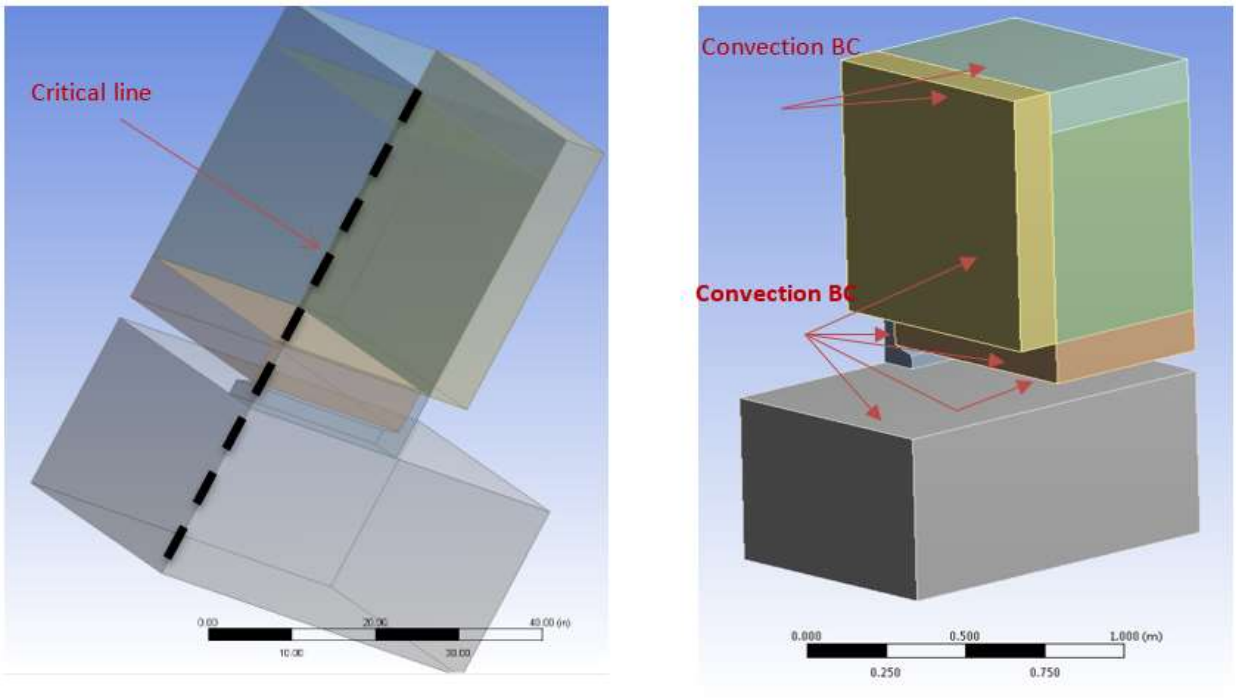

Figure 62: Temperature History Along the Centerline of the Model

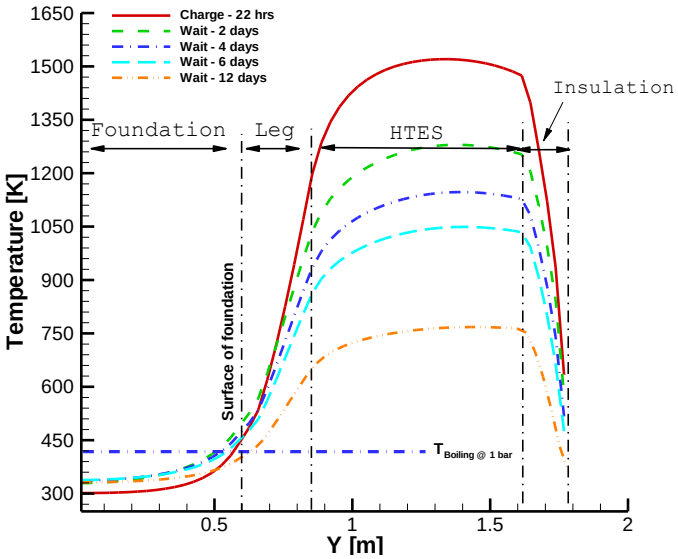

4.4.8 The Loss of Strength in Steel Rebar

As shown in Table 11, temperature in the foundation reaches the maximum of 509K = 456 F. The temperature rating of reinforcement rebar, shown in Figure 63, [1], indicates that at this temperature the rebar maintains over 80% of its yield strength which puts it within the safe zone. It is therefore concluded that the loss of strength of reinforcement rebars due to heat leak into foundation is a secondary issue.

Table 11: Temperature Values [Kelvin] at Different Depths in Foundation

	0[inch]	3.9[inch]	7.9[inch]	11.8[inch]
Charging for 22 hours	379.4 K	194.0 K	132.8 K	98.6 K
Waiting for 2 days post charge	**456.8** K	287.6 K	215.6 K	172.4 K
Waiting for 4 days post charge	**411.8** K	271.4 K	212.0 K	176.0 K
Waiting for 6 days post charge	**509.4 K**	255.2 K	203.0 K	174.2 K
Waiting for 12 days post charge	275.0 K	197.6 K	167.0 K	150.8 K

Depth is measured from the surface of foundation [inch]

Figure 63: Effect of High-Temperature on the Yield Strength of Steel

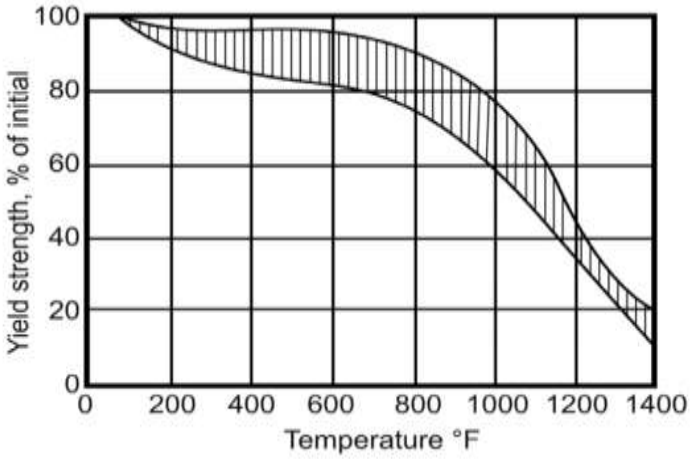

CHAPTER 5:
Managing Vendors and Third Party Entities

5.1 Vendors

The vendors and subcontractors search started at the beginning of the project with several different options for each of the pieces of equipment present in this project. The main components of this plant as mentioned in the previous chapters are the following: compressor, air tank, LTES, HTES and micro turbine. As the teamed explored the system processes in depth as the system parameters were being optimized through thermodynamic analyses and HYSYS, they were able to specify input and output parameters for the various components of the project. This in fact helped narrow down the search for the components by taking into consideration the now validated specifications at different stages of the process. As an example, while the team was researching the various different options for the rotary screw compressor, they went from a 125hp compressor to a 30hp thanks to the results that obtained from the models developed through the HYSYS software. The impact of HYSYS on the project was discussed in detail in Chapter 3 of this report.

When choosing valves for this system, several companies could not meet the high temperature, high pressure requirements. Some companies did not want to embark on a one-time basis research and development endeavor where they would have to assign a team to conduct R&D to be able to match the specifications. This was one area where it was more tedious to pinpoint a vendor that was willing to supply the project with equipment that matches the specific needs.

With regards to the HTES and LTES, the team contacted multiple vendors considering the fact that those system components were made up of several different smaller components. For instance, the team had to find a vendor for the resistance heating wires, and another one for the refractory concrete blocks.

After conducting extensive research, meeting with suppliers and receiving competitive bids, the appropriate vendors were chosen to purchase the various components for this system.

As for the various software required for this project UCLA computing facility was consulted and checked if there were any software that can license through the university.

The piping and instrumentation was an endeavor that the Murray Company decided to embark on, considering this was under their umbrella of mechanical contractor work.

5.2 California State Polytechnic University, Pomona (Cal Poly Pomona)

Cal Poly Pomona as per the Grant agreement was the subcontractor and provided the project location until the notice of involvement termination.

Cal Poly Pomona provided the team with technical expertise from their mechanical engineering department as they performed computational fluid dynamics and heat transfer modeling for the HTES component of this system. University staff implemented the design changes provided by the project team and would run multiple simulations and iterations for the thermal storage component of the system.

The senior manager from Cal Poly Pomona's Facilities Planning, Design & Construction division was the direct liaison to ensure all the necessary measures in planning and safety were covered. All the permitting processes and procedures were to be handled and implemented by that same division. For example, the delivery route for the heavy equipment, mainly the air tank, was undertaken by the senior manager.

Initially the Murray Company would be the team's subcontractor considering that Cal Poly Pomona was the major subcontractor as per the Grant agreement. Following the decision of Cal Poly Pomona to withdraw from the project, the Murray Company replaced them as the major subcontractor for this project.

5.3 The Murray Company Mechanical Contractor

The Murray Company provided the pipes, fittings, pumps, and all the minor pieces of equipment. They have a department in charge of welding and fabricating pipes in house eliminating the necessity to go through a third party vendor.

The Murray Company played a major consulting role throughout multiple stages of this project. The research team obtained industry help through the Murry Company connections and they had an array of subcontractors to tap into as necessary. The team consulted with the Murray Company with any questions and they would guide them to the correct for answers

The Murray Company was the project management on site during assembly of the system's components and was also in charge of the quality control tasks required during the fabrication, machining and assembly of the different parts of the system. All the work was to be performed according with the Murray Company's safety program.

CHAPTER 6:
Roadblocks in the Project

6.1 Cal Poly Pomona's Involvement Termination

The project team was surprised when Cal Poly Pomona withdrew from the project, resulting in the loss of the university site location. The research team looked for alternate locations to host this project. This new challenge came at a time where there was good momentum the project development. Fortunately, Clean Energy Systems Inc. offered a letter of commitment to provide a test site location in the City of Santa Clarita (Appendix A and B).

6.2 City of Santa Clarita's Permitting Process

The research team began exploring the City of Santa Clarita permits and process. The team contacted the city's planning division and discovered several hurdles since the city has multiple departments. The review was a complex one with three major entities to be consulted: the city's fire department, the planning manager and the Home Owner's Association of Santa Clarita. On September 25, the team was granted approval of a temporary use permit from the Planning Division of the City of Santa Clarita, however, the project still does not have any final permits. The temporary use permit is attached at the end of Appendix B.

6.3 Long Delivery Lead Times

The extremely high temperatures in different parts of this system made it difficult to find companies willing to manufacture high temperature valves to accommodate these specifications. Inconel, a material able to withstand high temperatures, was considered in the first discussions with valve manufacturers, however the cost was about $250,000 for one valve. The research team explored more viable alternative options, moving to stainless steel and other alloy options. The team discovered some of these valves take 16-18 weeks to manufacture and calibrate. The delivery was further delayed as the new tentative delivery date moved to early October 2017.

CHAPTER 7:
Conclusions/Future Work

A team of professors, researchers and engineers from UCLA proposed to design and build a fully-functional, low-cost 74 kW pilot high-temperature hybrid compressed air energy storage (HTH-CAES) system that can efficiently store grid-level energy and later release that energy for ancillary services and load following use-cases. The HTH-CAES system combines a state-of-the-art high-temperature energy storage unit with traditional compressed air energy storage to reduce the losses in air compression processes with a capital cost of $938/kW. By reducing losses in the compressed air storage system and shifting the storage capacity to the thermal side, in addition to using low cost components, the hybrid system is optimized for capital cost savings. The proposed system cost for energy storage is $156/kWh installed and 7 cents/kWh/cycle levelized with a system cycle efficiency of 85% over 15,000 cycles.

The proposed project had the following goals:

1. Construct a low capital cost, durable, and efficient pilot scale HTH-CAES system to address use-cases such as ancillary services and load following.
2. Demonstrate the cost saving advantages of combining low and high-temperature energy storage (LTES & HTES) units to improve the efficiency of the HTH-CAES system.

For years, conventional CAES has been recognized for its potential to be the leading large-scale energy storage system. However, the high costs of manufacturing combined with the low efficiency of conventional CAES are among the main reasons CAES has not lived up to its potential. Because optimization is based on overall costs, this proposed system can be the most economical energy storage system to date. The new technology will improve the round-trip efficiency of the conventional CAES system while reducing the capital cost. As an added benefit, with the exception of the thermal storage unit, the majority of components to the system are already available for purchase and do not require custom engineering, unlike AA-CAES and isothermal CAES. This keeps the overall cost of HTH-CAES below the state's statutory goals.

The team successfully designed and numerically studied HTH-CAES system using professional software such as Aspen HYSYS, Ansys, EES and Matlab. The initial thermodynamics of the system were modeled by EES and Matlab to explore the overall performance of the system. During the second stage of design, Aspen HYSYS was used to fully model the process during the charge and discharge processes. All of the components used in this model were the actual parts to be used in the system.

In parallel, Matlab software was used for optimizing the process with minimizing the cost and maximizing the overall efficiency. The Matlab results were used as inputs into the Aspen HYSYS software in the final design of the process.

Throughout the process design stage of the project, the Murray Company was consulted for design, viability and safety issues. As the result of this collaboration, the piping and instrumentation (P&ID) diagram of the process was finalized.

The heart of the system, high-temperature energy storage (HTES), was designed and modeled using Ansys software. The design went through several rigorous iterations to finally converge

to the lowest possible cost with highest effectiveness. This energy storage unit has the lowest $/kWh in the market which is one of the achievements of this project. The team constructed several small-scale models of HTES to test in the lab to make sure of its performance.

To summarize, a complete thermodynamic analysis of the HTH_CAES system was made along with parametric studies, to characterize how the operating pressure and thermal storage temperature affect the performance of the storage system. This is an essential part to design of such systems since the location of the energy storage system, being in hot/cold, high/low elevation, high/low humidity, etc. dictates the proper design of such machine. This analysis provides a road-map for design and installation of this type energy storage system at different locations in the state of California, that includes desert, mountains, ocean sides locations.

A significant challenge was to choose off-the-shelf components to maximize efficiencies and minimize throttling losses. It is essential for any energy storage system to have be economically viable otherwise, it cannot be practical. This is a lesson learned from previous efforts that spent lots of time and money to improve the efficiency of system, but jeopardize the capital cost of such unit which lead to the failure of the efforts. In this project, the researchers modeled and developed a design for an ultra-low cost system to satisfy this need. This resulted in a complete design for a 74kW energy storage system using off the shelf components ready for pilot demonstration.

This energy storage system can efficiently store grid-level energy and release that energy when it is needed to meet peak demand, particularly for ancillary services and load following use-cases. Such an energy storage system can be used for grid stabilization, peak-shaving, demand-respond as well as resiliency needed for places such as hospitals, ports and military bases at the time of need, when grid is down due to emergency.

Subcontractors are very important to the success of complex engineered energy storage systems. The Murray Company, an expert in installation and commissioning of such systems was instrumental to overcoming many barriers of the high temperature systems. During the course of this project, engineers of Murray company have provided expertise for design of piping, valves and creative way to reduce the costs for this system. This significantly reduces the cost of manufacturing and maintenance of this system by creatively using fewer high temperature valves, a big source of capital cost of the system. The experienced engineering team at Murray company has been a great compliment to the scientific team at UCLA.

Another challenge in this project was how HTH-CAES would respond to different type of demand from the grid and what type of services it can provide. The researchers were able to show that this system is fully capable of load following, ramp-up, ramp down, peak-shaving and energy arbitrage. In addition, it can provide long duration energy for high demand application during blackout/brownout situations.

The unique patented ultra-low cost high temperature energy storage unit, brought the price of energy stored to $156/kWh installed and 7 cents/kWh/cycle levelized with a system cycle efficiency of 85% over 15,000 cycles. These are numbers much lower than currently available batteries with similar capacities, with the additional advantages of longer life-time and lower maintenance costs for the HTH-CAES system.

One of the main hurdles encountered, as noted in the report, is that the original site for the construction of HTH-CAES was on the campus of Cal Poly Pomona. However, as Cal Poly

decided to terminate their involvement with the project, it was necessary to quickly start looking for an alternative site to host the project. A site location was offered through Clean Energy Systems at 20885 Placerita Canyon Rd. in the city of Santa Clarita. Even though the new location prospect looked promising, it was a slow process of applying for permits from the City of Santa Clarita to build the HTH-CAES. On September 25th, approval for the temporary use permit from the Planning Division of the City of Santa Clarita was obtained, but there were still 2 more permit applications needed from the LA County Fire Department and the Building & Safety Department. Unfortunately, these endeavors were not pursued as time ran out for the completion of the project. Educating the communities around California regarding the significance of such projects would help fostering the culture of expediting such permits.

GLOSSARY

Term	Definition
EPIC	Electric Program Investment Charge
Smart Grid	Smart Grid is the thoughtful integration of intelligent technologies and innovative services that produce a more efficient, sustainable, economic, and secure electrical supply for California communities.
ACFM	Actual Cubic Feet per Minute
CAES	Compressed Air Energy Storage
CFD	Computational Fluid Dynamics
CS	Carbon Steel
cu. ft.	Cubic Feet
cu. m.	Cubic Meters
F	Fahrenheit
FAD	Free Air Delivered
GPM	Gallons per Minute
HEX	Heat Exchanger
HP	Horsepower
HRS	Heat Recovery System
HTES	High Temperature Energy Storage
HTH-CAES	High Temperature Hybrid Compressed Air Energy Storage
IR	Ingersoll-Rand
K	Kelvin
kg	Kilogram
Kg/s	Kilogram per Second
kW	Kilowatt
kWh	Kilowatt Hour
LTES	Low Temperature Energy Storage
MDMT	Minimum Design Metal Temperatures
psia	Pounds per Square Inch, Atmosphere
psig	Pounds per Square Inch, Gauge `
PVC	Polyvinyl Chloride
SCFM	Standard Cubic Feet per Minute
SS	Stainless Steel
VFD	Variable Frequency Drive
VSD	Variable Speed Drive

REFERENCES

[1] Sun Can, Zhaohong Bie, Zijun Zhang, A new framework for the wind power curtailment and absorption evaluation, International Transactions on Electrical Energy Systems, 2016:2016 vol: 26 iss: 10 pg: 2134 -2147 doi: 10.1002/etep.2194

[2] Li CB, Shi HQ, Cao YJ, et al. Comprehensive review of renewable energy curtailment and avoidance: a specific example in China. Renewable & Sustainable Energy Reviews 2015; 41:1067–1079.

[3] Zou, J (Zou, Jin)[1]; Rahman, S (Rahman, Saifur)[2]; Lai, X (Lai, Xu)[1], Mitigation of Wind Output Curtailment by Coordinating with Pumped Storage and Increasing Transmission Capacity, 2015 IEEE POWER & ENERGY SOCIETY GENERAL MEETING

[4] Waite, M (Waite, Michael)[1]; Modi, V (Modi, Vijay)[1], Modeling wind power curtailment with increased capacity in a regional electricity grid supplying a dense urban demand, 2016, APPLIED ENERGY, Volume: 183 Pages: 299-317 DOI: 10.1016/j.apenergy.2016.08.078

[5] Wang, CX (Wang, Caixia)[1], Study of Unit Commitment Strategies in Combating Wind Curtailment in China, 2015 4TH INTERNATIONAL CONFERENCE ON ENERGY AND ENVIRONMENTAL PROTECTION (ICEEP 2015) Pages: 1137-1140

[6] Fan, XC (Fan, Xiao-chao)[1,2]; Wang, WQ (Wang, Wei-qing)[1,2]; Shi, RJ (Shi, Rui-jing)[1]; Li, FT (Li, Feng-ting)[1,2], Analysis and countermeasures of wind power curtailment in China, 2015, ENEWABLE & SUSTAINABLE ENERGY REVIEWS, Volume: 52. Pages: 1429-1436, DOI: 10.1016/j.rser.2015.08.025

[7] Gunter, N (Gunter, Niklas)[1,2]; Marinopoulos, A (Marinopoulos, Antonios)[3], Energy storage for grid services and applications: Classification, market review, metrics, and methodology for evaluation of deployment cases, 2016, JOURNAL OF ENERGY STORAGE, Volume: 8, Pages: 226-234, DOI: 10.1016/j.est.2016.08.011

[8] Zakeri, B (Zakeri, Behnam)[1]; Syri, S (Syri, Sanna)[1], Electrical energy storage systems: A comparative life cycle cost analysis, 2015, RENEWABLE & SUSTAINABLE ENERGY REVIEWS, Volume: 42, Pages: 569-596, DOI: 10.1016/j.rser.2014.10.011

[9] Zidar, Matija[1]; Georgilakis, PS (Georgilakis, Pavlos S.)[2]; Hatziargyriou, ND (Hatziargyriou, Nikos D.)[2]; Capuder, T (Capuder, Tomislav)[1]; Skrlec, D (Skrlec, Davor)[1], Review of energy storage allocation in power distribution networks: applications, methods and future research, 2016, IET GENERATION TRANSMISSION & DISTRIBUTION, Volume: 10, Issue: 3, Pages: 645-652, Special Issue: SI, DOI: 10.1049/iet-gtd.2015.0447

[10] A.G. Olabi, Renewable energy and energy storage systems, In Energy, Volume 136, 2017, Pages 1-6, ISSN 0360-5442, https://doi.org/10.1016/j.energy.2017.07.054.

[11] Anuta, OH (Anuta, Oghenetejiri Harold)[1]; Taylor, P (Taylor, Phil)[1]; Jones, D (Jones, Darren)[2]; McEntee, T (McEntee, Tony)[2]; Wade, N(Wade, Neal)[1], An international review of the implications of regulatory and electricity market structures on the emergence of grid scale electricity storage, 2014, RENEWABLE & SUSTAINABLE ENERGY REVIEWS, Volume: 38, Pages: 489-508, DOI: 10.1016/j.rser.2014.06.006

[12] Hameer, S (Hameer, Sameer)[1]; van Niekerk, JL (van Niekerk, Johannes L.)[1], A review of large-scale electrical energy storage, 2015, INTERNATIONAL JOURNAL OF ENERGY RESEARCH, Volume: 39, Issue: 9, Pages: 1179-1195, DOI: 10.1002/er.3294

[13] Freeman, E (Freeman, Eugene); Occello, D (Occello, Davide)[1]; Barnes, F (Barnes, Frank)[2], Energy storage for electrical systems in the USA, 2016, AIMS ENERGY, Volume: 4, Issue: 6, Pages: 856-875, DOI: 10.3934/energy.2016.6.856

[14] Zakeri, B (Zakeri, Behnam)[1]; Syri, S (Syri, Sanna)[1], Electrical energy storage systems: A comparative life cycle cost analysis, 2015, ENEWABLE & SUSTAINABLE ENERGY REVIEWS, Volume: 42, Pages: 569-596, DOI: 10.1016/j.rser.2014.10.011

[15] Obi, M (Obi, Manasseh)[1]; Jensen, SM (Jensen, S. M.)[2]; Ferris, JB (Ferris, Jennifer B.)[3]; Bass, RB (Bass, Robert B.)[1], Calculation of levelized costs of electricity for various electrical energy storage systems, 2017, RENEWABLE & SUSTAINABLE ENERGY REVIEWS, Volume: 67, Pages: 908-920, DOI: 10.1016/j.rser.2016.09.043

[16] Erren Yao, Huanran Wang, Ligang Wang, Guang Xi, François Maréchal, Multi-objective optimization and exergoeconomic analysis of a combined cooling, heating and power based compressed air energy storage system, Energy Conversion and Management, Volume 138, 15 April 2017, Pages 199-209, ISSN 0196-8904, http://dx.doi.org/10.1016/j.enconman.2017.01.071.

[17] Wei Ji, Yuan Zhou, Yu Sun, Wu Zhang, Baolin An, Junjie Wang, Thermodynamic analysis of a novel hybrid wind-solar-compressed air energy storage system, Energy Conversion and Management, Volume 142, 15 June 2017, Pages 176-187, ISSN 0196-8904, http://dx.doi.org/10.1016/j.enconman.2017.02.053.

[18] Adriano Sciacovelli, Yongliang Li, Haisheng Chen, Yuting Wu, Jihong Wang, Seamus Garvey, Yulong Ding, Dynamic simulation of Adiabatic Compressed Air Energy Storage (A-CAES) plant with integrated thermal storage – Link between components performance and plant performance, Applied Energy, Volume 185, Part 1, 1 January 2017, Pages 16-28, ISSN 0306-2619, http://dx.doi.org/10.1016/j.apenergy.2016.10.058.

[19] Daniel Wolf, Marcus Budt, LTA-CAES – A low-temperature approach to Adiabatic Compressed Air Energy Storage, Applied Energy, Volume 125, 15 July 2014, Pages 158-164, ISSN 0306-2619, http://dx.doi.org/10.1016/j.apenergy.2014.03.013.

[20] Hao Peng, Yu Yang, Rui Li, Xiang Ling, Thermodynamic analysis of an improved adiabatic compressed air energy storage system, Applied Energy, Volume 183, 1 December 2016, Pages 1361-1373, ISSN 0306-2619, http://dx.doi.org/10.1016/j.apenergy.2016.09.102.

[21] Adewale Odukomaiya, Ahmad Abu-Heiba, Kyle R. Gluesenkamp, Omar Abdelaziz, Roderick K. Jackson, Claus Daniel, Samuel Graham, Ayyoub M. Momen, Thermal analysis of near-isothermal compressed gas energy storage system, Applied Energy, Volume 179, 1 October 2016, Pages 948-960, ISSN 0306-2619, http://dx.doi.org/10.1016/j.apenergy.2016.07.059.

[22] Gayathri Venkataramani, Prasanna Parankusam, Velraj Ramalingam, Jihong Wang, A review on compressed air energy storage – A pathway for smart grid and polygeneration, Renewable and Sustainable Energy Reviews, Volume 62, September 2016, Pages 895-907, ISSN 1364-0321, http://dx.doi.org/10.1016/j.rser.2016.05.002.

[23] Seamus D. Garvey and Andrew Pimm, Chapter 5 - Compressed Air Energy Storage, In Storing Energy, edited by Trevor M. Letcher, Elsevier, Oxford, 2016, Pages 87-111, ISBN 9780128034408, http://dx.doi.org/10.1016/B978-0-12-803440-8.00005-1.

[24] Odukomaiya, A (Odukomaiya, Adewale)[1]; Abu-Heiba, A (Abu-Heiba, Ahmad)[2]; Gluesenkamp, KR (Gluesenkamp, Kyle R.)[2]; Abdelaziz, O(Abdelaziz, Omar)[2]; Jackson,

RK (Jackson, Roderick K.)[2]; Daniel, C (Daniel, Claus)[2]; Graham, S (Graham, Samuel)[1,2]; Momen, AM (Momen, Ayyoub M.)[2], Thermal analysis of near-isothermal compressed gas energy storage system, 2016, APPLIED ENERGY, Volume: 179, Pages: 948-960, DOI: 10.1016/j.apenergy.2016.07.059

[25] Kilic, M (Kilic, M.)[1]; Mutlu, M (Mutlu, M.)[2], A novel design of a compressed air storage system with liquid pistons, 2016, BULGARIAN CHEMICAL COMMUNICATIONS, Volume: 48, Pages: 318-324, Special Issue: E2

[26] Li, PY (Li, Perry Y.)[1]; Saadat, M (Saadat, Mohsen)[1], An approach to reduce the flow requirement for a liquid piston near-isothermal aircompressor/expander in a compressed air energy storage system, 2016, IET RENEWABLE POWER GENERATION, Volume: 10, Issue: 10, Pages: 1506-1514, Special Issue: SI, DOI: 10.1049/iet-rpg.2016.0055

[27] Qin, C (Qin, Chao)[1]; Loth, E (Loth, Eric)[1], Liquid piston compression efficiency with droplet heat transfer, 2014, APPLIED ENERGY, Volume: 114, Pages: 539-550, Special Issue: SI, DOI: 10.1016/j.apenergy.2013.10.005

[28] Daniel Buhagiar, Tonio Sant, Modelling of a novel hydro-pneumatic accumulator for large-scale offshore energy storage applications, In Journal of Energy Storage, 2017, ISSN 2352-152X, https://doi.org/10.1016/j.est.2017.05.005.

[29] Marcus Budt, Daniel Wolf, Roland Span, Jinyue Yan, A review on compressed air energy storage: Basic principles, past milestones and recent developments, In Applied Energy, Volume 170, 2016, Pages 250-268, ISSN 0306-2619, https://doi.org/10.1016/j.apenergy.2016.02.108.

[30] Qin, C (Qin, C.)[1]; Loth, E (Loth, E.)[1], Simulation of spray direct injection for compressed air energy storage, 2016, APPLIED THERMAL ENGINEERING, Volume: 95, Pages: 24-34. DOI: 10.1016/j.applthermaleng.2015.11.008

[31] McBride T, Bell A, Kepshire D. ICAES innovation: foam-based heat exchange. USA: Seabrook; 2013.

[32] Kentschke T. Druckluftmaschinen als Generatorantrieb inWarmluftspeichern. Dissertation. Clausthal; 2004.

[33] Lukasz Szablowski, Piotr Krawczyk, Krzysztof Badyda, Sotirios Karellas, Emmanuel Kakaras, Wojciech Bujalski, Energy and exergy analysis of adiabatic compressed air energy storage system, In Energy, Volume 138, 2017, Pages 12-18, ISSN 0360-5442, https://doi.org/10.1016/j.energy.2017.07.055.

[34] Hao Peng, Yu Yang, Rui Li, Xiang Ling, Thermodynamic analysis of an improved adiabatic compressed air energy storage system, In Applied Energy, Volume 183, 2016, Pages 1361-1373, ISSN 0306-2619, https://doi.org/10.1016/j.apenergy.2016.09.102.

[35] Baghaei Lakeh R., Villanava, I., Houssainy, S., Anderson, K., Kavehpour, H.P., 2016, Design of a Modular Solid-Based Thermal Energy Storage for a Hybrid Compressed Air Energy Storage System, Paper No. PowerEnergy2016-59160, Proc. of 2016 ASME Int. Conference on Energy Sustainability Charlotte, NC

[36] Houssainy, S Baghaei Lakeh R., Kavehpour, H.P., 2016, A Thermodynamic Model of High-Temperature Hybrid Compressed Air Energy Storage System for Grid Storage, Paper No. PowerEnergy2016-59431, Proc. of 2016 ASME Int. Conference on Energy Sustainability Charlotte, NC

[37] Ip PP, Houssainy S, Kavehpour. Modeling of a Low Cost Thermal Energy Storage System to Enhance Generation From Small Hydropower Systems. 2017, ASME Power Conference, doi:10.1115/POWER-ICOPE2017-3684

[38] Sammy Houssainy, Mohammad Janbozorgi, Peggy Ip, Pirouz Kavehpour, Thermodynamic Analysis of a High-Temperature Hybrid Compressed Air Energy Storage (HTH-CAES) System, Renewable Energy, Available online 12 September 2017, ISSN 0960-1481, https://doi.org/10.1016/j.renene.2017.09.038.

[39] Peng, H (Peng, Hao)[1]; Yang, Y (Yang, Yu)[1]; Li, R (Li, Rui)[1]; Ling, X (Ling, Xiang)[1], Thermodynamic analysis of an improved adiabatic compressed air energy storage system, 2016, APPLIED ENERGY, Volume: 183, Pages: 1361-1373, DOI: 10.1016/j.apenergy.2016.09.102

[40] Wolf D, Budt M. LTA-CAES – a low-temperature approach to adiabatic compressed air energy storage. Appl Energy 2014;125:158–64.

[41] Luo, X (Luo, Xing)[1]; Wang, JH (Wang, Jihong)[1,3]; Krupke, C (Krupke, Christopher)[1]; Wang, Y (Wang, Yue)[1]; Sheng, Y (Sheng, Yong)[2]; Li, J (Li, Jian)[3]; Xu, YJ (Xu, Yujie)[2]; Wang, D (Wang, Dan)[3]; Miao, SH (Miao, Shihong)[3]; Chen, HS (Chen, Haisheng)[2],Modelling study, efficiency analysis and optimisation of large-scale Adiabatic Compressed Air Energy Storage systems with low-temperature thermal storage, 2016, APPLIED ENERGY, Volume: 162, Pages: 589-600, DOI: 10.1016/j.apenergy.2015.10.091

[42] B. Cárdenas, A.J. Pimm, B. Kantharaj, M.C. Simpson, J.A. Garvey, S.D. Garvey, Lowering the cost of large-scale energy storage: High-temperature adiabatic compressed air energy storage, In Propulsion and Power Research, Volume 6, Issue 2, 2017, Pages 126-133, ISSN 2212-540X, https://doi.org/10.1016/j.jppr.2017.06.001.

[43] V. de Biasi, Fundamental analyses to optimize adiabatic CAES plant effi- ciencies, Gas Turbine World 39 (2009) 26e28.

[44] Doetsch C, Budt M, Wolf D, Kanngießer A. Adiabates Niedertemperatur-Druckluftspeicherkraftwerk zur Unterstützung der Netzintegration von Windenergie. Abschlussbericht zu FKZ 0325211; 2012.

[45] Barbour E, Mignard D, Ding Y, Li Y. Adiabatic compressed air energy storage with packed bed thermal energy storage. Appl Energy 2015;155:804–15.

[46] Dreißigacker V, Zunft S, Müller-Steinhagen H. A thermo-mechanical model of packed-bed storage and experimental validation. Appl Energy 2013;111:1120–5.

[47] Yang Z, Wang Z, Ran P, Li Z, Ni W. Thermodynamic analysis of a hybrid thermal-compressed air energy storage system for the integration of wind power. Applied Thermal Engineering 2014;66:519-527.

[48] Ibrahim Dincer, Marc Rosen, Thermal Energy Storage Systems and Applications (2nd Edition), 2011, John Wily & Sons Ltd, United Kingdom

[49] Fire and Concrete Structures , David N. Bilow, et al., Structures 2008: Crossing Borders, http://www.cement.org/docs/default-source/th-buildings-structures-pdfs/fire-concrete-struc-sei-08.pdf

APPENDIX A:
E-mail Conversations with Cal Poly Pomona

This appendix highlights conversations leading to the permitting process and the progress towards moving equipment to the site location prior to Cal Poly Pomona.

Re: Construction Permits for CPP/UCLA project in Lyle Center

1 message

Ariana Thacker <arianathacker@yahoo.com> Thu, Apr 21, 2016 at 1:18 PM
Reply-To: Ariana Thacker <arianathacker@yahoo.com>
To: Reza Baghaei Lakeh <rblakeh@cpp.edu>
Cc: Pirouz Kavehpour <pirouz@seas.ucla.edu>, WALID ISMAIL <walidi86@ucla.edu>

Hi Reza,

Thanks for forwarding the information.

We'd rather not wait until the very last minute (until we have obtained construction drawings) to determine if what we are planning to build is acceptable (in case it would require major modifications). Especially since we have already started purchasing equipment.

1. Does he have any literature on what permits/codes/regulations we would need to follow on campus? Eg, CCOR Title 22, 23, etc.
2. How long is the approval process for issuing these permits? What's the procedure?
3. May we ask if we can forward the P&ID as a preliminary review so we can modify our design if necessary?
4. Could I discuss the details of this drawing and our process with him over the phone? Or, schedule an in-person meeting with the people responsible for issuing the approval.
5. Does he have any soil information on the site? I would assume so since soil testing probably would have been conducted when installing those solar panels.

Thank you!

Ariana

From: Reza Baghaei Lakeh <rblakeh@cpp.edu>
To: Ariana Thacker <arianathacker@yahoo.com>; Pirouz Kavehpour <pirouz@seas.ucla.edu>; Mohammad Janbozorgi <mjanbozorgi@gmail.com>
Sent: Thursday, April 21, 2016 1:12 PM
Subject: FW: Construction Permits for CPP/UCLA project in Lyle Center

---

From: Bruyn Bevans
Sent: Thursday, April 21, 2016 1:11 PM
To: Reza Baghaei Lakeh <rblakeh@cpp.edu>
Cc: Kyle D. Brown <kdbrown@cpp.edu>
Subject: RE: Construction Permits for CPP/UCLA project in Lyle Center

Reza,
We will most likely handle all of the permitting items here in Facilities Planning & Management. However, I still need to see the site plans and any construction plans or shop drawings for occupied space equipment that might be brought to the site for use. A final determination of what will be required, in the way of reviews and approvals for the issuance of a building permit will be

made once we have received the documents listed above. Please email them directly to me if possible.
Thank you,
Bruyn

Bruyn Bevans, LEED AP
Sr. Project Manager
Facilities Planning, Design & Construction
California State Polytechnic University, Pomona
CAL POLY POMONA
Office:(909) 979-5517 Fax: (909) 869-2292
bbevans@cpp.edu

From: Reza Baghaei Lakeh
Sent: Wednesday, April 20, 2016 5:08 PM
To: Bruyn Bevans
Cc: Kyle D. Brown
Subject: Construction Permits for CPP/UCLA project in Lyle Center

Hi Bruyn,

We met a few months back in Lyle center regarding a joint compressed air project between UCLA and Cal Poly that is going to be constructed in Lyle center (under the large solar PV panels). As we are moving to the construction phase, UCLA and the consulting company (Murray) would like to know about the permits that they need to acquire in order to get the work started on our campus. Would you please share your thoughts on this issue ?

Thanks,
Reza

Reza Baghaei Lakeh, Ph.D.
Assistant Professor
California State Polytechynic University, Pomona
909-869-2493
rblakeh@cpp.edu
http://www.cpp.edu/~rblakeh

First line of communication with Bruyn Bevans, the senior project manager at Cal Poly Pomona, informing the project team that CPP will handle the permitting items. He requested site plans and construction plans and drawings from our end.

RE: Skype

1 message

Bruyn Bevans <bbevans@cpp.edu> Wed, May 4, 2016 at 2:23 PM
To: Ariana Thacker <arianathacker@yahoo.com>
Cc: Reza Baghaei Lakeh <rblakeh@cpp.edu>, WALID ISMAIL <walidi86@ucla.edu>

Ariana,

Please find attached a copy of the Building Permit Application Form. Please complete as much of the requested information that you or Reza have and return the completed for via email for processing. Don't worry about anything below the Status of Project line of the form.

As for the items we will require for the review and approval of the building permit:

- Full set of plans including site plan, tank layout plans with details and anchorage
- Structural plans indicating the foundations necessary for all equipment including specification for materials to be installed.
- Stamped signed structural calculations, plans, details for the anchorage, restraints, and foundation for the equipment.
- Electrical plans indicating the conduit feeds with voltage and amps for all runs and types of electrical gear to be supplied with the installation
- Documentation of the containment enclosures for the high temp equipment
- Details of and high temperature discharge pipelines or flues for the equipment.
- Any other items you feel will be helpful in the understanding of the project and the safety features that will be installed for the safety and wellbeing of the engineers conducting the tests as well as students that may join as observers.

I think that's it. If anything pops up I will let you know.

Thank you,

Bruyn

Bruyn Bevans, LEED AP

Sr. Project Manager

Facilities Planning, Design & Construction

California State Polytechnic University, Pomona

CAL POLY POMONA

Office:(909) 979-5517 Fax: (909) 869-2292

Bruyn's requests from site plans to containment enclosures information, etc.

RE: ** External ** Foundation Engineering

3 messages

Bruyn Bevans <bbevans@cpp.edu> Thu, May 5, 2016 at 3:51 PM
To: Ariana Thacker <arianathacker@yahoo.com>
Cc: WALID ISMAIL <walidi86@g.ucla.edu>

Ariana,

No, the jurisdic on having authority is not requiring another report as nothing has changed in the area in ques on for years. The work completed by Amonix regarding the two solar arrays caused addi onal compac on to the area so you are good.

Bruyn

Bruyn Bevans, LEED AP

Sr. Project Manager

Facilities Planning, Design & Construction

California State Polytechnic University, Pomona

CAL POLY POMONA

Office:(909) 979-5517 Fax: (909) 869-2292

bbevans@cpp.edu

Bruyn Informed us that the site location is under the jurisdiction of CPP and not the City of Pomona

CSUP Equipment Installation - JAMA Proposal

1 message

Jenni Shishido <jshishido@johnmartin.com> Tue, May 10, 2016 at 10:27 AM
To: "pirouz@seas.ucla.edu" <pirouz@seas.ucla.edu>
Cc: "arianathacker@yahoo.com" <arianathacker@yahoo.com>, "Bruyn Bevans (bbevans@cpp.edu)" <bbevans@cpp.edu>, "walidi86@ucla.edu" <walidi86@ucla.edu>, Barry Schindler <BARRY@johnmartin.com>

Good Morning – on behalf of Barry Schindler, attached is JAMA's proposal for the CSU Pomona *Installation of Equipment* project.

If the proposal is acceptable, please sign and return a copy of the proposal (via email is fine).

Thank you – and please call with any questions or comments.

Jenni Ervin-Shishido
Director – Contracts & Risk Management

John A. Martin & Associates, Inc.

Structural Engineers

950 South Grand Avenue, 4th Floor

Los Angeles, California 90015

213.785.3108 (direct)

213.483.6490 (general)

818.522-4144 (mobile)

213.483.3084 (fax)

jshishido@johnmartin.com

www.johnmartin.com

John A. Martin & Associates, Inc.'s quote for the CSU Pomona Installation of Equipment

Delivery Route at CPP Lyle Center

1 message

Reza Baghaei Lakeh <rblakeh@cpp.edu> Tue, Aug 2, 2016 at 2:38 PM
To: Ariana Thacker <arianathacker@yahoo.com>
Cc: Mohammad Janbozorgi <mjanbozorgi@gmail.com>, WALID ISMAIL <walidi86@ucla.edu>, Pirouz Kavehpour <pirouz@seas.ucla.edu>, "Kyle D. Brown" <kdbrown@cpp.edu>

Hi Ariana,

I met with Kyle today and we assessed the delivery route. Here are some visual slides that you may want to share with the delivery guys: https://www.dropbox.com/s/lplox54oeey5nt3/Delievery.pptx?dl=0

In short, 14 ft of clearance is available. There are two bottle necks: There is a permanent steel bollard (see slides 9-12) and some vegetation that need trimming (slides 13-16). Once the contract between UCLA and CPP is finalized, Kyle can instruct his staff to trim those trees. Kyle would also need to be informed about the day of delivery in advance, so that he manages his staff to assist with the process.

Please feel free to let us know If the delivery guys need any other information.

Thanks,

Reza

Reza Baghaei Lakeh, Ph.D.

Assistant Professor

California State Polytechnic University, Pomona

909-869-2493

rblakeh@cpp.edu

http://www.cpp.edu/~rblakeh

Cal Poly Pomona's assessment of the delivery route for the air tank

APPENDIX B:
E-mail Conversations with the City of Santa Clarita

This appendix highlights conversations with the City of Santa Clarita and the lengthy process of applying for permits through the city so we can construct our project at 20885 Placerita Canyon Rd. It can be inferred by the highlighted text and the conversation that the process was delayed due to the slow progress from the City.

RE: Walid Ismail from UCLA
1 message

David Peterson <DPETERSON@santa-clarita.com> Thu, Dec 15, 2016 at 2:25 PM
To: WALID ISMAIL <walidi86@ucla.edu>

Hi Walid,

So the best thing for you to do at this time is submit for a One Stop application. The application does not result in any approvals but will allow us to give you comments on the project that will tell you how to best proceed and what permits will be required.

You can find the application on our website at:

http://www.santa-clarita.com/city-hall/departments/community-development/planning

You'll want to click on and download the "One Stop Application". Prepare the materials outlined on the form and submit them to us with the associated fee of $1, 315 and we'll review it. Generally takes about 4 weeks to review and will result in a meeting with your organization and all of the commenting agencies on my end. If you decide to proceed to a formal submittal we will credit the one stop fee to the cost of any formal entitlement fees that we'd charge.

If you have questions let me know.

D

First communication with David Peterson. Stated that the process takes about 4 weeks to review

Proposed Project

6 messages

David Peterson <DPETERSON@santa-clarita.com> Wed, May 17, 2017 at 4:21 PM
To: WALID ISMAIL <walidi86@ucla.edu>

Hi Walid,

I received your one stop application. Can you call me and explain exactly what the project is? Also, we can't proceed until we've received payment. What's the status on that?

D

David Peterson
Associate Planner
Planning Division
City of Santa Clarita
23920 Valencia Blvd.
Santa Clarita, CA 91355

Phone: (661) 284-1406
Email: DPETERSON@santa-clarita.com
Web: http://www.santa-clarita.com

Think before you print

WALID ISMAIL <walidi86@ucla.edu> Thu, May 18, 2017 at 2:01 PM
To: David Peterson <DPETERSON@santa-clarita.com>
Cc: Pirouz Kavehpour <pirouz@seas.ucla.edu>

Hello David,

My boss, Professor Kavehpour, would like to set up a call with you at your earliest convenience to discuss our project. Please let us know what times work best for you.

--

Regards,

Walid Ismail | UCLA
walidi86@ucla.edu | (818)324-6554 Mobile

Setting up a call to explain what the project is about after talking to him several times about the project.

One stop
2 messages

David Peterson <DPETERSON@santa-clarita.com> Wed, May 31, 2017 at 1:14 PM
To: WALID ISMAIL <walidi86@ucla.edu>

Hi Walid,

Sorry for the delay. I'm having the conversation with my boss about the permit type we'll need for this project tomorrow at 8 am. He was out of the office for the past few days. I'll be able to advise tomorrow.

D

David Peterson
Associate Planner
Planning Division
City of Santa Clarita
23920 Valencia Blvd.
Santa Clarita, CA 91355

Phone: (661) 284-1406
Email: DPETERSON@santa-clarita.com
Web: http://www.santa-clarita.com

Think before you print

WALID ISMAIL <walidi86@ucla.edu> Wed, May 31, 2017 at 1:17 PM
To: David Peterson <DPETERSON@santa-clarita.com>
Cc: Mohammad Janbozorgi <mjanbozorgi@gmail.com>, Pirouz Kavehpour <pirouz@seas.ucla.edu>

Hi David,

Thank you for the update. Looking forward to hearing from you soon.

--

Regards,

Walid Ismail | UCLA
walidi86@ucla.edu | (818)324-6554 Mobile

Potential change in the permit type.

Questions

4 messages

David Peterson <DPETERSON@santa-clarita.com> Wed, Jul 12, 2017 at 1:53 P
To: WALID ISMAIL <walidi86@ucla.edu>

Hi Walid,

Sorry that this never got to you and your team.

Questions:

1) Do you have any examples or of other units in operation currently?

2) What is the noise level associated with this equipment? I'm looking for a dB spec if you have it.

3) Does the system emit any kind of gas or other exhaust that AQMD has to permit?

4) How is the equipment installed? How long does it take?

5) Describe how the equipment will be operated? Is it a continual thing or is it only operated intermittently?

6) How long will the equipment be on site?

7) How will it be dismantled and removed? How long will that take?

8) What kinds of danger to the public does this equipment represent? Is there a potential that it could explode? Are there hazardous materials associated with it? Are there combustible materials associated with it?

9) Is the Fire Department familiar with this kind of equipment? We'll want Fire to make conditions on this project.

10) We'll also need to see how the equipment is mounted to the ground – but that wont happen until you submit for a building permit.

D

David Peterson
Associate Planner
Planning Division
City of Santa Clarita
23920 Valencia Blvd.
Santa Clarita, CA 91355

Phone: (661) 284-1406
Email: DPETERSON@santa-clarita.com
Web: http://www.santa-clarita.com

WALID ISMAIL <walidi86@ucla.edu> Wed, Jul 19, 2017 at 3:46 PM
To: David Peterson <DPETERSON@santa-clarita.com>
Cc: Mohammad Janbozorgi <mjanbozorgi@gmail.com>, Pirouz Kavehpour <pirouz@seas.ucla.edu>

Good afternoon David,

Please find below our answers:

1) Do you have any examples or of other units in operation currently?

Our system is a combination of 2 mature technologies, compressed air and thermal storage. Both technologies have been used across industries and have been proven to be effective. It is their combination that makes our technology novel.

2) What is the noise level associated with this equipment? I'm looking for a dB spec if you have it.

Noise level is 78dB at 1meter.

3) Does the system emit any kind of gas or other exhaust that AQMD has to permit?

No. The plant does not emit any air polluting gases. It operates with compressed air only.

4) How is the equipment installed? How long does it take?

The equipment used is standard industry equipment, except that the working fluid is compressed air. There will be an air tank, an air compressor, water tanks, heat exchangers, a micro-turbine and a refractory-based energy storage medium, which are connected together via a piping system. Also, the projected installation time span is one month.
The equipment will be installed on a concrete slab where the foundation will be set in place prior to mobilization of the equipment on site. The standalone pieces of equipment will be anchored to the foundation. The reputable Murray Company Mechanical Contractors (http://murraycompany.com) will be in charge of installing the equipment as per the California building standards codes.

5) Describe how the equipment will be operated? Is it a continual thing or is it only operated intermittently?

The system will be powered up twice a week maximum, for 12 hours each time.
Each phase, charge and discharge will take 6 hours.

6) How long will the equipment be on site?

The equipment will be on site for 6 months.

7) How will it be dismantled and removed? How long will that take?

It will be decommissioned as per the Murray Company (reference above) standards and best practices. It will be dismantled within a month.

8) What kinds of danger to the public does this equipment represent? Is there a potential that it could explode? Are there hazardous materials associated with it? Are there combustible materials associated with it?

None! There will be no danger to the public. Our operation does not introduce any risk to the surrounding. There are no hazardous nor any combustible materials used in the plant.

9) Is the Fire Department familiar with this kind of equipment? We'll want Fire to make conditions on this project.

The Fire Department should be familiar with this kind of equipment. We have an air tank, an air compressor, water tanks, heat exchangers, a micro-turbine and a refractory-based energy storage medium; all of which constitute a normal set of industry equipment.

10) We'll also need to see how the equipment is mounted to the ground – but that wont happen until you submit for a building permit.

We can provide that, as well as foundation drawings.

Please let us know if you need any clarification for the answers above.
Also, could you please inform us of the next steps in order to get the necessary permits in place?

--

Regards,

Walid Ismail | UCLA
walidi86@ucla.edu | (818)324-6554 Mobile

[Quoted text hidden]

David Peterson <DPETERSON@santa-clarita.com> Wed, Jul 19, 2017 at 4:14 PM
To: WALID ISMAIL <walidi86@ucla.edu>
Cc: Mohammad Janbozorgi <mjanbozorgi@gmail.com>, Pirouz Kavehpour <pirouz@seas.ucla.edu>

Thank you, Walid! I'm talking to my senior planner tomorrow and will see if we can do this at a lesser permit level than I had anticipated. Will contact you tomorrow.

From: WALID ISMAIL [mailto:walidi86@ucla.edu]
Sent: Wednesday, July 19, 2017 3:47 PM
To: David Peterson
Cc: Mohammad Janbozorgi; Pirouz Kavehpour
Subject: Re: Questions

[Quoted text hidden]

WALID ISMAIL <walidi86@ucla.edu> Wed, Jul 19, 2017 at 4:42 PM
To: David Peterson <DPETERSON@santa-clarita.com>
Cc: Mohammad Janbozorgi <mjanbozorgi@gmail.com>, Pirouz Kavehpour <pirouz@seas.ucla.edu>

Thank you.

Looking forward to talking to you tomorrow.

--

Regards,

Walid Ismail | UCLA
walidi86@ucla.edu | (818)324-6554 Mobile

David's technical questions answered by our team

Call today

3 messages

David Peterson <DPETERSON@santa-clarita.com> Thu, Aug 3, 2017 at 8:31 AM
To: WALID ISMAIL <walidi86@ucla.edu>

Hi Walid,

Do you have time for a phone call today? I need to chat with you about a few issues. This review has been somewhat complex and has taken a while based on several different factors. I wanted to go over some things with you.

D

David Peterson
Associate Planner
Planning Division
City of Santa Clarita
23920 Valencia Blvd.
Santa Clarita, CA 91355

Phone: (661) 284-1406
Email: DPETERSON@santa-clarita.com
Web: http://www.santa-clarita.com

Think before you print

WALID ISMAIL <walidi86@ucla.edu> Thu, Aug 3, 2017 at 9:43 AM
To: Pirouz Kavehpour <pirouz@seas.ucla.edu>, Mohammad Janbozorgi <mjanbozorgi@gmail.com>

Good morning gents,

After talking with David briefly, he'd like to have a call this afternoon around 2pm.

Pirouz, we will follow up with an e-mail highlighting the main topics discussed during our call.

--

Regards,

Walid Ismail | UCLA
walidi86@ucla.edu | (818)324-6554 Mobile

WALID ISMAIL <walidi86@ucla.edu> Thu, Aug 3, 2017 at 2:37 PM
To: Pirouz Kavehpour <pirouz@seas.ucla.edu>, Mohammad Janbozorgi <mjanbozorgi@gmail.com>

Good afternoon,

During the call, David confirmed that his efforts are still in full force to get us the adequate permits for our project, and he thanks us for being patient throughout the process.

He still has 3 meetings and should have an update for us by the end of next week:

- Fire department meeting
- Planning manager
- Home Owner's Association (HOA) of Santa Clarita near the Placerita Canyon site

David specifically said that our project can gain traction through his office because it is green, but the HOA hates the Placerita Canyon plant and might be the biggest opposing force against this project.

Regarding the extra money that was paid for the OneStop application, we will be either reimbursed or the extra amount can be used to pay for the building and fire permits.

--

Regards,

Walid Ismail | UCLA
walidi86@ucla.edu | (818)324-6554 Mobile

David stating that there might be some issues with the permitting for our project. He mentions that there are 3 important meetings pending.

Air Tank

3 messages

David Peterson <DPETERSON@santa-clarita.com> Tue, Aug 8, 2017 at 1:21 PM
To: WALID ISMAIL <walidi86@ucla.edu>

Hi Walid,

Do you know how many gallons the air tank can hold? Fire Department is asking.

Thanks

D

David Peterson
Associate Planner
Planning Division
City of Santa Clarita
23920 Valencia Blvd.
Santa Clarita, CA 91355

Phone: (661) 284-1406
Email: DPETERSON@santa-clarita.com
Web: http://www.santa-clarita.com

Think before you print

WALID ISMAIL <walidi86@ucla.edu> Wed, Aug 9, 2017 at 11:37 AM
To: David Peterson <DPETERSON@santa-clarita.com>

Hello David,

The volume of the air tank is 100 cubic meters, which converts to about 26417 gal.
The air tank is 122 inches ID, approximately 40 feet seam to seam.

Please let me know if you need more specs or drawings.

–

Regards,

Walid Ismail | UCLA
walidi86@ucla.edu | (818)324-6554 Mobile

David Peterson <DPETERSON@santa-clarita.com> Wed, Aug 9, 2017 at 1:03 PM
To: WALID ISMAIL <walidi86@ucla.edu>

I think this will do for now.

Question from the Fire Department answered by our team.

Project

7 messages

David Peterson <DPETERSON@santa-clarita.com> Thu, Aug 10, 2017 at 3:42 PM
To: WALID ISMAIL <walidi86@ucla.edu>

Hi Walid,

So the Fire Department is familiar with what you're proposing so I'll add a condition to have them review it after we do. I'm working on getting a meeting scheduled with the HOA people in Placerita Canyon and will advise you when that's done.

D

David Peterson
Associate Planner
Planning Division
City of Santa Clarita
23920 Valencia Blvd.
Santa Clarita, CA 91355

Phone: (661) 284-1406
Email: DPETERSON@santa-clarita.com
Web: http://www.santa-clarita.com

Think before you print

WALID ISMAIL <walidi86@ucla.edu> Thu, Aug 10, 2017 at 3:45 PM
To: David Peterson <DPETERSON@santa-clarita.com>

Thank you David.

Should we expect an update before the end of the week?

--

Regards,

Walid Ismail | UCLA
walidi86@ucla.edu | (818)324-6554 Mobile

David Peterson <DPETERSON@santa-clarita.com> Thu, Aug 10, 2017 at 3:46 PM
To: WALID ISMAIL <walidi86@ucla.edu>

I'm hoping so.

From: WALID ISMAIL [mailto:walidi86@ucla.edu]
Sent: Thursday, August 10, 2017 3:45 PM
To: David Peterson
Subject: Re: Project

[Quoted text hidden]

David Peterson <DPETERSON@santa-clarita.com> Thu, Aug 10, 2017 at 4:26 PM
To: WALID ISMAIL <walidi86@ucla.edu>

Is there a way you could move the facility to the back of the existing energy plant? I would be less visible and eliminate the oak tree issue. That would be more ideal for the City.

D

From: WALID ISMAIL [mailto:walidi86@ucla.edu]
Sent: Thursday, August 10, 2017 3:45 PM
To: David Peterson
Subject: Re: Project

Thank you David.

[Quoted text hidden]

WALID ISMAIL <walidi86@ucla.edu> Thu, Aug 10, 2017 at 4:50 PM
To: David Peterson <DPETERSON@santa-clarita.com>

Hello David,

We've had numerous talks with Clean Energy Systems and we were allocated this part of the energy plant considering the setup and the 3-D layout of our project.

--

Regards,

Walid Ismail | UCLA
walidi86@ucla.edu | (818)324-6554 Mobile

[Quoted text hidden]

David Peterson <DPETERSON@santa-clarita.com> Thu, Aug 10, 2017 at 5:18 PM
To: WALID ISMAIL <walidi86@ucla.edu>

Honestly, that could prove problematic with the HOA folks. Will advise shortly.

WALID ISMAIL <walidi86@ucla.edu> Sat, Aug 12, 2017 at 5:44 PM
To: David Peterson <DPETERSON@santa-clarita.com>

Hello David,

We have been to the site and had no issues with the oak tree being there. We should not be conducting any work near the oak tree.
Could you please elaborate on where the problem might be?

--

Regards,

Walid Ismail | UCLA
walidi86@ucla.edu | (818)324-6554 Mobile

Still working on scheduling a meeting with the HOA. David asks us if we can move the project to the back of the facility away from the oak tree

PCPOA

5 messages

David Peterson <DPETERSON@santa-clarita.com> Wed, Aug 16, 2017 at 12:58 PM
To: WALID ISMAIL <walidi86@ucla.edu>

Hi Walid,

I talked with the president of the Placerita Canyon Property Owners Association. I'm sending her a copy of the site plan and elevations and she's going to give that information to her board. She did have a couple questions:

1) She wanted to verify that there are no emissions from the mechanism.

2) She wanted to know if the heavy rains that are forecast for this winter will impact the operation of the mechanism.

Will let you know when I hear back from them.

D

David Peterson
Associate Planner
Planning Division
City of Santa Clarita
23920 Valencia Blvd.
Santa Clarita, CA 91355

Phone: (661) 284-1406
Email: DPETERSON@santa-clarita.com
Web: http://www.santa-clarita.com

Think before you print

WALID ISMAIL <walidi86@ucla.edu> Wed, Aug 16, 2017 at 4:19 PM
To: David Peterson <DPETERSON@santa-clarita.com>
Cc: Pirouz Kavehpour <pirouz@seas.ucla.edu>, Mohammad Janbozorgi <mjanbozorgi@gmail.com>

Thank you David,

With regards to the president of the Placerita Canyon Property Owners Association's questions:

1) There will be no emissions from the mechanism
2) The heavy rains will not impact the operation of the mechanism, as the equipment is elevated and we will have adequate drainage to prevent any damage to the equipment.

Regards,

Walid Ismail | UCLA
walidi86@ucla.edu | (818)324-6554 Mobile

WALID ISMAIL <walidi86@ucla.edu> Fri, Aug 18, 2017 at 11:33 AM
To: David Peterson <DPETERSON@santa-clarita.com>
Cc: Pirouz Kavehpour <pirouz@seas.ucla.edu>, Mohammad Janbozorgi <mjanbozorgi@gmail.com>

Good morning David,

We were just wondering if the Placerita Canyon Property Owners Association gave you a timeframe as to when they might get back to you?

--

Regards,

Walid Ismail | UCLA
walidi86@ucla.edu | (818)324-6554 Mobile

[Quoted text hidden]

WALID ISMAIL <walidi86@ucla.edu> Tue, Aug 22, 2017 at 10:01 AM
To: David Peterson <DPETERSON@santa-clarita.com>
Cc: Pirouz Kavehpour <pirouz@seas.ucla.edu>, Mohammad Janbozorgi <mjanbozorgi@gmail.com>

Hello David,

Any updates from your end?

On another note, how long would the building, fire and encroachment permits take usually?

--

Regards,

Walid Ismail | UCLA
walidi86@ucla.edu | (818)324-6554 Mobile

[Quoted text hidden]

WALID ISMAIL <walidi86@ucla.edu> Wed, Aug 23, 2017 at 11:38 AM
To: David Peterson <DPETERSON@santa-clarita.com>
Cc: Mohammad Janbozorgi <mjanbozorgi@gmail.com>, Pirouz Kavehpour <pirouz@seas.ucla.edu>

Good afternoon David,

We are getting close to some deadlines with the California Energy Commission and would like to keep the momentum going with obtaining the necessary permits for building our project.
I haven't been able to get a hold of you at the office, please give us some updates at your earliest convenience or call me at (818)324-6554.

Your help is greatly appreciated.

--

Regards,

Walid Ismail | UCLA
walidi86@ucla.edu | (818)324-6554 Mobile

Two questions from the HOA that our team answered. We attempt to get a timeframe with regards to the permits.

Sorry to keep you waiting
3 messages

David Peterson <DPETERSON@santa-clarita.com> Wed, Aug 23, 2017 at 5:28 PM
To: WALID ISMAIL <walidi86@ucla.edu>

I've yet to hear back from the HOA board that I met with. Reaching out to them to get a status on their feelings.

D

David Peterson
Associate Planner
Planning Division
City of Santa Clarita
23920 Valencia Blvd.
Santa Clarita, CA 91355

Phone: (661) 284-1406
Email: DPETERSON@santa-clarita.com
Web: http://www.santa-clarita.com

Think before you print

WALID ISMAIL <walidi86@ucla.edu> Thu, Aug 24, 2017 at 11:04 AM
To: David Peterson <DPETERSON@santa-clarita.com>

Thank you David,

Could you also please let us know if we can start the paperwork for the building and fire permits?

--

Regards,

Walid Ismail | UCLA
walidi86@ucla.edu | (818)324-6554 Mobile

[Quoted text hidden]

David Peterson <DPETERSON@santa-clarita.com> Fri, Aug 25, 2017 at 12:09 PM
To: WALID ISMAIL <walidi86@ucla.edu>

Let me get back to you on that as the HOA is telling me they want to consider this at their board meeting which isn't until the 7th of September. I'll be on a business trip until next Thursday but I'll check in with my Senior Planner on your question.

D

Still waiting for the HOA, apparently they have a board meeting on the 7th of September

City of
SANTA CLARITA

23920 Valencia Boulevard • Santa Clarita, California 91355-2196
Phone: (661) 259-2489 • FAX: (661) 259-8125
www.santa-clarita.com

CITY OF SANTA CLARITA
COMMUNITY DEVELOPMENT DEPARTMENT
MASTER CASE NO. 17-184
TEMPORARY USE PERMIT 17-028
PER CODE SECTION 17.23.200 OF THE
UNIFIED DEVELOPMENT CODE

Date:	September 25, 2017
Applicant:	Pirouz Kavehpour 420 Westwood Plaza, Room 46-147A Los Angeles, CA 90095
Location:	North of Placerita Canyon Road, west of the intersection of Sierra Highway and Placerita Canyon Road (APN: 2833-023-036)
Request:	The applicant is requesting approval of a Temporary Use Permit to temporarily operate one 75 kW energy storage system. The energy storage system would be operated by the University of California of Los Angeles. The subject property is located in the Business Park (BP) zone and operate for a period not to exceed 6 months.
Findings:	In granting this approval, the Director finds that the required Burden of Proof set forth in Section 17.23.200 of the Santa Clarita Municipal Code has been met by the applicant. The Director further finds that the use is categorically exempt since it meets the criteria set forth in Class 4 of Section 15304(e) of the California Environmental Quality Guidelines. This approval is pursuant to the following conditions:

CONDITIONS OF APPROVAL

GENERAL CONDITIONS

GC1. The approval of this project shall expire if the approved use is not commenced within two (2) years from the date of this approval, unless it is extended in accordance with the terms and provisions of the City of Santa Clarita's Unified Development Code (UDC).

GC2. To the extent the use approved with this project is a different use than previously approved for the property, the prior approval shall be terminated along with any associated vested rights to such use, unless such prior approved use is still in operation, or is still within the initial pre-commencement approval period. Once commenced, any discontinuation of the use approved with this project for a continuous period of one hundred eighty (180) calendar days or more shall terminate the approval of this use along with any associated vested rights to such use. The use shall not be re-established or resumed after the one hundred eighty (180) day period. Discontinuation shall include cessation of a use regardless of intent to resume.

GC3. The applicant may file for an extension of the conditionally approved project prior to the date of expiration. If such an extension is requested, it must be filed no later than sixty (60) days prior to expiration.

GC4. The applicant shall be responsible for notifying the Director of Community Development, in writing, of any change in ownership, designation of a new engineer, or change in the status of the developer, within thirty (30) days of said change.

GC5. Unless otherwise apparent from the context, the term "applicant" shall include the applicant and any other persons, corporation, or other entity making use of this grant. The applicant shall defend, indemnify, and hold harmless the City of Santa Clarita, its agents, officers, and employees from any claim, action, or proceeding against the City or its agents, officers, or employees to attack, set aside, void, or annul the approval of this project by the City, including any related environmental approvals. In the event the City becomes aware of any such claim, action, or proceeding, the City shall promptly notify the applicant. If the City fails to cooperate fully in the defense, the applicant shall not thereafter be responsible to defend, indemnify, or hold harmless the City. Nothing contained in this condition prohibits the City from participating in the defense of any claim, action, or proceeding, if both of the following occur: 1) the City bears its own attorneys' fees and costs; and 2) the City defends the action in good faith. The applicant shall not be required to pay or perform any settlement unless the settlement is approved by the applicant.

GC6. The property shall be developed and maintained in substantial conformance with the approvals granted by the City. Any modifications shall be subject to further review by the City.

GC7. The applicant and property owner shall comply with all inspections requirements as deemed necessary by the City of Santa Clarita.

GC8. The owner, at the time of issuance of permits or other grants of approval agrees to develop the property in accordance with City codes and other appropriate ordinances including, but not limited to, the California Building Code (Building, Mechanical, Plumbing, Electrical, Green Building, and Energy Codes), Fire Code, Unified Development Code (Grading Code and Undergrounding of Utilities Ordinance), Utilities Code (Sanitary Sewer and Industrial Waste Ordinance), and Highway Permit Ordinance.

GC9. This grant shall not be effective for any purpose until the applicant has filed with the Director of Community Development, their affidavit (Acceptance Form) stating that they are aware of, and agree to accept, all of the conditions of this grant.

GC10. Details shown on the site plan are not necessarily approved. Any details which are inconsistent with the requirements of state or local ordinances, general conditions of approval, or City policies and not modified by this permit must be specifically approved.

GC11. It is hereby declared and made a condition of this permit that if any condition hereof is violated, or if any law, statute, or ordinance is violated, the City may commence proceedings to revoke this approval.

PLANNING DIVISION

PL1. The applicant is approved to temporarily operate one 75 kW energy storage system (system) in accordance with the site plan and elevations on file with the City of Santa Clarita's Planning Division.

PL2. The system shall cease operation on a date six-months from the date of installation. The system shall be removed from the site completely fourteen days after the date operation ceases.

PL3. The system shall comply with the City of Santa Clarita's Noise Ordinance and shall not be operated in a manner that disturbs the residents of the Placerita Canyon neighborhood.

PL4. The system shall not emit any offensive odors.

PL5. The system shall comply with all state and local air quality emission requirements.

PL6. The system shall not encroach within the public right of way.

PL7. Signs are not a part of this approval. Prior to installing any temporary banners, the applicant shall receive approval from the Planning Division.

PL8. All requirements of the Zoning Ordinance and of the specific zoning of the subject property must be complied with unless set forth in this permit.

PL9. All applicable provisions of the Los Angeles County Health Department, Los Angeles County Fire Department, Los Angeles County Business License, or the provisions of any other affected agency shall be met.

PL10. The applicant shall obtain all necessary building permits from the Building and Safety Division for any temporary structures.

PL11. The applicant shall obtain all necessary permits from the City of Santa Clarita Public Works Department prior to location of the proposed system on site.

PL12. The applicant shall follow best management practices for preservation of the existing oak trees on site. The applicant shall contact the City of Santa Clarita's Oak Tree Specialist, Robert Sartain, at (661) 294-2556 prior to commencement of construction.

PL13. This approval shall not supersede the approvals of any other agency.

If you have any questions regarding this application, I can be reached at (661) 255-4330 or by email at mmanion@santa-clarita.com.

Sincerely,

David Peterson,
Associate Planner

S:\CD\PLANNING DIVISION\CURRENT\2017\MC17-184 (TUP 17 028UCLA Energy)\Conditions of Approval 17 184.doc

CC: Daniel Rivas, Community Preservation Manager

Our project receiving a temporary use permit from the Planning Division of the City of Santa Clarita.

APPENDIX C:
Mechanical (3D) Layout

3D Renderings of the mechanical layout.

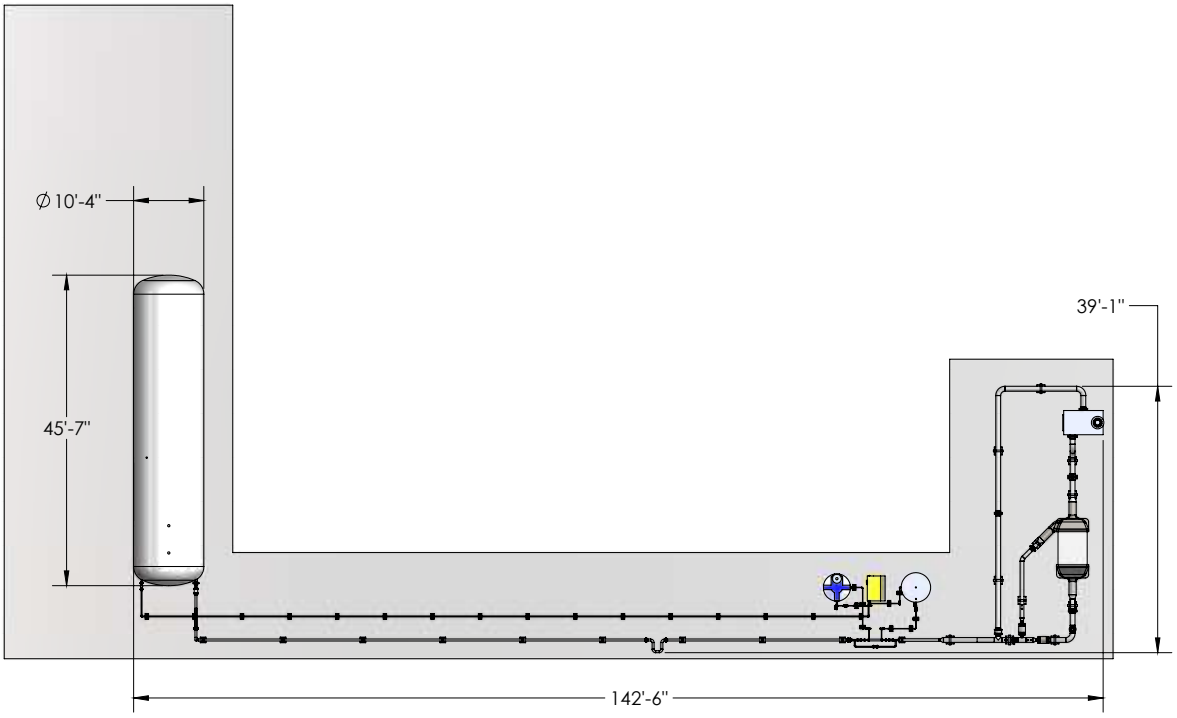

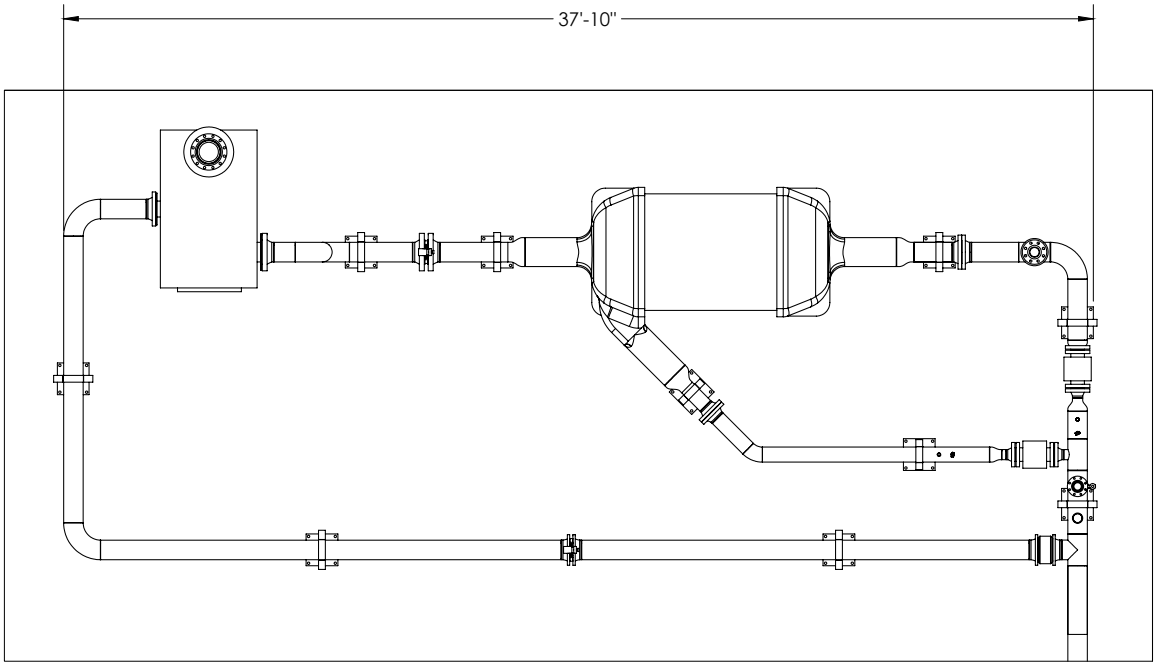
37'-10"

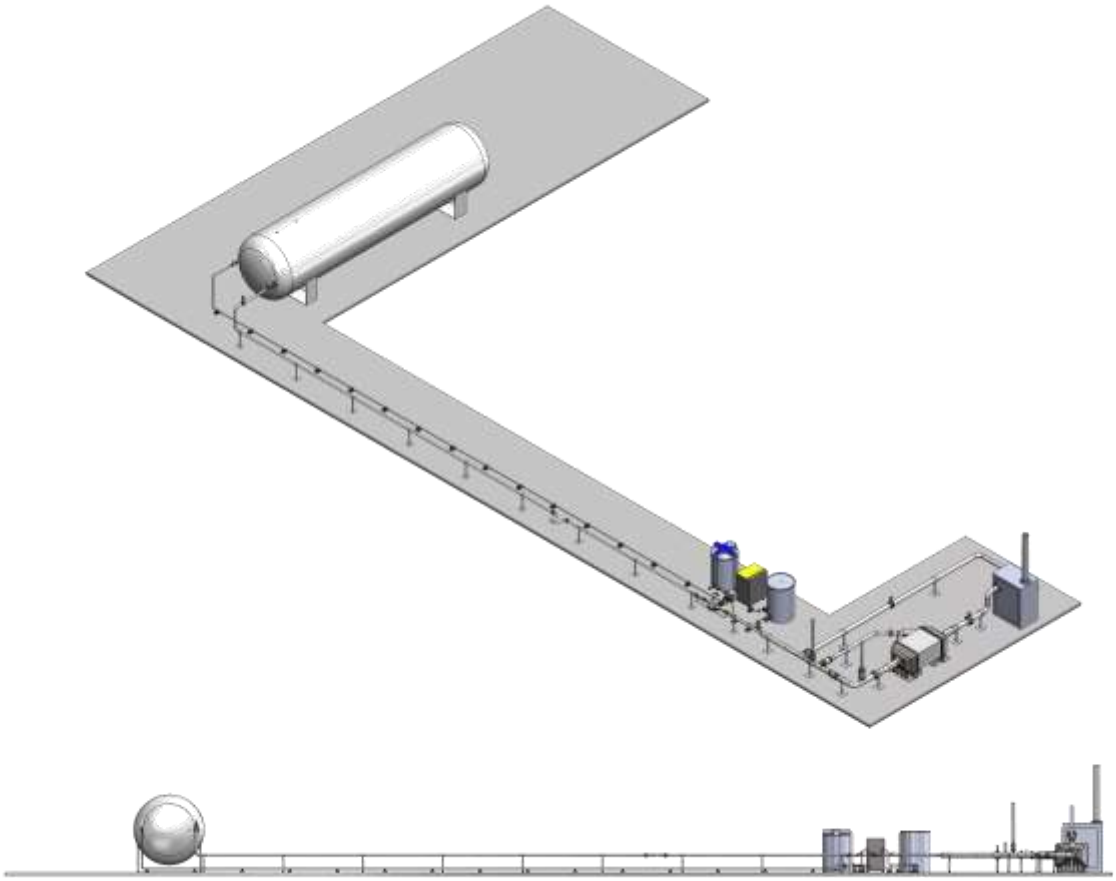

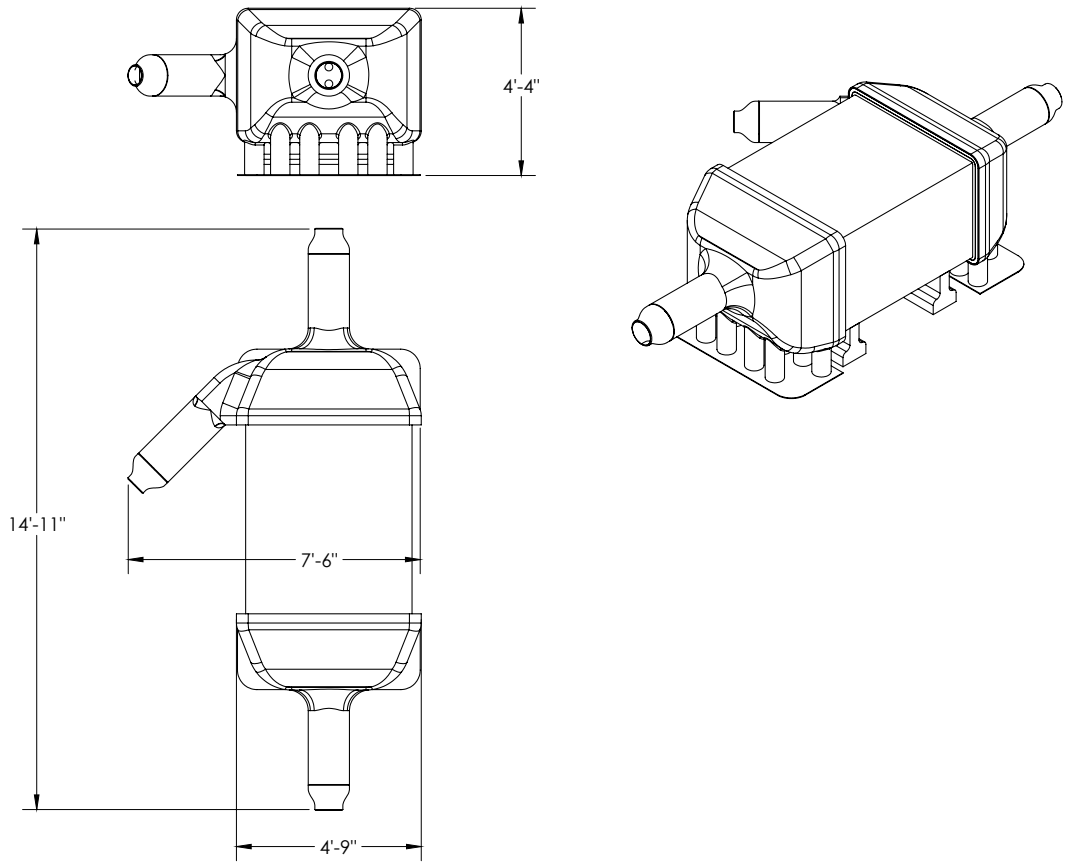
4'-4"
14'-11"
7'-6"
4'-9"

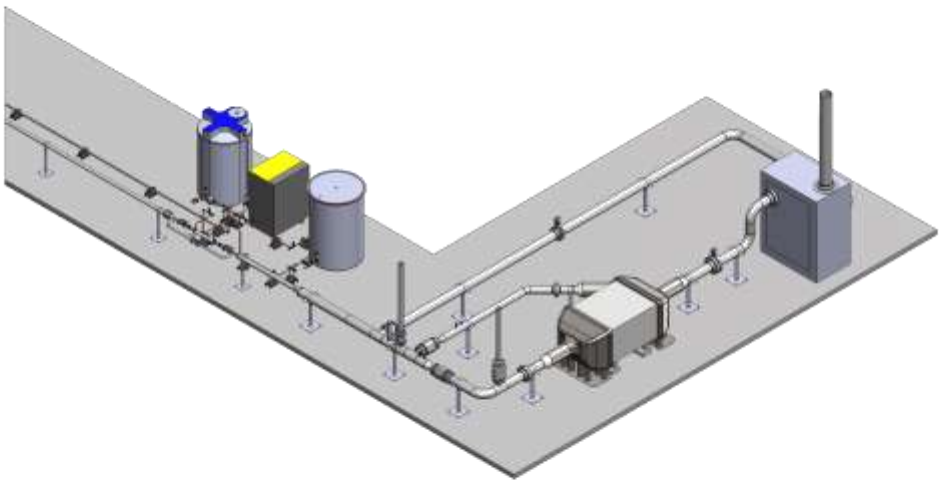

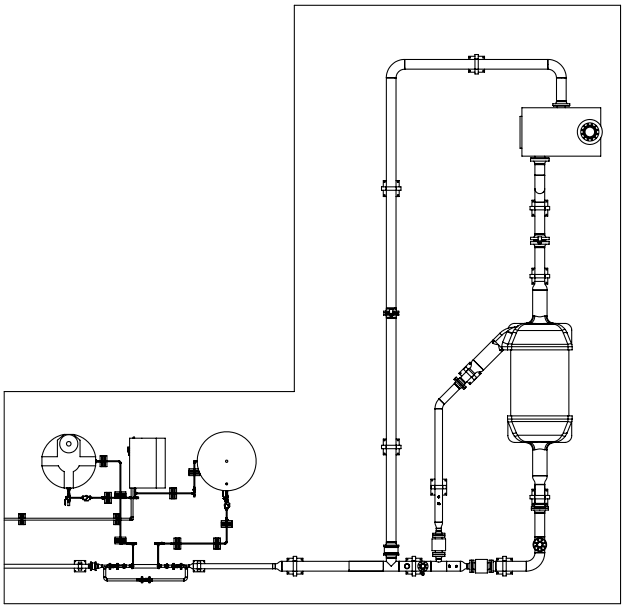

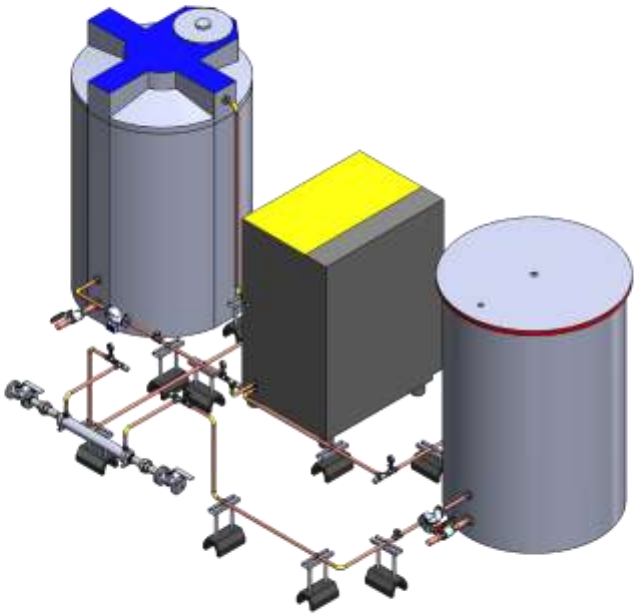

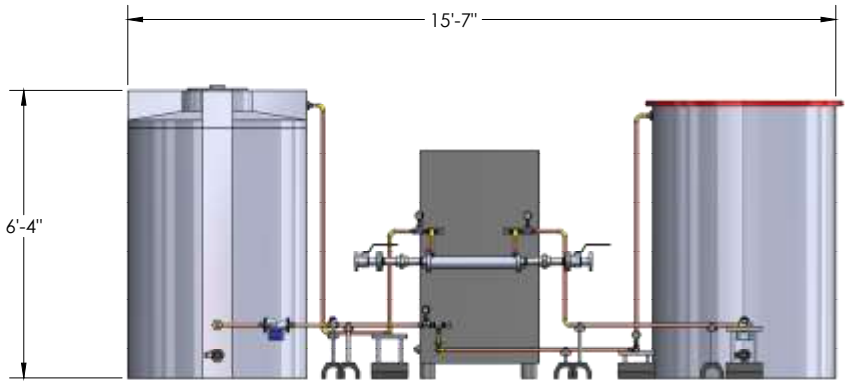
15'-7"
6'-4"

APPENDIX D:
Snapshots from Aspen HYSYS Software

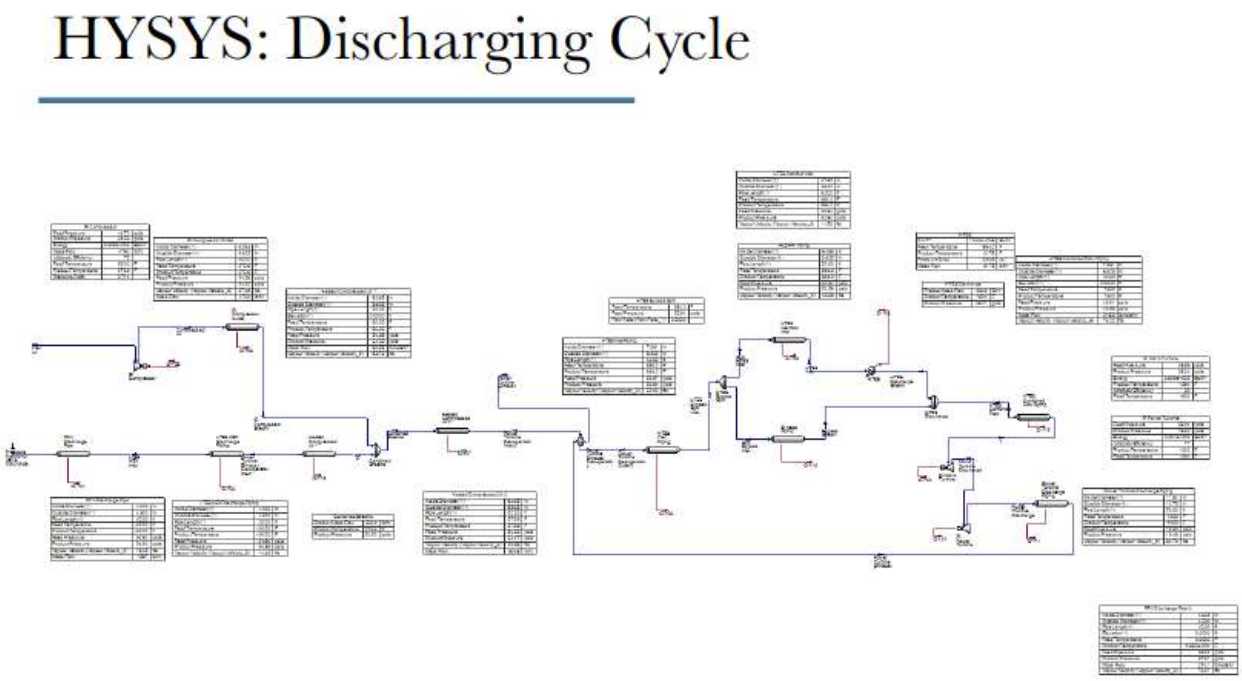

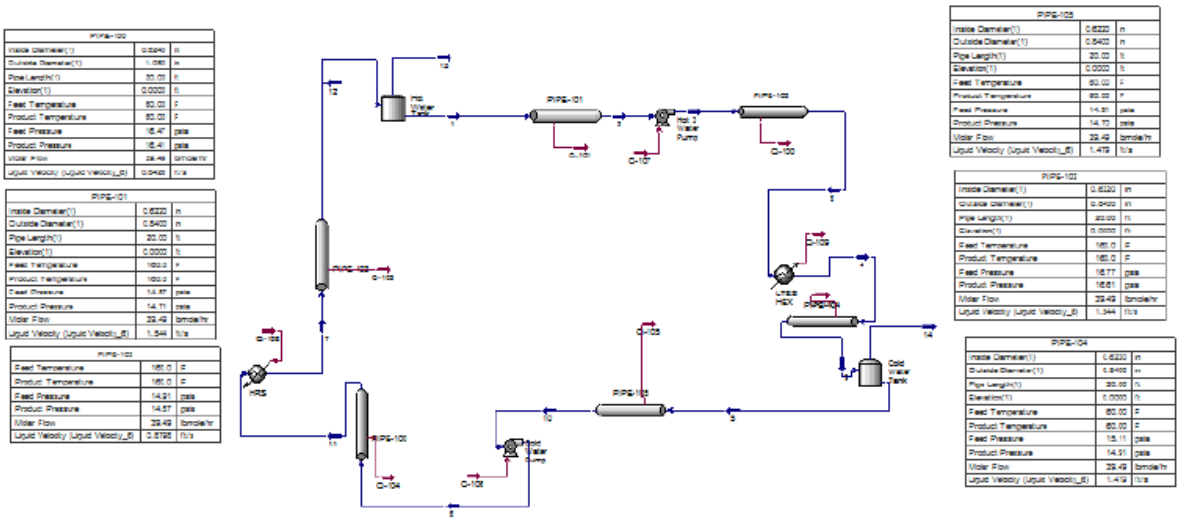

HYSYS: Power Turbine Exhaust Heat Recovery Cases

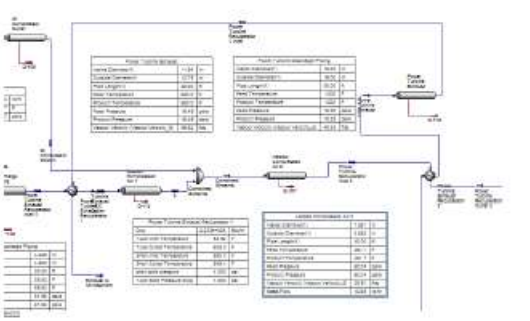

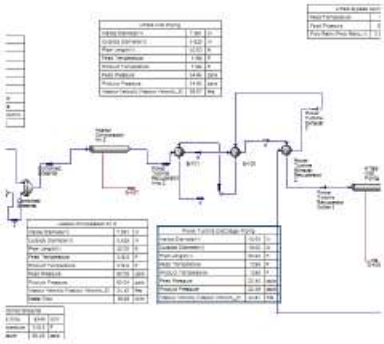

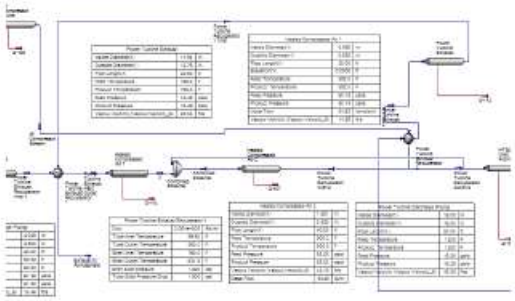

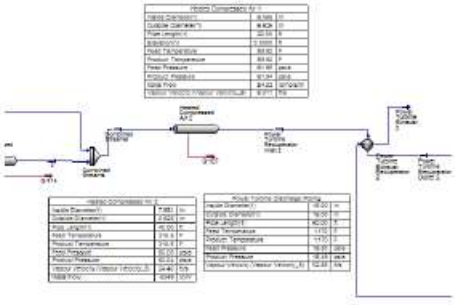

HYSYS: Conventional CAES (Competing Technologies)

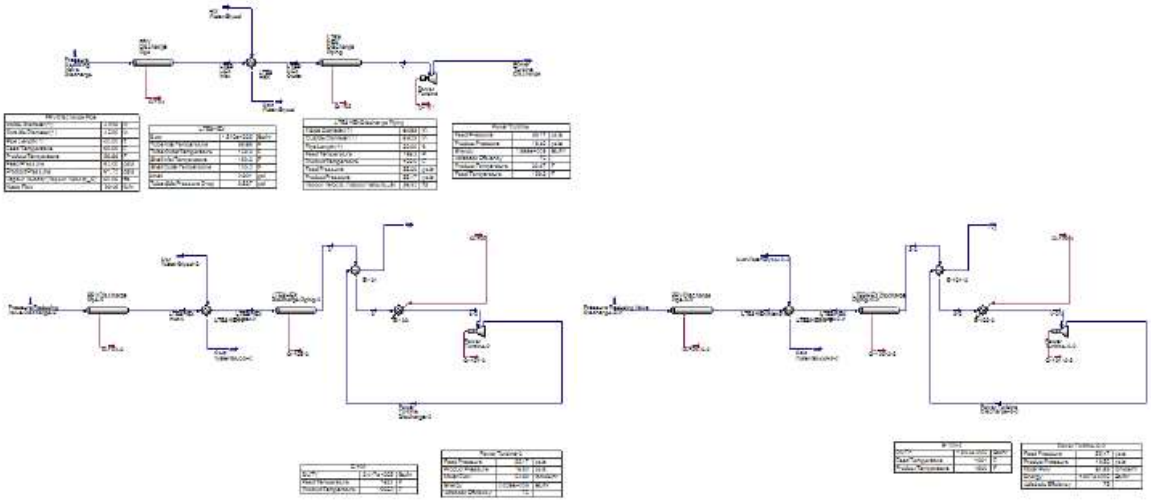

HYSYS: HTES Regeneration